UNIVERSITÀ DI PARMA

UNIVERSITÀ DEGLI STUDI DI PARMA

DOTTORATO DI RICERCA IN

"Scienze del Farmaco, delle Biomolecole

e dei Prodotti per la Salute"

CICLO XXXI

Human serine racemase: regulation by divalent metals, NADH and S-nitrosylation

Coordinatore:

Chiar.mo Prof. Marco Mor

Tutore:

Chiar.mo Prof. Stefano Bruno

Dottorando: Francesco Marchesani

Anni 2015/2018

INDEX

Chapter 1 - INTRODUCTION

Serine racemase is a pyridoxal 5'-phosphate (PLP)-dependent enzyme involved in the reversible racemization of L-serine and D-serine and their deamination to pyruvate and ammonia.

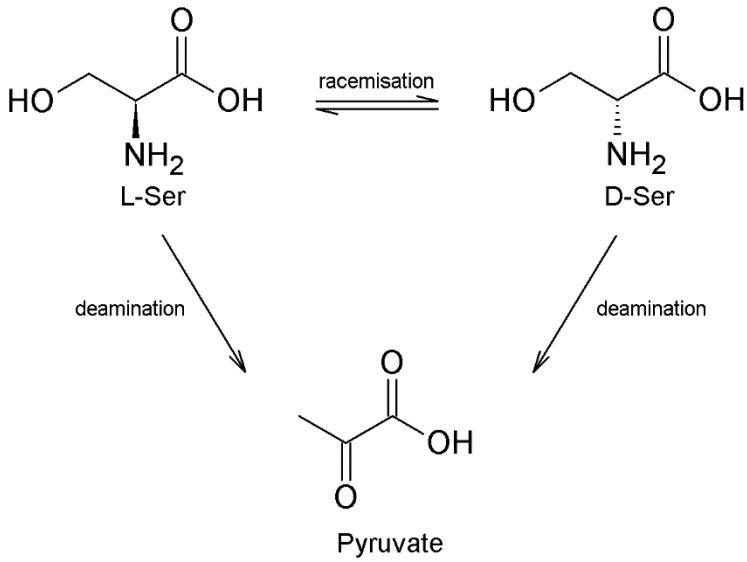

Figure 1.1: General reactions catalyzed by serine racemase

In vertebrates, D-serine is the co-agonist of the N-methyl D-aspartate (NMDA) receptors for glutamate, the most abundant excitatory neurotransmitter in the brain. The NMDA receptors are ligand-gated ion channels involved in several biological events, including synapse formation, synaptic plasticity, learning and memory potentiation (Paoletti et al. 2013). NMDA receptors are the only neurotransmitter receptors the activation of which requires two distinct agonists, glutamate and either glycine or D-serine.

Increased levels of D-serine and the resulting over-excitation of NMDA receptors in the brain are associated with neuronal excitotoxicity, observed in several pathological conditions, including Parkinson and Alzheimer diseases, stroke and amyotrophic lateral sclerosis. On the other hand, low levels of D-serine are associated with schizophrenia (Wolosker et al. 2008).

Other D-amino acids were detected in the brain but, for most of them, the racemase involved in their production has not yet been identified (Conti et al. 2011). SR itself was proposed to be responsible for the production of D-aspartate, an agonist of the NMDA receptors (Ito et al. 2016).

1.1 LOCALIZATION OF SERINE RACEMASE IN THE BRAIN

Serine racemase (SR) was first localized in astrocytes, leading to the assumption that D-serine, its product, was a 'gliotrasmitter', i.e. a neuroactive molecule directly released by astrocytes. There was also evidence that D-serine was concentrated in vesicle-like structures in cultured astrocytes (Henneberger et al. 2010), thus apparently confirming this '*gliotransmitter hypothesis*'. The experimental results that led to this model have been put into question (Wolosker et al. 2016).

Today, the prevalent view is that the main production of D-serine takes place in neurons and that astrocytes do not produce a physiologically relevant amount of it (Wolosker et al. 2016). However, astrocytes produce most of L-serine, the substrate of SR, from glucose. Indeed, astrocytes express 3-phosphoglycerate dehydrogenase (PhgDH), which catalyzes a crucial step in the L-serine synthesis pathway. Its silencing in mouse brain astrocytes

dramatically reduces both L- and D-serine in the brain by about 80%. L-serine would then shuttled to neurons, where it is converted to D-serine by SR. D-serine is then released by neurons at the synaptic interface. Finally, D-serine is re-uptaken by neurons, and possibly astrocytes, through serine transporters (ASC-1 and others). A simplified model of this '*shuttle hypothesis'* is represented in Figure 1.2.

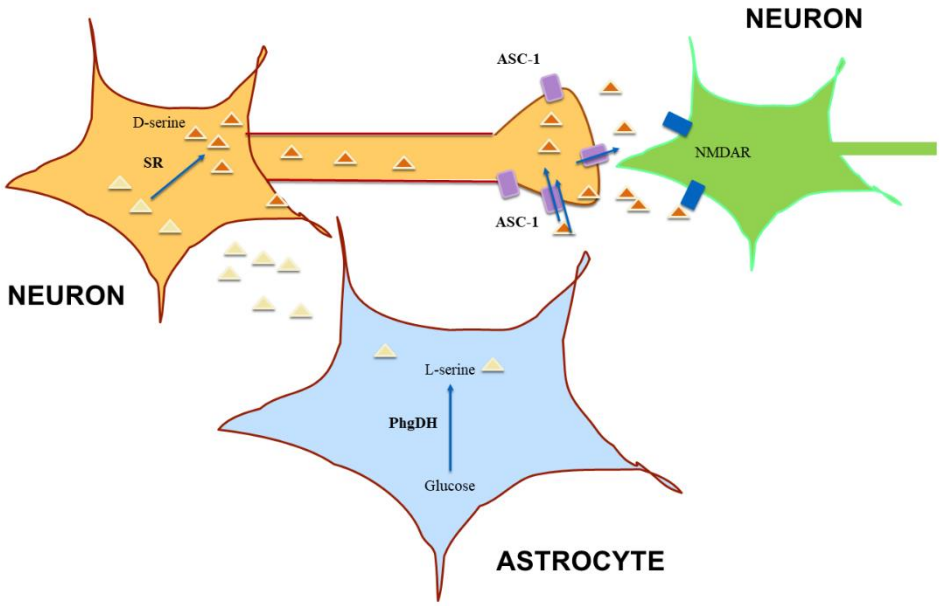

Figure 1.2: Shuttle model as proposed by Wolosker (Wolosker et al. 2016).

1.2 STRUCTURE OF SERINE RACEMASE

PLP-dependent enzymes are classified into 7 groups depending on their fold-type. Serine racemase belongs to the fold-type II, which also includes tryptophan synthase, O-acetylserine sulfhydrylase, threonine deaminase and serine dehydratase (Bettati et al. 2000; Campanini et al. 2003; Raboni et al. 2003). Fold-type II PLP-dependent enzymes are characterized by a large and a small domain with a similar α/β architecture constituted of a central β-sheet surrounded by helices. In hSR, the large domain is formed by residues 1-68 and 157-340, while the small domain comprises residues between 78 and 155. The PLP cofactor is covalently bound to a lysine residue of the large domain in a cleft between the two domains (Figure 1.3). Ten SR X-ray crystallographic structures have been deposited in the Protein Data Bank, including three structures of the human orthologue.

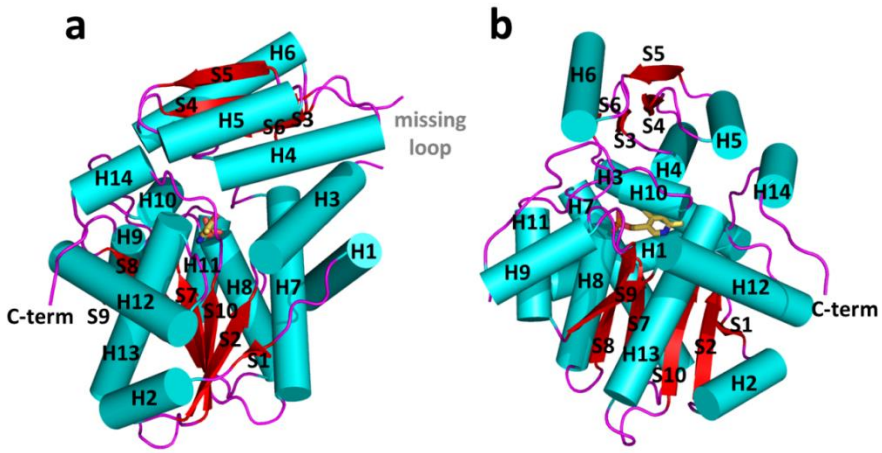

Figure 1.3: Structure of human serine racemase (PDB 3L6B) shown in two orthogonal views (**a, b**).

SR is present as a symmetric dimer in solution (Figure 1.4), as confirmed by different techniques, including exclusion chromatography, X-ray crystallography and glutaraldehyde cross-linking (Wang et al. 2012). The formation of the dimer is crucial for enzyme activity. Dimer formation involves regions that have high degree of flexibility. The equilibrium with a tetrameric form under specific conditions is discussed in chapter 3.

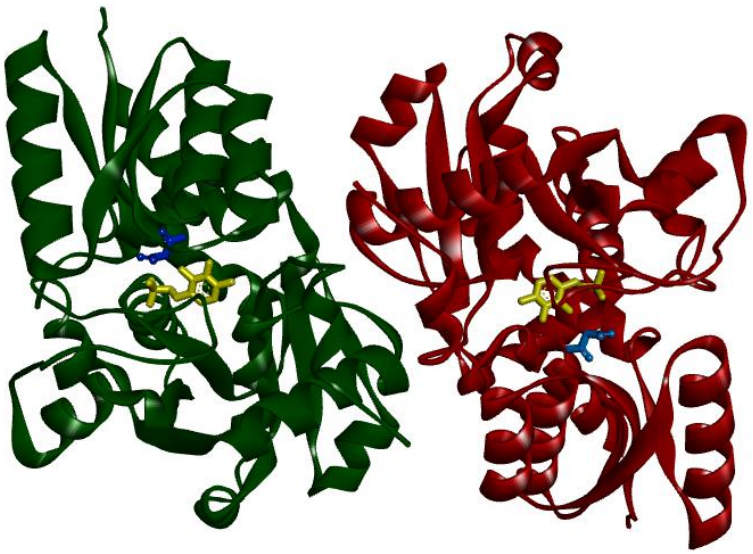

Figure 1.4. Dimeric structure of hSR (pdb code: 3L6B). PLP is represented in yellow sticks.

The structural investigation of SR in different ligation states allowed for the detection of an open-closed conformational shift occurring upon binding of the substrate or other active-site ligands. This mechanism was described previously for fold-type I PLP-dependent aspartate aminotransferases (Jager et al. 1994; Jansonius and Vincent 1987; Okamoto et al. 1994) and for several fold-type II enzymes such as OASS and tryptophan synthase (Mozzarelli et al. 2011; Raboni et al. 2009).

The structure of *Schizosaccharomices pombe* serine racemase (SpSR), which exhibits 35.1% sequence identity with hSR, crystallized in the absence of ligands at the active site in an open conformation (PDB code: 1V71) (Goto et al. 2009). SpSR modified at the active site with a lysino-D-alanyl group – which mimics the substrate – was found to be in a closed conformation (PDB code: 2ZPU) (Yamauchi et al. 2009), where the small domain undergoes a 20° rotation towards the large domain to close the active site (Figure 1.5a). A particularly large conformational change occurs in the asparagine loop Ser-Ser-Gly-Asn (residues 81-84 for SpSR, 83-86 for rat and human SR), at the N-terminal part of α-helix H5 (H4 in rat and human SR, since in SpSR an extra helix is present after helix H3), which forms the binding site for the carboxylate moiety of the substrate serine. Moreover, the carboxylate is involved in a salt bridge with the N-terminal Arg133 of α-helix H7 (H6 in rat and human SR) (Goto et al. 2009b).

An analogous open-closed conformational change was described for rat SR (rSR) by Smith and coworkers (Smith et al. 2010). The structure of rSR converts from an open conformation (PDB code: 3HMK) of the holo-enzyme to a closed conformation upon binding with the competitive inhibitor malonate (PDB code: 3L6C), which exerts a conformational effect similar to that of the substrate. Arg135 (corresponding to Arg133 in SpSR) and the arginine loop move towards the ligand bound to the active site, similarly to what is observed for SpSR (Figure 1.5b).

The structure of hSR bound to malonate was also reported (PDB code: 3L6B). Its comparison with a recently published structure of hSR in the unbound form (PDB code: 5X2L) (Takahara et al. 2017), confirmed that also hSR undergoes an open-closed conformational change when a ligand is present at the active site (Figure 1.5c). The relevance of this conformational

equilibrium for hSR post-translational modifications, particularly S-nitrosylation, was explored in the work described in Chapter 5.

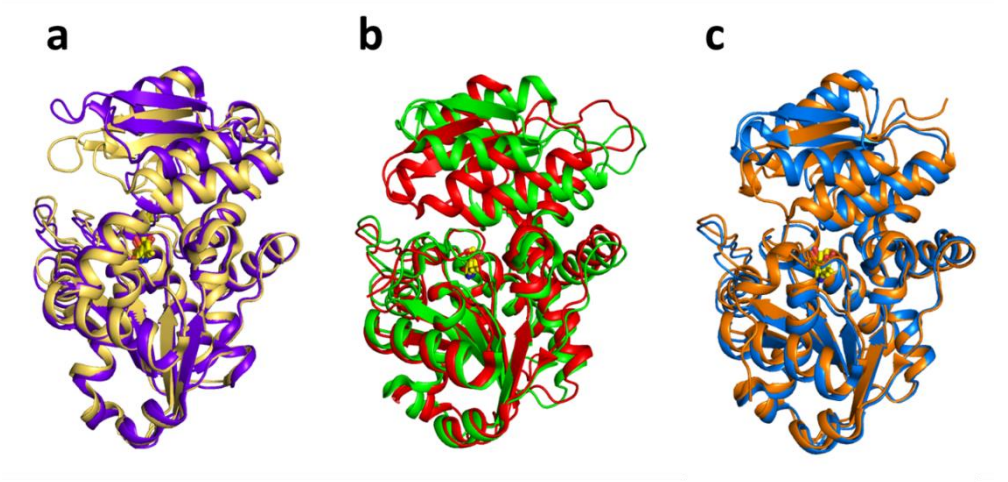

Figure 1.5: Overlay of **a)** the open (PDB 1V71, purple) and closed (PDB 2ZR8, yellow) structures of SpSR; **b)** the open (PDB 3HMK, green) and closed (PDB 3L6C, red) structures for rat SR; **c)** the open (PDB 5X2L, blue) and closed (PDB 3L6B, orange) structures of hSR. PLP is in yellow sticks.

The currently available crystal structures also clarify the binding site of two positive allosteric effectors: divalent cations and ATP (Figure 1.6).

The divalent cations binding site is in the large domain and is physiologically occupied by Mg^{2+}. The presence of divalent cations is critical for the enzyme correct folding, stability and activity (see below) (Bruno et al. 2017; Cook et al. 2002; Ito et al. 2012). The metal binding site is formed by ionic interactions with the carboxylate groups of Glu208 and Asp214 (Glu210 and Asp216 in rSR and hSR), the backbone carbonyl group of Gly212 (Ala214 in rSR and hSR) and three water molecules (Goto et al. 2009; Smith et al. 2010). The metal ion is coordinated by the six coordination points in an octahedral geometry (Figure 1.6). This site is not directly involved in catalysis,

although it is connected through water molecules to a tetra-glycine loop (Gly 183-184-185-186 for SpSR and 185-186-187-188 for rSR and hSR) at the N-terminal of α-helix H9 (in SpSR numbering, H8 in rSR and hSR), which forms a series of H-bonds with the phosphate group of PLP, contributing to the correct positioning of the cofactor. The PLP ring is covalently linked as internal aldimine to a Lys residue in the active site (Lys57 in SpSR and Lys56 in rat SR and hSR).

As for ATP, the structure of SR bound to 5′-adenylyl methylene diphosphonate (AMP-PCP) a stable analog of ATP was solved for SpSR (Goto et al. 2009) (Figure 1.6). AMP-PCP in complex with Mg^{2+} binds between the subunits at two symmetric sites in the dimer. The allosteric effector interacts both with the small domain and the large domain of one subunit, as well as with the large domain of the other subunit. ATP binding involves Ala115 (SpSR numbering) and Tyr119 in the small domain. The large domain interacts with Asn25, Phe-50, Asn51, Lys52, Met53, and Asn31, all found in the loop region. On the opposite side, the ligand interacts with Ser32, Ser33, Thr34, and Arg275, Met276, Lys277, of the large domain of the other monomer in the dimer.

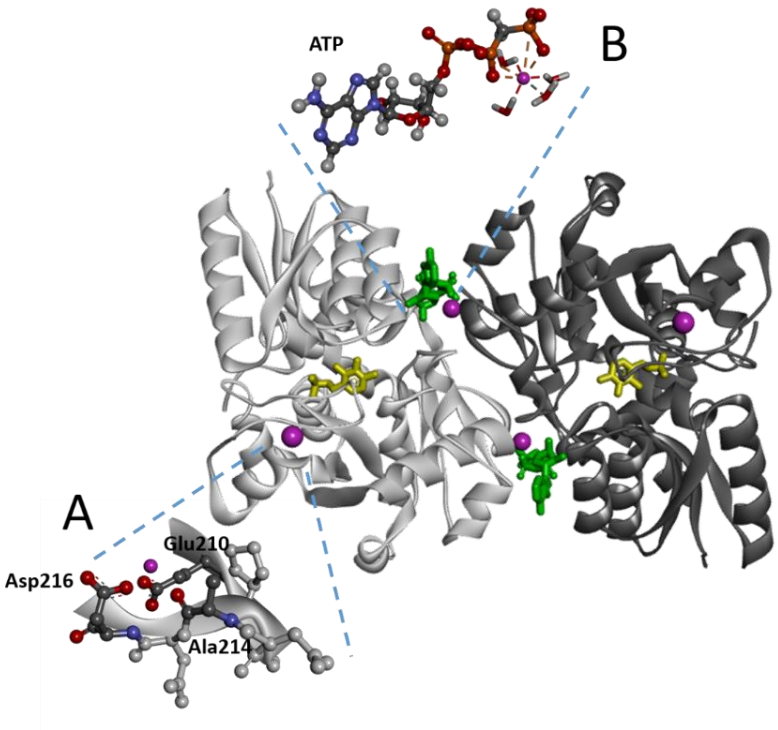

Figure 1.6. Model of human SR indicating the positions of Mg^{2+}, ATP-Mg^{2+} and pyridoxal 5′-phosphate, represented in purple, green and yellow, respectively. The model is based on PDB entry 3L6B, reported as a homodimer, which binds Mg^{2+} at the metal binding site but not ATP. The ATP binding site was approximately defined by overlapping the structure of hSR with that from *Schizosaccharomyces pombe* (PDB 1WTC) in complex with the ATP analog AMP-PCP. Insets: (A) detail of the metal-binding site; (B) details of the ATPMg^{2+} (Ca^{2+}) binding sites

The binding of AMP-PCP to SR changes the relative position of the two subunits, increasing the width of the groove formed by the two monomers (Figure 1.7).

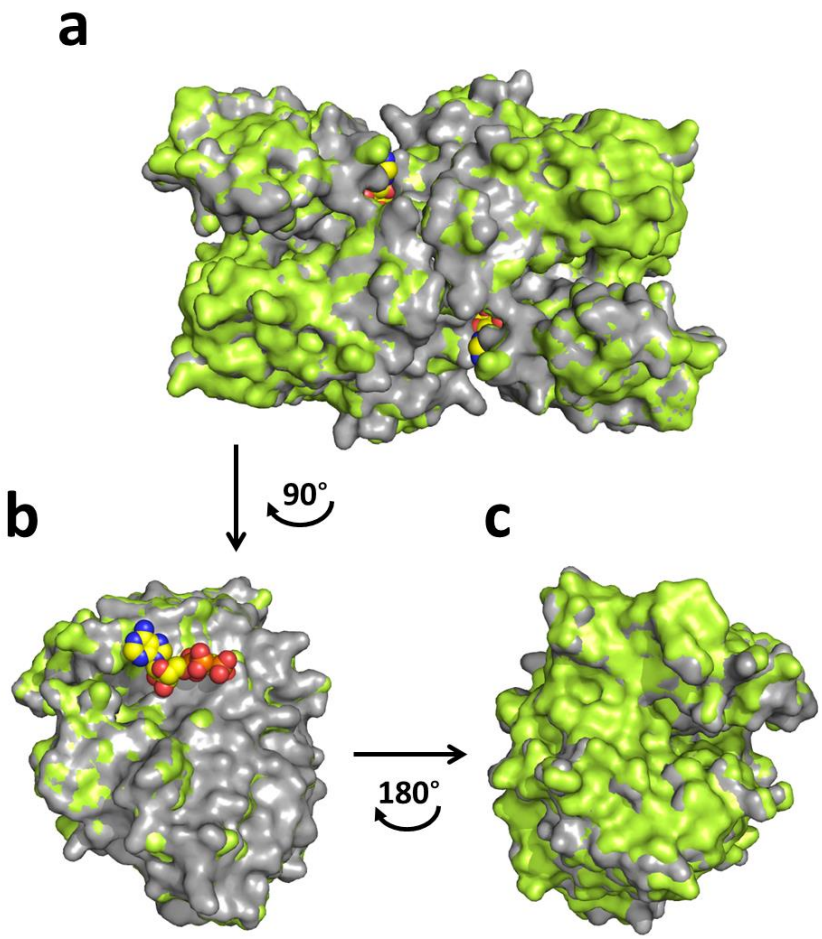

Figure 1.7: Surface representation of spSR in the open form in the presence (PDB 1WTC, grey) and absence (PDB 1V71, light green) of AMP-PCP bound to two symmetric sites at the dimer interface. The superposition of only one monomer is shown **b)** facing the direction of the dimer interface, upon rotation of 90° of the dimer, and **c)** from the opposite side of the subunit, upon rotation of 180° of the monomer, i.e. rotation of the dimer of 90° in the opposite direction. AMC-PCP is in yellow. In **b)**, only the molecule of AMP-PCP bound to the monomer is shown.

Overall, SR exists as an equilibrium of several conformations (Figure 1.8), some of which have been defined crystallographically. Others were inferred from spectrofluorimetric studies (vide infra).

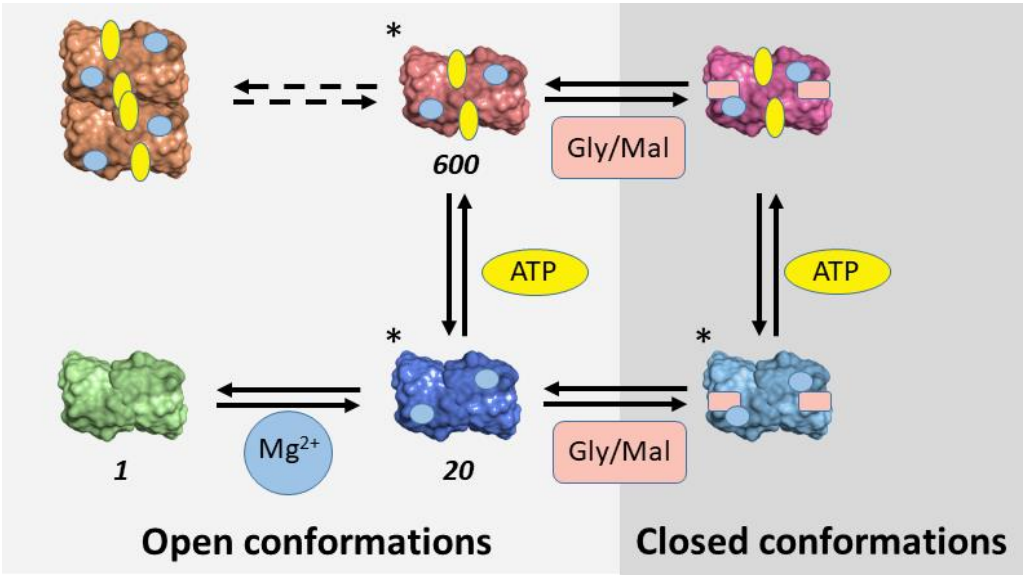

Figure 1.8. General model of the conformational equilibria of SR in the presence of different ligands. The structures marked with * have been reported in crystal structures of either hSR, SpSR or rat SR.

1.3 CATALYSIS

SR catalyses both the racemization and deamination of L- and D-serine. Racemization starts with the formation of an external aldimine and the subsequent extraction of a proton; a quinonoid intermediate is formed, followed by re-protonation from the opposite side of the intermediate. The mechanism of racemization involves specific residues in the active site, depending on the substrates. When L-serine forms the external aldimine with the co-factor, a neutral Lys56 can abstract the alpha proton, bringing the formation of an anionic quinonoid intermediate. When D-serine binds, Lys56 is protonated and positively charged and Ser84 is deprotonated, thus allowing the proton abstraction from the opposite side of the amino acid. Finally, there is reprotonation by either Ser84 or Lys56 and reconstitution of the internal aldimine in the active site (Scheme 1). The abstraction of the proton of D-Ser by Ser84 is strongly dependent on the pKa of this residue. Lys114 has been proposed to increase the acidity of Ser84 through a hydrogen bond involving a water molecule (Nelson et al. 2017).

After the formation of the external aldimmine and the extraction of the alpha proton, the quinonoid negatively charged intermediate can undergo a deamination reaction with formation of the α-aminoacrylate; this unstable intermediate is rapidly hydrolyzed to pyruvate and ammonia, with restoration of the internal aldimmine (Scheme 1).

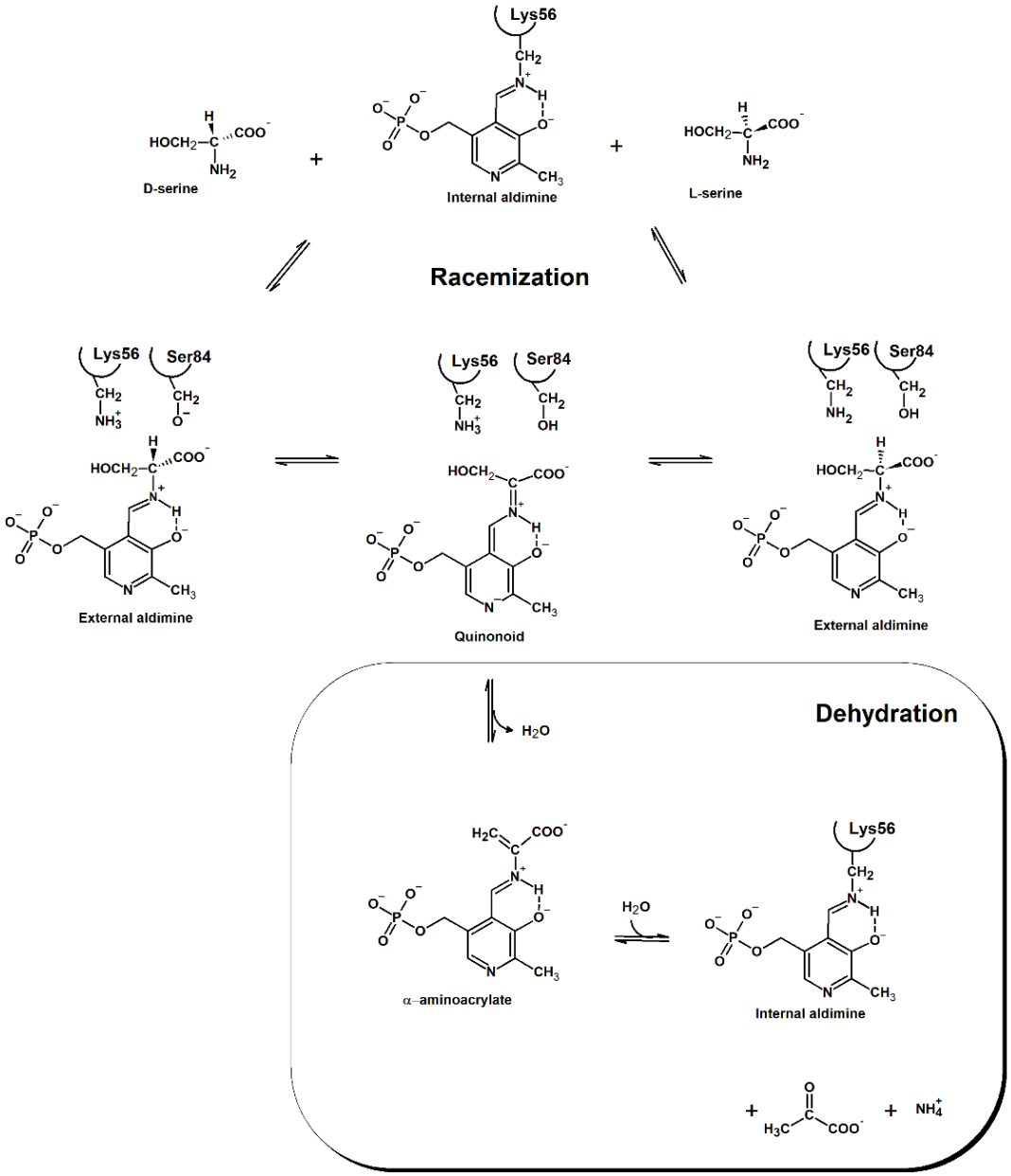

Scheme 1: Catalysis of hSR

Both racemization and deamination are activated, to a different extent, by the positive allosteric effector ATP, with the deamination of L-Ser being much more affected - 31-fold - in catalytic efficiency upon ATP binding (Canosa et al. 2018; de Miranda et al. 2002) (Table 1). As hSR, under physiological conditions, is fully saturated with ATP, the deamination is several times more efficient than the racemization. The efficiency of D-serine synthesis by SR is very low even in the presence of ATP (Table 1), possibly reflecting the low metabolic requirement for this amino acid and the need for a tight modulation of its production. It is also very important to consider the wide interactome of SR, whose effects are still under investigation and could dramatically affect its activity in vivo.

Reaction	**K_M (mM)**		**k_{cat} (min^{-1})**		**k_{cat}/K_M ($s^{-1}\cdot M^{-1}$)**		**Increase**
	-ATP	+ATP	-ATP	+ATP	-ATP	+ATP	
L-Ser racemization	35 ± 5	34 ± 4	19 ± 1	35 ± 1	9.2 ± 1.4	17.5 ± 2.1	1.9
L-Ser deamination	76 ± 10	12 ± 1	37 ± 4	183 ± 3	8.1 ± 1.1	253.0 ± 15.0	31.0
D-Ser deamination	46 ± 3	167 ± 16	1.7 ± 0.1	23 ± 1	0.6 ± 0.1	2.4 ± 0.1	4.0

Table 1. Enzymatic parameters of hSR (Canosa et al. 2018; Marchetti et al. 2013).

Knock-out mice for SR have been used to demonstrate the relevance of SR in the production of D-serine in the brain. In this animal model, the concentration of D-serine is less than 10% in comparison to normal mice (Balu et al. 2013; Labrie et al. 2009). On the other hand, the *in vivo* role of deamination is still discussed, but it was proposed to be relevant for D-serine degradation in brain areas where D-amino acid oxidase is lacking (de Miranda et al. 2002).

Recently, it was demonstrated that mouse SR (mSR) is able to catalyze also the racemization of L-Asp (Ito et al. 2016). The efficiency of SR in D-Asp racemization is 500-fold lower than that of D-Serine production. However, the over-expression of SR in cultivated cells increases the concentration of D-Asp, suggesting another relevant role *in vivo* for this enzyme. Phylogenetic analysis in invertebrates SRs suggests a role as aspartate racemase (Uda et al. 2016).

1.4 REGULATION BY SMALL LIGANDS

1.4.1 ATP

ATP is the most relevant positive modulator of hSR (Table 1). The activation of SR activity by ATP was first observed by Neidle and Dunlop in 2002 (Neidle and Dunlop, 2002) on the murine orthologue. Subsequent experiments demonstrated that SR is also activated by ATP, CTP and GTP in the presence of the divalent cations Ca^{2+} or Mg^{2+}. Although ATP is well known to provide energy through its hydrolysis to ADP or AMP in several enzymatic reactions, the activation of SR by non-hydrolysable ATP analogs (de Miranda et al. 2002; Neidle and Dunlop 2002) demonstrated that ATP acts as a structural co-factor in this case.

The catalytic efficiency of deamination of L-serine is strongly enhanced by ATP (31-fold), with a k_{cat}/K_M of 8.1 ± 1.1 and 253.0 ± 15.0 s^{-1} M^{-1} in the absence and presence of ATP, respectively (Marchetti et al. 2013). Surprisingly, the catalytic efficiency of the deamination of D-serine increases just 4-fold and that of L-serine racemization only two-fold (from 9.2 to 17.5 s^{-1} M^{-1}). Therefore, the net effect of ATP binding is a strong stimulation of L-serine degradation, with an increment from 0.9 to 14.5 of the ratio between deamination and racemization efficiency in the absence and presence of ATP, respectively (Marchetti et al. 2013).

As the intracellular concentration of ATP is in the millimolar range, it was first suggested that hSR is always saturated *in vivo*. *In vitro* studies showed that ATP binds with a strong cooperativity (Hill n close to 2) with K_Ds for the high and low affinity states of 11.5 µM and 200 µM, respectively. These values fall within the physiological range of ATP concentration (Marchetti et al. 2013), suggesting that hSR could be very sensitive to ATP intracellular

fluctuations. ATP binds 15 Å far from the active site, and the two symmetric ATP sites are 24 Å apart. Binding cooperativity was therefore associated to a network involving Thr52, Asn-86, Gln89, Glu283 and Asn316 in hSR (Met53, Gln87, Glu281, Asn311 in SpSR) and two water molecules (Goto et al. 2009) (Canosa et al. 2018); Asn-316 directly binds ATP on the hydroxyl groups of the ribose ring.

The comparison of the K_D for ATP binding to hSR measured through fluorimetric titrations (0.26 ± 0.02 mM) and through activity assays (0.22 ± 0.01 mM, 0.41 ± 0.02 mM and 0.22 ± 0.05 mM for L-serine and D-serine deamination and for L-serine racemization, respectively) it appear clear that that reaction intermediates do not allosterically affect ATP binding site (Marchetti et al. 2013). Moreover, in the presence of ligands of the active site, such as glycine, which forms a stable complex with PLP, ATP binds to hSR in a non-cooperative fashion and with a 50-fold stronger affinity. In the same way, ATP increase the affinity of ligands for the active site which bind covalently (i.e. glycine, 15-fold) or non-covalently (i.e. malonate, 10-fold) (Marchetti et al. 2013) (Marchetti et al. 2015). This mechanism revealed a possible role of glycine in tuning of the glutamatergic neurotransmission, being the alternative co-agonist together with D-serine for the NMDA receptor.

1.4.2 DIVALENT CATIONS

Serine racemase is also activated by divalent metals, particularly calcium and magnesium. *In vivo,* the metal binding site has always been assumed to be occupied by magnesium, because of its intracellular concentration. Deamination and racemization activities in conditions close to the physiological ones (i.e. 1 mM L-serine and 2 mM ATP) revealed a 2.5-fold larger effect of magnesium on the catalytic efficiency in comparison to calcium (Foltyn et al. 2005; Genc et al. 2011; Gribble et al. 2000).

1.4.3 HALIDES

The activity of hSR is also affected by halides (Marchetti et al. 2015), with chloride being the only physiologically relevant one. Chloride act as an 'uncompetitive activator' (Maruyama 1990; Wild et al. 1976), since it influences both k_{cat} and K_M, without altering the catalytic efficiency (Marchetti et al. 2015).

1.4.4 NADH

The reduced form of NADH was found to inhibit SR activity, possibly connecting the modulation of D-serine levels to the glycolytic flux (Suzuki et al. 2015). This topic is a part of my PhD work and will be discussed in details in chapter 1.

1.5 PROTEIN INTERACTORS

Many proteins have been proposed to interact with hSR, especially proteins associated with glutamatergic neurotransmission and the AMPA and NMDA glutamatergic receptors. Particularly, it seems that the C-terminal part of hSR is the most relevant for the interaction of protein partners, as it is capable to interact with PDZ domains (Baumgart et al. 2007).

- **GRIP** (Glutamate Receptor Interacting Protein) induces conformational changes in SR, which increased its enzymatic activity and also enhance D-serine release from glia (Jiraskova-Vanickova et al. 2011).
- **PICK1** (Protein Interacting with C-kinase) is activated by the erythropoietin-producing hepatocellular receptor (Eph) and subsequently released in the cytosol of astrocytes, where it interacts with SR. Specifically, upon Eph receptor activation, PICK1 dissociates from Eph and the interaction with SR is promoted (Kiriyama and Nochi 2016; Zhuang et al. 2010) together with an increase in D-serine synthesis (Fujii et al. 2005; Hanley 2008; Hikida et al. 2008). GRIP and PICK1 both interact with other proteins through a PDZ domain, which is recognized by three residues (-Val-Ser-Val-) at the carboxyl-terminal of SR (Baumgart et al. 2007). The structural basis of the interaction of hSR with PICK1 and GRIP are still unclear, but it seems that they are both dependent on the phosphorylation status of AMPA receptors (Fujii et al. 2005; Wolosker et al. 1999).
- **Stargazin** and **PSD-95 (**postsynaptic density proteins 95), also regulate AMPA receptors (Ma et al. 2014). It has been proposed that SR interact with Stargazin and PSD-95 forming a ternary complex, possibly

affecting SR activity and, therefore, glutamatergic transmission (Ma et al. 2014).

- **Golga-3** is a protein that binds at the cytosolic face of the Golgi apparatus. It stabilizes SR and prevents its ubiquitination (Canu et al. 2014; Dumin et al. 2006b; Fujii et al. 2005; Wolosker et al. 1999).
- **DISC1** (Disrupted in Schizophrenia 1) is the only protein that was proven to be involved in schizophrenia, and it binds SR through its C-terminus portion, preventing its ubiquitination and degradation (Ma et al. 2013).
- **Glyceraldehyde 3-phosphate dehydrogenase** is a glycolytic enzyme and interacts with hSR, inhibiting its enzymatic activity (Suzuki et al. 2015). The inhibitory effect seems also to be dependent on the presence of GAPDH substrate, glyceraldehyde 3-phosphate, which is important for inhibition to take place (Suzuki et al. 2015).

1.6 S-NITROSYLATION

Nitrosylation is an emergent post translational modification (PTM) which consists in the reactivity of nitroso group donors with cysteine residues, through different mechanisms; one of the most relevant endogenous nitroso donors is S-nitroso glutathione (GSNO) with an *in vivo* concentration in the nanomolar range. There are also proteins that known to act as nitrosylases, transferring nitroso groups on cysteine residues of other proteins. Nitrosylation can also take place by direct reaction of nitric oxide with cysteine residues in the presence of molecular oxygen or transition metals, like iron (Anand and Stamler, 2012). Proteins are often nitrosylated on specific cysteine residues, probably reflecting the pKa of the thiol or a higher stabilization by the chemical environment of the cysteine group; some works demonstrate that an acid-base

dyad close to the cysteine residues and hydrophobic interactions are critical for the stabilization of the nitroso thiol to be formed (Anand and Stamler, 2012). S-nitrosylation can induce different biological events, such enzyme regulation, subcellular localization and protein-protein interaction

S-nitrosylation was first characterized in murine SR. Through site-directed mutagenesis, Cys113 was discovered to be the one undergoing S-nitrosylation (Mustafa et al. 2007). Cys113 is close to the ATP binding site and was shown to inhibit the enzyme activity of about 10-fold (Mustafa et al. 2007). This regulation mechanism was proposed to act as a feedback control of NMDA transmission (Mustafa et al. 2007).

Further aspects of S-nitrosylation on the human orthologue are part of my PhD work. They are described in chapters 3 and 4. Some results were published (Marchesani et al. 2018).

1.7 SR INHIBITORS

Increased concentrations of D-serine in the brain are associated with high NMDA receptors activity and high glutamatergic neurotransmission, leading to severe excitotoxicity, as observed in Alzheimer and Parkinson diseases, ischemia and amyotrophic lateral sclerosis. Thus, in the last fifteen years, many drug discovery programs were conducted for the development of active-site inhibitors with potential therapeutic effects (Conti et al. 2011; Jiraskova-Vanickova et al. 2011). From the different drug discovery programs that have been conducted on SR, actually no compound was found with drug-like properties, revealing hSR as a difficult target.

Malonate was identified as the most active compound in a screening of a series of dicarboxylic acids (Strisovsky et al. 2005) (compound **1**, **Scheme 2**) with a K_i of 27 μM for mSR, and 77 and 710 μM for hSR, in the presence and absence of ATP, respectively (Marchetti et al. 2015). In order to improve the affinity, the structure of malonate was modified, leading to 2,2-dichloromalonate, which has a slightly higher affinity, with a K_i of 19.3 μM for mSR (Vorlova et al. 2015). Compounds containing the 3-phenylpropanoic acid moiety (Dixon et al. 2006) or other hydroxamic acids (Hoffman et al. 2009) were also identified to inhibit the activity of SR, but with lower affinity than 2,2-dichloromalonate.

A small library of differentially substituted cyclopropane derivatives was synthetized to mimic malonate. These compounds were docked into hSR structures and tested *in vitro*. The most active compound was dicarboxylic cyclopropane, with a K_i of 0.9 mM (Beato et al. 2015).

Compound **2** was identified by *in silico* screening and *de novo* synthesis (Mori et al. 2014), and further optimized to obtain compound **3**, which exhibits an IC_{50} *in vitro* of 14 μM for mSR and suppresses neuronal over-activation *in vivo* in a mouse model (Mori et al. 2017). Compound **4** has an IC_{50} of 1 mM and was further optimized to yield compound **5,** with an IC_{50} of 0.84 mM (Takahara et al. 2017).

In order to enlarge the chemical space of hSR inhibitors, *in silico* structure-based screening was performed on the human enzyme, using both the open and the closed conformations (Dellafiora et al. 2015). The study unveiled compounds with completely different chemical structures in comparison to reported inhibitors, with K_i values in the low millimolar range (Dellafiora et al. 2015).

The characterization of analogs of NADH, including β-1,4-dihydronicotinamide monucleotide (NMN-red) (compound **6**, Scheme 2) is part of my PhD work and are reported in chapter 2.

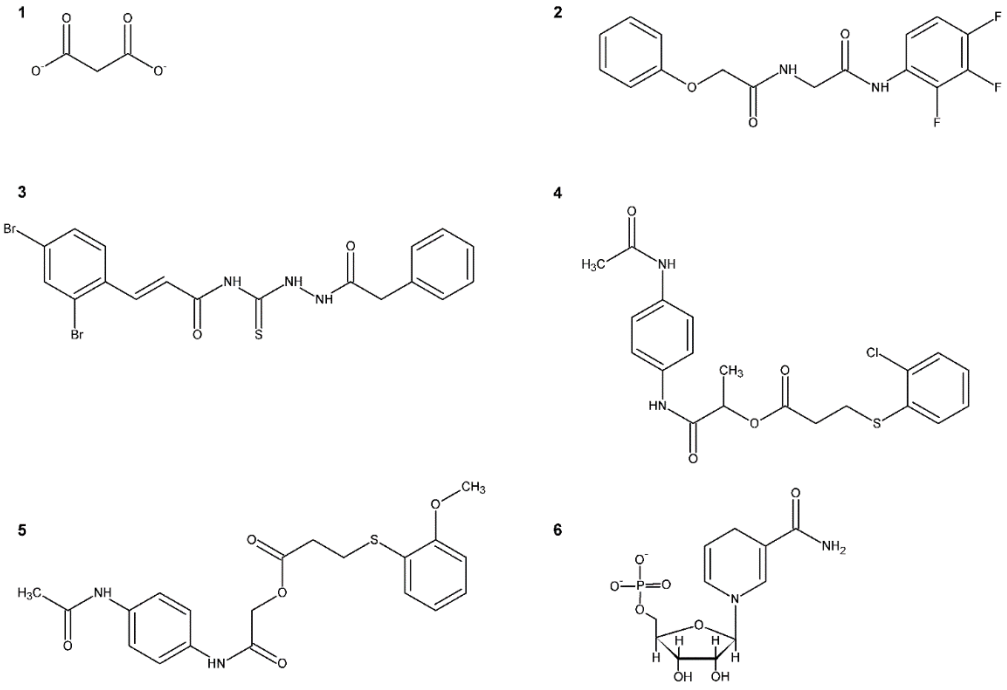

Scheme 2: Examples of SR inhibitors

Chapter 2 - INHIBITION OF hSR BY NADH

As mentioned in the introduction, NADH was found to inhibit SR activity, possibly connecting the modulation of D-serine levels to the glycolytic flux (Suzuki et al. 2015). In the work described herein, NADH was found to exert its effect by allosterically interacting with hSR at a new binding site, close to the one for ATP.

This work was published:

Stefano Bruno, Francesco Marchesani, Luca Dellafiora, Marilena Margiotta, Serena Faggiano, Barbara Campanini, Andrea Mozzarelli; "Human serine racemase is allosterically modulated by NADH and reduced nicotinamide derivatives". Biochemical Journal (2016) DOI: 10.1042/BCJ20160566. Permission for reproduction of the figures and parts of the text was obtained by the publisher.

Candidate's contribution: My contribution consisted in the full characterization of the inhibitory effect and the mechanism of action of NADH.

2.1. MATERIALS AND METHODS

Materials

Chemicals were of the best commercial quality available and were purchased from Sigma-Aldrich (St. Louis, MO, USA), with the exception of tris(2-carboxyethyl)phosphine (TCEP), from Apollo Scientific (Bredbury, UK), $NADP^+$ and NADPH, from Boehringer Ingelheim and 1-methyl-1,4-dihydronicotinamide (MNA-red) from Toronto Research Chemicals (Toronto, Canada). Recombinant D-amino acid oxidase (DAAO) from *Rhodotorula gracilis* was a generous gift from Professor L. Pollegioni, University of Insubria, Varese, Italy. Porcine DAAO was acquired from Sigma Aldrich.

Protein expression

The following protocol was followed:

- BL21 (DE3) cells co-transformed with pET28(b) plasmid containing the gene encoding for human serine racemase (pET28(b)_hSR) and TAKARA2 plasmid, which allow for the expression of chaperonins GroEL and GroES, were cultured in 5 ml of LB medium at 37 C° under shaking for six hours. The co-expression of hSR in the presence of chaperonins, allow for a higher yield of purification of the enzyme in a soluble form. pET28(b)_hSR and TAKARA 2 allow for resistance from kanamycin and chloramphenicol respectively; antibiotics were added to overcome contamination.

- One ml of the culture was added in three flask containing 100 ml of LB medium plus the same antibiotics and cultured overnight at 37 °C under shaking
- 100 ml of the overnight culture were added in three flask containing 1l of LB medium in the presence of antibiotics. Cell were cultured for 4-5 hours, until an optical density at 600 nm of about 0.5 was reached.
- Arabinose and benzylic alcohol were added at final concentration of 0.3 mg/ml and 1 ml/l respectively. Arabinose induced the expression of the chaperonins GroEL and GroES, benzylic alcohol induces the expression of endogenous chaperonins in bacteria.
- After 20 minutes Isopropyl β-D-1-thiogalactopyranoside (IPTG) at the final concentrations of 0.05 mM was added to induce the expression of hSR. IPTG is a stable analog of lactose, which induces the expression of proteins under the control of the *lac* operon. The culture is incubated at 20 °C overnight
- The morning after the cells are harvested and extensively washed with phosphate buffered saline (PBS)
- The obtained pellet is store at -80 °

Protein purification

The following protocol was followed:

- Cells were re-suspended in 50 ml of lysis buffer (50 mM Na_2HPO_4, 150 mM NaCl, 5 mM TCEP, 50 μM PLP, 0.2 mM PMSF, 0.2 mM benzamidine, 1.5 μM pepstatin A at pH 8.0 at 4 °C)
- Lysozyme was added at a final concentration of 1 mg/ml and incubated at 4 °C under shaking. Lysozyme was used to broke the cell membrane.

- Five cycles of sonication were performed to completely break cells. The release of cytosolic extract from cells is detected spectrophotometrically
- Cells were harvested to separate the non-soluble fraction from the soluble one
- The soluble part was loaded in to a TALON® His-Tag Purification Resin (Clontech, CA, USA) and incubated under shaking at 4 °C for one hour. The resin consists in a functionalized sepharose with Cobalt ion, which are able to specifically interact with a poly-histidine tag linked to the recombinant protein.
- After one hour the crude lysate was eluted from the resin and collected in a tube. The resin was washed several times with 150 to 200 ml of wash buffer (50 mM Na_2HPO_4, 300 mM NaCl, 5 mM imidazole, pH 8.0 at 4°C). The presence of 5 mM imidazole allowed for the removal of the aspecific binding of histidine rich proteins in the crude extract.
- hSR was eluted by adding 10 ml of elution buffer (50 mM Na_2HPO_4, 300 mM NaCl, 250mM imidazole, pH 8.0 at 4°C). The higher concentration of imidazole allows for the elution of the target recombinant protein.
- hSR was then concentrated through diafiltration and desalted in 50 mM TEA pH 8 with a HiTrap Desalting (Sephadex G-25)
- The protein was then stored in small aliquots at -80 °C.

hSR deamination activity assay

The deamination assay is a continuous assay coupled with enzyme lactate dehydrogenase (LDH). Pyruvate produced by SR reacts with a molecule of NADH producing NAD^+ and lactate. NADH has a characteristic absorption peak at 340 nm while its oxidized form does not absorb at this wavelength. The

reaction can then be monitored by evaluating the absorption reduction at 340 nm, which allows us to estimate the reaction rate.

- A 4X master solution was prepared containing the fixed components of the assay (200 mM TEA, 150 mM NaCl, 200 mM PLP, 20 mM DTT)
- At the 4X solution, ATP, MgCl2 or L-Ser were then added at a double concentration to the final one present in the assay, obtaining a 2X master solution
- The various components of the assay excluding SR were added to the cuvette; A quartz shielded cuvette with 1 cm of optical length was used; The total volume of the assay is 150 µl, the assay was conducted at 37 ° C. In some case a cuvette with shorter optical length was used to obtain the right signal to noise signal (l = 0.2 cm or 0.1 cm).
- After carefully mixing the solution, the cuvette was incubated for 2 minutes inside the thermostated cuvette holder at 37 ° C.
- Once the reading at 340 nm was started, a trace of 1 - 2 minutes was recorded in the absence of protein. The slope of this trace reflected the contribution of a possible auto-oxidation of NADH
- At this point the protein was added and the solution was carefully mixed;
- Once the kinetic started, it was expected about the fourth minute before recording the slope; the speed was calculated on one minute of track, dividing the ΔOD / min for the molar coeffcient of NADH (6200 M^{-1} cm^{-1}), taking into account the optical length.

hSR racemization activity assay

- A 2M L-Ser solution was prepared in MilliQ water and the pH was adjusted to 8.5 so that it was compatible with the enzymes that will be used later.
- D-amino acid oxidase from Rhodotorula gracilis (rgDAAO), catalase and Flavin adenine dinucleotide (FAD) were added in catalytic quantities.
  - DAAO: 15 µl rg-DAAO 0.4 U / µl
  - CATALASE: 2 µl Catalase 106 U / ml
  - FAD: 6 µl FAD 100 µM
- The solution was incubated at 37 ° C and followed for 72h. Twice a day (morning and evening), enzymes and cofactors were refreshed.
- At the end of the process 3 cycles of boiling and centrifugation of 15 minutes were carried out to block the reaction and eliminate the enzymes in solution. The solution is aliquoted.
- Twenty µl of 200 mM phosphoric acid was seeded into the wells of a 96 well-plate
- The reaction mixtures were prepared in tubes. Reactions took place in a buffered solution containing 50 mM TEA, 2 mM ATP, 2 mM MgCl2 and 150 mM NaCl pH 8; other components are added depending from the experiments.
- The reactions started after the addition of hSR at a final concentration of 1.5 µM.
- During time 20 µl of reaction mixtures was withdrawn and put into the wells containing phosphoric acid to stop the reaction.
- The pH of the reaction mixtures was then adjusted to a more alkaline one adding 5 µl of 10 M NaOH, in order to allow for the enzymatic detection to take place.
- The detection solution was then added to every well and incubated at 37 °C for one hour. The detection solution was composed by 100 mM

$Na_4O_7P_2$, 1 mM O-Dianisidine, 2 μM FAD, 2 U of horseradish peroxidase (HRP) and 0.04 U of rgDAAO. DAAO is responsible for the conversion of D-Serine in 3-OH pyruvate, NH_3 and H_2O_2; HRP catalyze the colorimetric redox reaction between the H_2O_2 produced by DAAO and an electrons acceptor which is o-Dianisidine.

- The reaction catalyzed by HRP produced oxidized o-dianisidine, which can be quantified by measuring its absorption at 550 nm after acidification with H_2SO_4. The acidic pH leads to a change in color from brown to pink, which allow a better detection of the product. The amount of oxidized o-dianisidine is proportional to the amount of D-serine produced in each sample collected during the racemization reaction. An accurate quantification of the product was carried out by building a calibration curve using pure D-serine as substrate for DAAO.

Inhibition assays

The inhibitory effect on hSR deamination or racemization activities by different compounds was first evaluated at 2 mM concentration. For compounds showing activity, the IC_{50} was determined through deamination assays at different concentrations. The potential effect of each compound to modulate the activity of the coupled enzymes (i.e. LDH, DAAO or HPR) was evaluated in the presence of their own substrates (i.e. pyruvate, D-serine and H_2O_2).

Preparation of 1-methyl-1,4-dihydronicotinamide and 1,4-dihydronicotinamide mononucleotide

The reduced form of NMN **(**NMN-red) was prepared starting from the oxidized derivative NMN-ox (Sigma-Aldrich) by reduction with stoichiometric sodium dithionite under deoxygenated conditions (Blankenhorn

and Moore 1980)(Figure 2.1.1). The product was then purified by desalting in an acetone:water mixture, dryed in SpeedVac™ (Thermo Scientific™) and resuspended in a 50% DMSO:water solution. The obtaining of the desired product was confirmed by 1H NMR spectra recorded on a Bruker 400 MHz spectrometer in 20 mM Na2HPO4 buffer, pH 8.0 (10% D2O), by the presence of a peak at 7.07 ppm, typical of the protons of the 1,4 di-hydro nicotinamidic. The concentration of the reduced species was spectrophotometrically determined based on the reported extinction coefficients at 340 nm (Blankenhorn and Moore 1980).

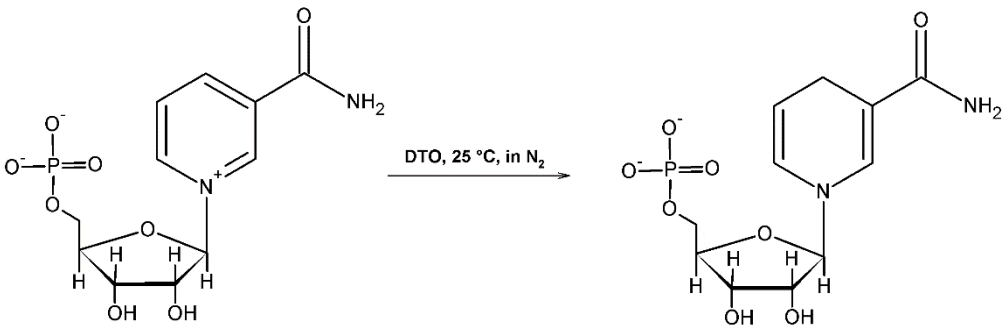

Figure 2.1.1. Preparation of NMN-red starting from NMN-ox with sodium dithionite (DTO)

Molecular Modelling

The work related to molecular modelling for the identification of the binding site for NADH and its analogs was performed in collaboration with Luca Dellafiora, PhD, from the Department of Food Science, University of Parma, Parma, Italy (now Department of Food and Drug).

2.2 RESULTS AND DISCUSSION

Effect of NADH and NADPH

The effect of NADH, NAD^+, NADPH and $NADP^+$ on hSR racemization and deamination activities was tested in a buffered solution containing 50 mM TEA, 150 mM NaCl, 50 mM PLP, 5 mM DTT, 50 mM L-serine, 2 mM ATP, 2 mM $MgCl_2$ and 2 mM of each compound (Figure 2.2.1). The effect on racemization and deamination of NADH and NADPH is an inhibition of about 50% and 36% respectively. A different incubation time of hSR with NADH or the presence of reducing agents as TCEP or DTT, do not alter the inhibition brought by the dinucleotides. The oxidized forms NAD^+ and $NADP^+$ at the same concentration do not exhibit any effect, possibly reflecting the importance of the redox state of nicotinamidic ring for the inhibition to take place.

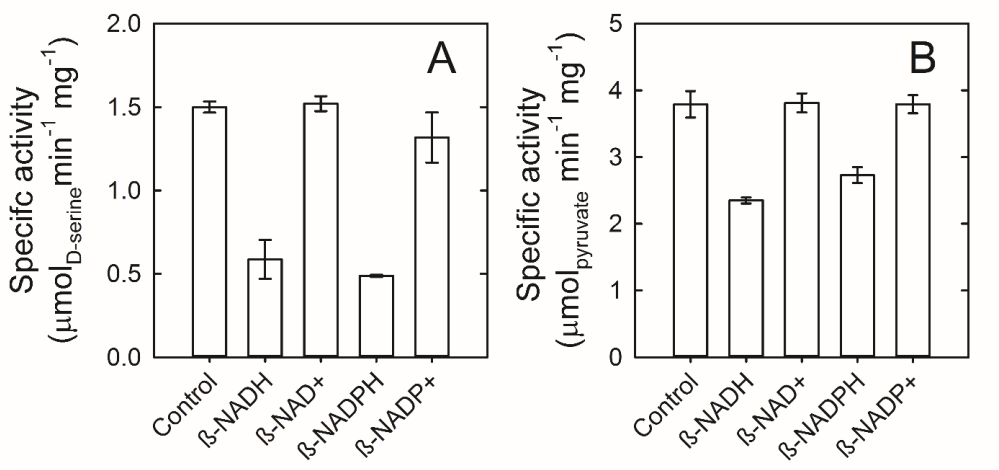

Figure 2.2.1. Inhibition by NADH and NAPDH. (A) Effect of NADH, NAD^+, NADPH and $NADP^+$ on L-serine racemization activity. (B) Effect of NADH, NAD^+, NADPH and $NADP^+$ on the L-serine deamination reaction. All compounds were tested at 2 mM. The error bars are the s.e.m. of two replicates.

NADH and ATP are structurally very similar, suggesting a competition for the same binding site. The ATP binding properties to hSR in the presence of 2 mM NADH changed significantly. The dissociation constant increased from 168±12 to 370±30 μM, and the cooperativity is completely lost (Figure 2.2.2a).

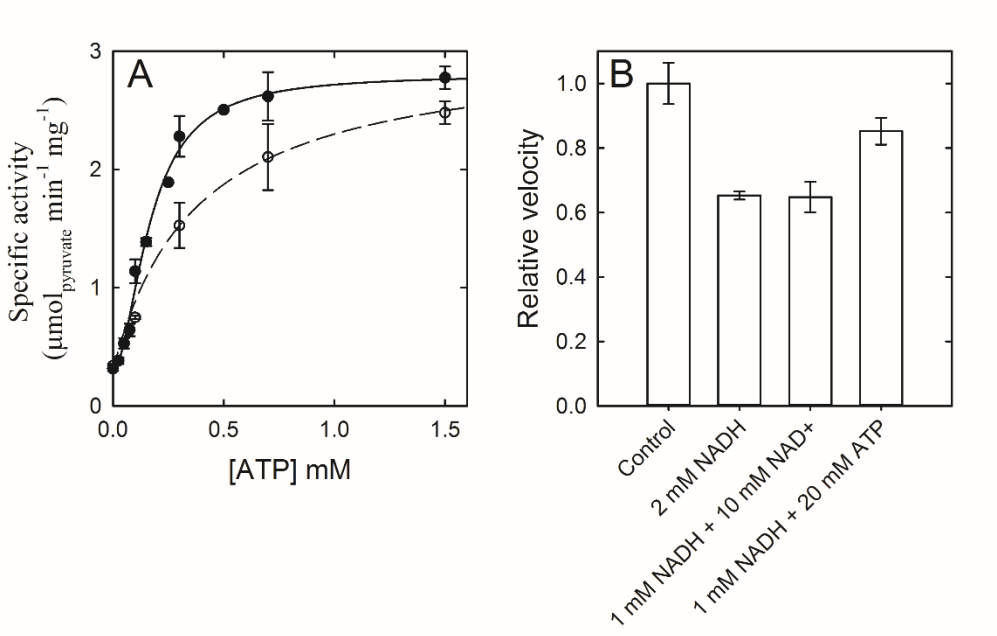

Figure 2.2.2. Competition of NADH with ATP and NAD^+. (A) Dependence of hSR activity on ATP concentration in the absence (closed circles) and presence of 2 mM NADH (open circles). The solid line is the fitting to a Hill equation; The dashed line is the fitting to a binding isotherm. The alternative fitting with the Hill equation shows no cooperativity (Hill coefficient of 1.1 ± 0.1). (B) Comparison between the activity of untreated hsr with the residual activity of hSR in the presence of 2 mM NADH, 1 mM NADH plus an excess of NAD+ and 1 mM NADH plus an excess of ATP. Error bars are means of two replicates ± s.e.m.

However, the effect of NADH in the presence of a 20-fold excess of ATP brings about only a partial restoration of the enzyme activity (Figure 2.2.2b), suggesting only a partial displacement of NADH.

Identification of the inhibitory determinants of nadh and mechanism of inhibition

The molecule of NADH was dissected to understand what are the main structural features that bring about the inhibition of SR. The 1-methyl-1,4-dihydronicotinamide (MNA-red), 1,4-dihydronicotinamide mononucleotide (NMN-red), their oxidized forms 1-methylnicotinamide (MNA-ox) and β-nicotinamide monucleotide (NMN-ox), the fully reduced form of MNA-ox–1-methyl 3-piperidinecarboxamide (MPCA) (Scheme 1), adenosine diphosphate (ADP) and sodium pyrophosphate were tested at 2 mM concentration using the deamination assay (Figure 2.2.3). ADP did not bring about any inhibition, as already observed (De Miranda et al. 2002). Pyrophosphate led to an inhibition of around 60%, which has been associated to Mg^{2+} chelation (Marchetti et al. 2015); moreover, the inhibitory effect of pyrophosphate is completely abolished by adding an excess of Mg^{2+} (Figure 2.2.4).

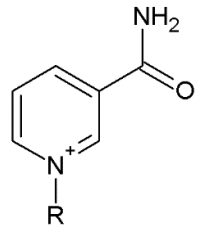

R= -Rib-P-P-Ade (NAD^+)

R= -Rib-P-P-Ade-P ($NADP^+$)

R= -Rib-P (NMN-ox)

R= $-CH_3$ (MNA-ox)

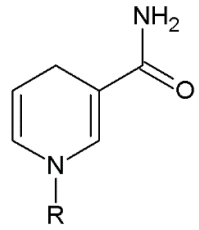

R= -Rib-P-P-Ade (NADH)

R= -Rib-P-P-Ade-P (NADPH)

R= -Rib-P (NMN-red)

R= $-CH_3$ (MNA-red)

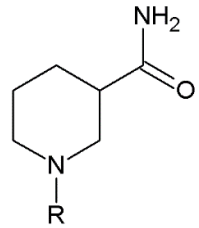

R= $-CH_3$ (MPCA)

Scheme 1

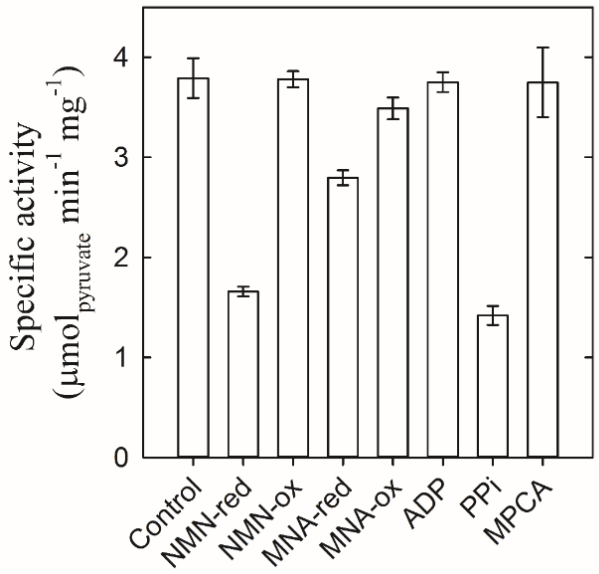

Figure 2.2.3. Inhibition by NADH fragments on the demination activity. Compounds were tested at 2 mM concentration. Error bars are means of two replicates ± s.e.m.

The dependence of the activity of hSR on the concentration of sodium pyrophosphate was biphasic (Figure 2.2.4), possibly reflecting the chelation of Mg^{2+} from both the ATP-Mg2+ complex and the Mg^{2+} bound to the divalent cations binding site. MNA-red and NMN-red and inhibited hSR by 25% and 46% respectively (Figure 2.2.3). The analysis of the results clearly claims that the inhibition is related to the N-substituted 1,4-dihydronicotinic ring. The redox state of the 1,4-dihydronicotinic ring is crucial, as a matter of fact, neither the oxidized forms (NAD+, NADP+, NMN-ox and MNA-ox) nor the fully reduced piperidinic form (MPCA) showed any effect on enzyme activity. The redox forms of the nicotinamidic ring differ both in net charge and conformation, giving indications on the binding properties of the Nam pocket.

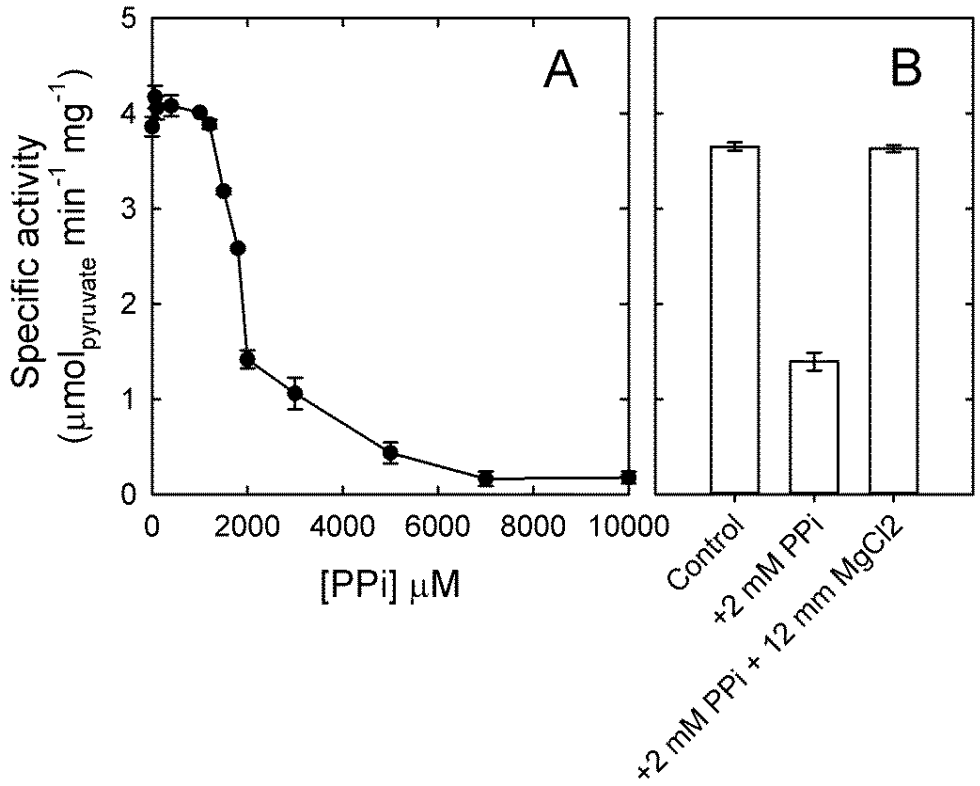

Figure 2.2.4. (A) Inhibition of hSR deamination activity by pyrophosphate (PPi). The error bars are the s.e.m. of two replicates. (B) deamination activity of hSR in the presence of 2 mM pyrophosphate (PPi) and in the presence of 2 mM PPi and 12 mM MgCl2. Each error bar is the s.e.m. of two replicates.

For the identification of the binding site for NADH, MNA-red and NMN-red by molecular docking, both the malonate-bound and -unbound dimeric structures of hSR were investigated by Luca Dellafiora. The highest docking scores for all compounds were close the ATP binding site, at the dimeric interface. NADH and NADPH partially occupied the ATP binding site, with a good overlapping for the P-P-Ade moiety with that of ATP, the

binding of which was crystallographically defined using the stable analogue 5-adenylyl methylenediphosphonate (Goto et al. 2009) (Figure 2.2.5).

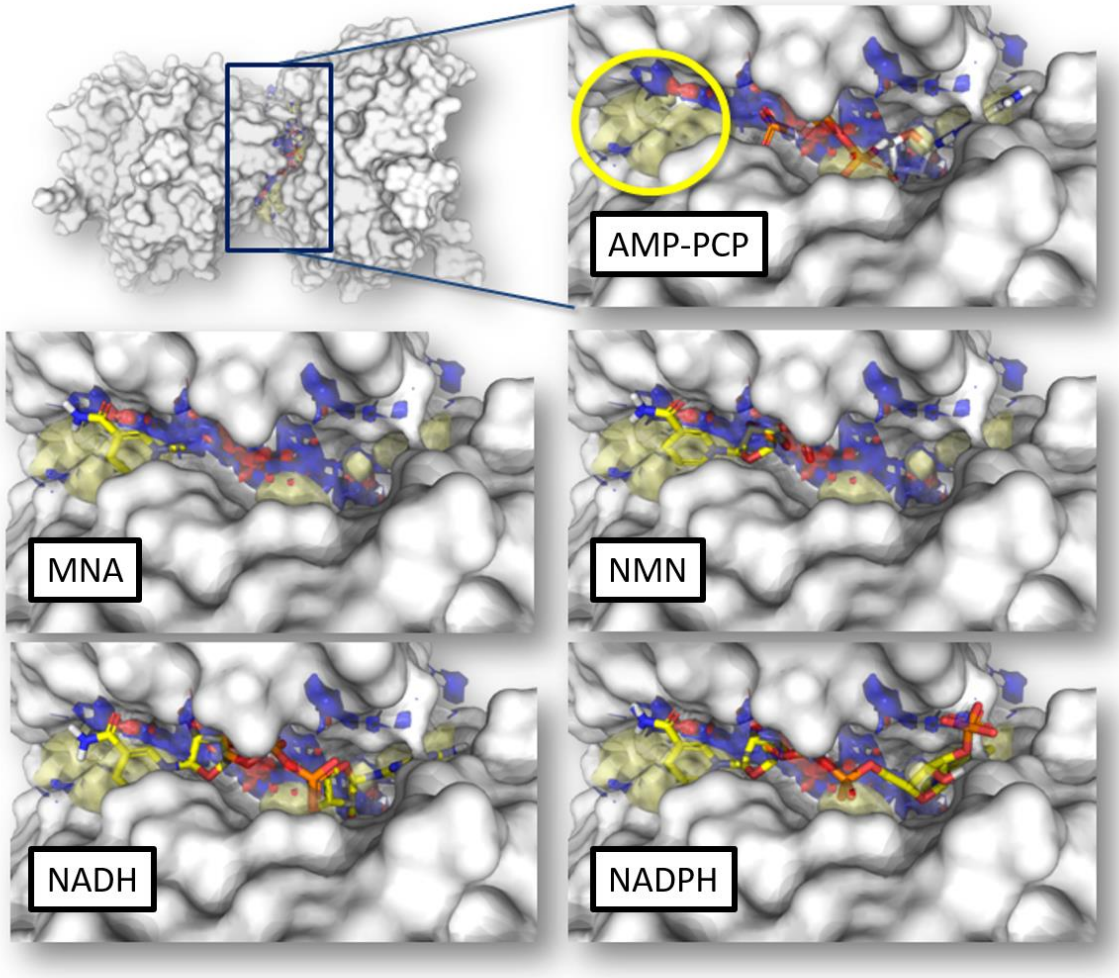

Figure 2.2.5. Binding poses of the ATP analog 5′-adenylyl methylenediphosphonate (AMP-PCP), MNA, MNM, NADH, and NADPH. In yellow, red and blue are represented protein regions energetically favorable for undergoing hydrophobic interactions, act as H-bond acceptor and H-bond donor, respectively. The yellow circle points out the unoccupied hydrophobic cleft next to the ATP binding site, where the nicotinic ring is positioned. The pose for AMP-PCP was obtained by overlapping the structure of *Schizosaccharomyces pombe* SR-AMP-PCP complex with that of hSR.

The nicotinamidic moiety of all compounds positioned itself into an unoccupied hydrophobic site next to that of ATP, which is the binding pocket for MNA-red and NMN-red (Figure 2.2.5). For NADH, NADPH and NMN-red further bonds are formed with the ribose ring (Met278, Arg277) and the phosphate group (Ser32, Ile33) (Figure 2.2.6). In the Nam pocket, hydrophobic residues, such as Leu29 and Phe49 were found, possibly explaining the selectivity towards the reduced Nam derivatives and the loss of inhibitory effect for the oxidized forms. Indeed, the oxidized forms are positively charged, preventing the hydrophobic interactions between ligand and protein (Figure 2.2.6).

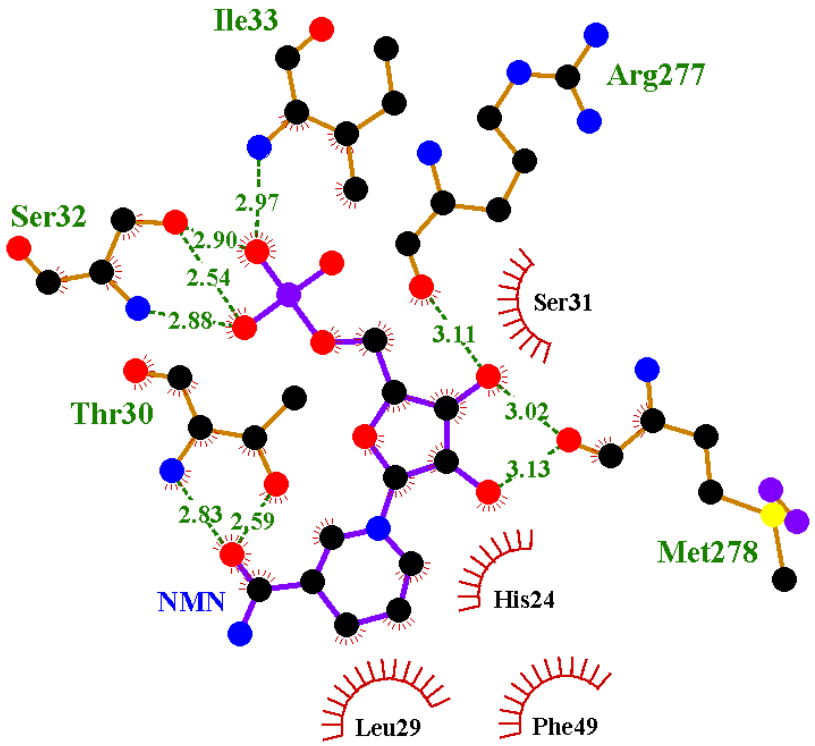

Figure 2.2.6. Interaction pattern of NMN-red in the Nam binding site.

The partial superimposition of the ATP binding site with the NADH-, NADPH- and NMN-red-binding sites (Figure 2.2.5), might explain the observed competition of NADH with ATP (Figure 2.2.2a). However, MNA-red was still active as inhibitors, binding different site from that of ATP. Besides, we observed a partial competition between NADH and ATP, with ATP incapable of restoring full activity also in a large molar excess (Figure 2.2.2b). All these findings suggest that the inhibitory effect of NADH is a complex mechanism, which involves the competition with ATP and the interaction at the Nam binding pocket.

Understanding the mechanism of action of NADH analogs

The dependence of the initial rate of the hSR deamination activity in the presence increasing concentrations of NADH, NMA-red and NMN-red was determined at 50 mM L-serine and 2 mM ATP – Mg^{2+} (Figure 2.2.7). All compounds act as partial inhibitors with different residual activities at saturating concentrations. The resulting IC50 values were 246 ±63μM for NADH, 177±63μM for MNA-red and 51±15 μM for NMN-red.

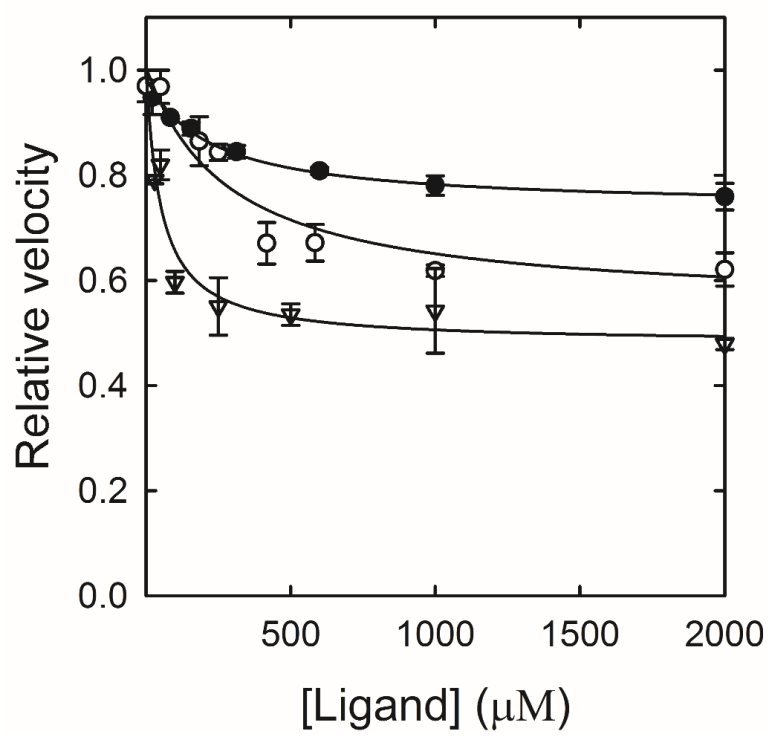

Figure 2.2.7. Determinations of the IC50 for NADH (open circles), NMN-red (closed circles) and MNA-red (closed triangles). The solid lines are the fitting to a binding isotherm. Error bars are the s.e.m. of two replicates.

The maximum inhibition was 36% for NADH, 25% for MNA-red and 47% for NMN-red. However, in the absence of ATP, NADH was still able to inhibits hSR by 30%, (Figure 2.2.8), suggesting not only a competition with ATP, but also an ATP-independent allosteric inhibition of hSR.

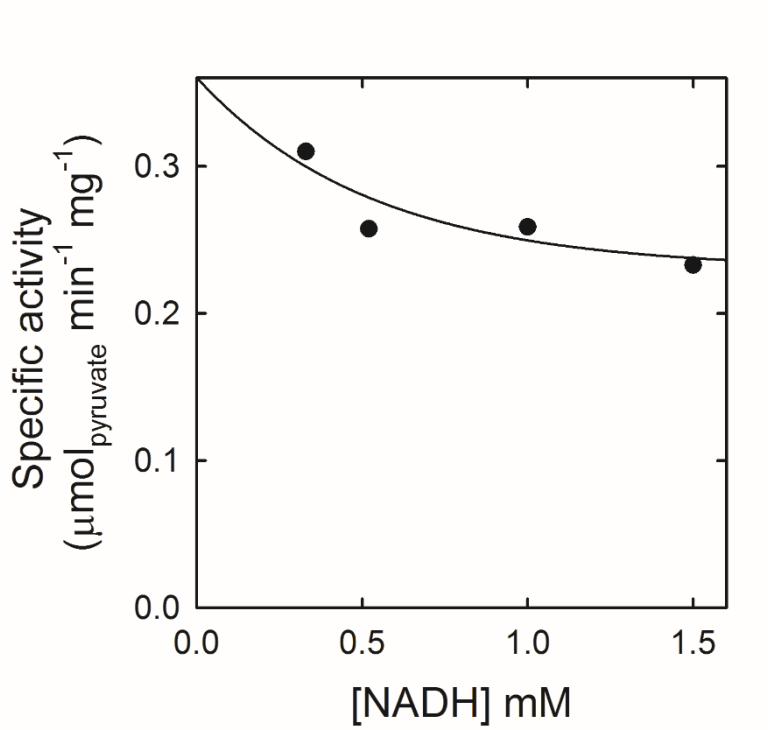

Figure 2.2.8. Inhibition of NADH in the absence of ATP. In this experiment, the concentration of hSR is 10-fold higher in comparison to the other deamination assays. The solid lines are the fitting to a binding isotherm.

The inhibition constant (KI) for the most active compound, NMN-red was estimated using the deamination assay. The initial rate of the deamination activity was measured in the presence of L-serine concentrations ranging from 5 to 200 mM in the presence of different concentrations of NMN-red (Figure 2.2.9). Experimental data points were then fitted to equation 1 — which describes a hyperbolic mixed-type inhibition — obtaining the following

parameters: KI =18±7μM, K_M =14±3 mM, kcat=166±11 min−1, α=5±2 and β=0.8±0.1. KM and kcat are very similar to those measured in a previous work (Marchetti et al. 2013). The KI calculated for NMN-red is comparable with that of 2,2-dichloromalonate, the most potent inhibitor identified so far (Vorlova et al. 2015). Moreover, an α-value higher than 1 indicated that NMN binds with higher affinity to the free enzyme in comparison with the enzyme-substrate (ES) complex. The non-zero value of the β-coefficient indicated that NMN-red acts as a partial inhibitor. Partial inhibition takes place when the enzyme-inhibitor–substrate complex still remains catalytically active, although at a reduced rate in comparison to the ES complex (Copeland 2000).

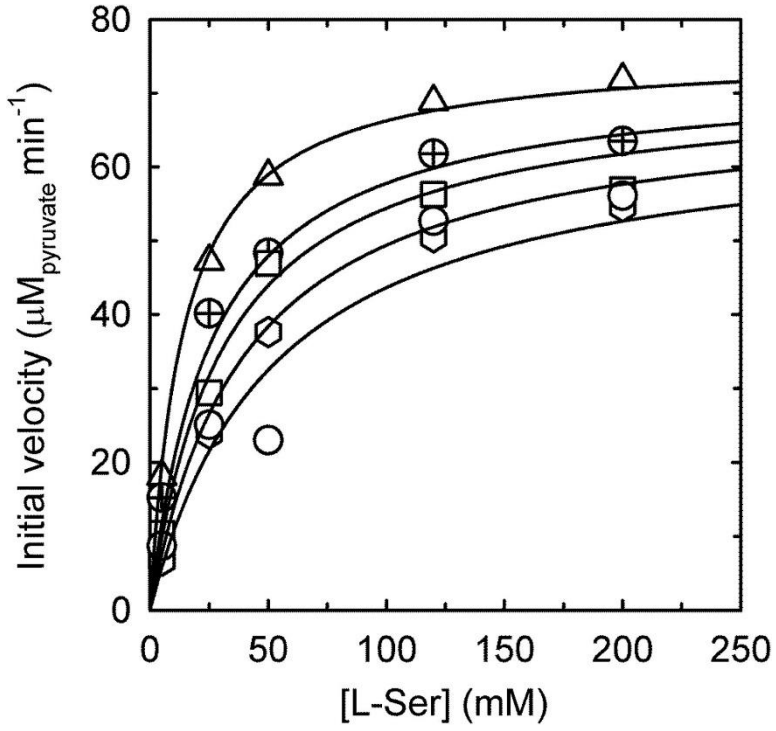

Figure 2.2.9. Dependence of the initial velocity of hSR on L-serine concentration in the absence of NMN-red (triangles), and presence of 24 (crossed circles), 40 (squares), 120 (diamonds) and 400 μM (circles) NMN-red. The solid lines represent the global fitting to equation 1.

Equation 1:

$$v = \frac{V_{max}\frac{[S]}{K_M} + \beta V_{max}\frac{[S][I]}{\alpha K_M K_I}}{1 + \frac{[S]}{K_M} + \frac{[I]}{K_I} + \frac{[S][I]}{\alpha K_M K_I}}$$

The deamination assays reported in the literature for SR are based on a coupled assay involving the conversion of pyruvate to lactate by LDH, in the presence of its co-substrate NADH. For a NADH concentration of 200–300 μM, as reported in the original protocols (Foltyn et al. 2005), a partial inhibition of hSR could be observed, suggesting that experimental biases have to be taken into account.

Inside cells, NAD+/NADH species concentration is estimated at around 300 μM and the ratio between them is strongly shifted towards the oxidized form of about 700-fold (Ying 2008). Considering the partial inhibition carried out by NADH and the relatively low potency, it appears that NADH could not have a role in hSR modulation under physiological conditions. NADPH is the prevalent form in comparison to NADP+, but its intracellular concentration is much lower than NADH. NMN is an intermediate of the NADH biosynthesis and its intracellular concentration is usually very low (Magni et al. 2004). Nevertheless, the cytosolic concentration of NMN was recently shown to increase to micromolar range after nerve injury, promoting axon degeneration (Di Stefano et al. 2015). These findings suggested NMN to be involved in hSR modulation during response to nerve injury.

Chapter 3 - CHARACTERIZATION OF THE OLIGOMERIC STATE OF hSR

In this work, the oligomeric state of hSR will be discussed in detail. Serine racemase has a wide interactome, which can affect not only its tertiary conformation, but also its quaternary state; here I report the discovery of dimer-tetramer equilibrium in hSR, which is affected by the presence of allosteric effectors and ions.

Part of this work was published on:

Stefano Bruno, Marilena Margiotta, Francesco Marchesani, Gianluca Paredi, Valentina Orlandi, Serena Faggiano, Luca Ronda, Barbara Campanini, Andrea Mozzarelli, Magnesium and Calcium ions differentially affect human serine racemase activity and modulate its quaternary state toward a tetrameric form", BBA – Protein and Proteomics (2016). DOI: 10.1016/j.bbapap.2017.01.001. Some of the parts reported in this thesis are from the reported manuscript as per authorization of the publisher.

Candidate's contribution: My contributions in the published work consisted in the gel filtration experiments on a HPLC system to measure the apparent molecular weight of hSR in different conditions.

3.1 MATERIALS AND METHODS

Materials

Chemicals were of the best commercial quality available and were purchased from Sigma-Aldrich (St. Louis, MO, USA), with the exception of tris(2-carboxyethyl) phosphine (TCEP), from Apollo Scientific. The plasmid for His-tagged TEV protease expression and the plasmid containing His-tagged thioredoxin were both generously provided by Professor Christopher S. Hayes, UC Santa Barbara, Santa Barbara, CA, USA.

Enzyme preparation

To remove the polyhistidine tag, a potential metal chelator, the gene encoding for hSR in a pET-28-derived plasmid (Marchetti et al. 2013) was amplified by PCR using the primers 5'-TTTGGATCCGAGAATCTATATTTTCAATCTGGTACTTGTGCTCAGTACTGCATCTC-3' and 5'-CCCCTCGAGCTAAACAGAAACAGACTGATAGGAAGCTGGCC-3'. The construct was subcloned into a pET21b-derived expression vector, generously provided by Professor Christopher S. Hayes, MCDB, University of California, Santa Barbara (Koskiniemi et al. 2014; Ruhe and Hayes 2010), in frame with the gene encoding for His-tagged thioredoxin. The expression vector contains a site for the TEV protease (Miladi et al. 2012) at the N-terminus for trxA-tag removal. The fusion protein was expressed in BL21 (DE3)-RIL cells, which were lysed by lysozyme incubation (45 minutes at 4°C), followed by sonication in a buffer containing 50 mM Na2HPO4, 150 mM NaCl, 4 mM TCEP, 50 μM PLP, 0.2 mM PMSF, 0.2 mM benzamidine, 1.5 μM pepstatine, pH 8.0. The fusion protein was purified using a TALON®

Resin (Clontech, CA, USA) and incubated with His-tagged-TEV protease (60 µg per mg of protein) for 3 hours at 4 °C to remove the His-tagged thioredoxin fragment. After dialysis to remove imidazole, the uncleaved protein and the His-tagged TEV protease were removed by further incubation with the TALON® matrix. The cleaved protein was supplemented of 400 µM EDTA to remove all residual metal ions from the Co2+ resin that could promote protein precipitation (Marchetti et al. 2015) and then extensively dialyzed into a buffer containing 50 mM TEA, 150 mM NaCl, at pH 8.0. Finally, hSR was concentrated to 33.6 µM and flash-frozen in 20 µl aliquots.

Gel filtration analysis

10 µl aliquots of 15 µM hSR solutions were loaded onto a Superdex 200 increase 3.2/300 column (GE Healthcare) mounted on a Prominence HPLC system (Shimadzu). Aliquots at higher (100 µM) or lower (5 µM) concentrations were also used in some experiments to evaluate the effect of protein concentration on the quaternary equilibria. The column was equilibrated and developed with 50 mM TEA-buffered solutions and 5 mM DTT in the presence – in different combinations as specified for each experiment – of NaCl in the 0-150 mM concentration range, 5 mM EDTA, 2 mM MgCl2, 2 mM CaCl2, 2 mM mM ATP, at pH 8.0. Solutions not containing NaCl were used because low ionic strengths enhance the quaternary effects of ligands. Calibration curves in the absence of NaCl were carried out to avoid bias assciated to the interaction of proteins with the matrix. No differences were observed. The hSR samples were preincubated with the same solution for 5 minutes before loading. The UV-vis detector was set at 412 nm – the absorption maximum of PLP bound as internal aldimine to hSR – to avoid interference with ATP, which, when present, would hide the hSR absorption band centered at 280 nm. The flow rate was 1 mL/min. The experiments were

carried out at room temperature. The column was calibrated with gel-filtration standards (Sigma-Aldrich), including carbonic anhydrase (29 kDa), conalbumin (75 kDa), glyceraldehyde-3-phosphate dehydrogenase (150 kDa), ferritin (440 kDa), blue dextrane (2000 kDa).

3.2 RESULTS AND DISCUSSION

Gel filtration experiments were carried out in different conditions and at different NaCl concentrations. To overcome possible experimental bias, preliminary measurements of calibrants were performed at different NaCl concentration, with negligible differences (Fig.3.2.1). All the experiments were performed at a hSR initial concentration of 15 μM, which is diluted approximately 30-fold during elution, reaching a concentration comparable to the one used for enzyme assays. (0.5 μM).

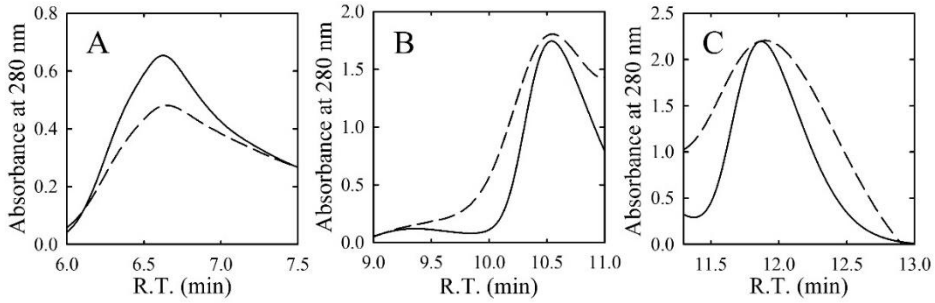

Figure3.2.1. Chromatogram of blue dextran (A), conalbumin (B) and carbonic anhydrase in the presence (continuous line) and absence (dashed lines) of 150 mM NaCl

In the presence of EDTA (i.e. in the absence of divalent metals) and in the absence of NaCl, the apparent molecular weight (AMw) of hSR was 67 ± 2 kDa (Fig. 3.2.2), which is close to the theoretical molecular weight of hSR dimers (73.3 kDa). At higher NaCl concentrations, the AMw remained identical (Fig. 3.2.2B). In the presence of EDTA, the measurements were repeated at different hSR concentrations, ranging from 5 μM to 100 μM, observing a higher oligomerisation state only at the highest concentration (89.9 kDa)

The AMw significantly increased when 2 mM Mg^{2+} was added to the elution buffer, (Fig. 3.2.2) suggesting a role of Mg^{2+} in the stabilization of a higher oligomer. This effect was particularly evident in the absence of NaCl, in which hSR eluted with an AMw of 124 ± 1 kDa, a value that was between the theoretical values for the dimer (73.3 kDa) and the tetramer (146.7 kDa). At higher NaCl concentrations, the AMw significantly decrease, reaching 66 ± 2 kDa at 300 mM NaCl (Fig. 3.2.2B). These results suggest a critical role for ionic strength in the oligomeric equilibrium, with a possible role for polar interactions in the stabilization of the tetramer.

When also ATP was added, a further increase in AMw was observed. (Fig. 3.2.2B); particularly, in the absence of NaCl, an AMw of 152 ± 2 kDa was detected, coeherent with the hSR tetramer (148 kDa).

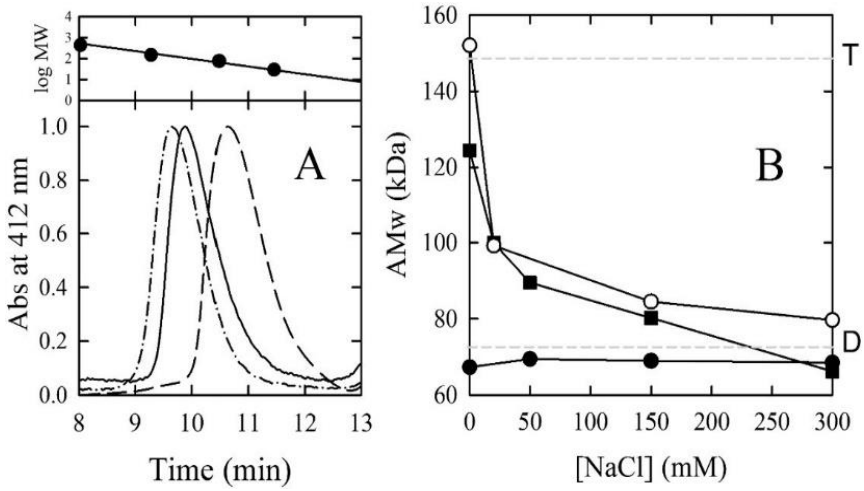

Figure 3.2.2. Gel filtration analysis of hSR in different conditions. (A) chormatograms of hSR in the presence of 5 mM EDTA (metals stripped hSR, dashed line), 2 mM $MgCl_2$ (continuous line) and 2 mM ATP Mg (dash-dot line); The chromatograms were normalized to unity. in the inset are reported the calibration standards; From the higher to the lower Mw: ferritin (440 kDa), glyceraldehyde-3-phosphate dehydrogenase (150 kDa), conalbumin (75 kDa), and carbonic anhydrase (29 kDa). (B) Dependence of the apparent molecular weight (AMw) on NaCl concentration in the presence of 5 mM EDTA (metals-stripped hSR, closed circles), 2 mM $MgCl_2$ (closed squares) and 2 mM ATP Mg (open circles). Horizontal dashed lines represent the theoretical AMw for the dimer and tetramer.

An experiment carried out with a higher concentration of hSR (100 μM) did not affect the measured AMw (149 ± 2 kDa), validating the full shift of the equilibrium toward the tetramer (Figure 3.2.3). In the presence of ATP and Mg^{2+}, a decrease of the AMw toward the dimer was observed at higher NaCl concentration, (Fig. 3.2.2B), as detected for the experiments carried out with only Mg^{2+}.

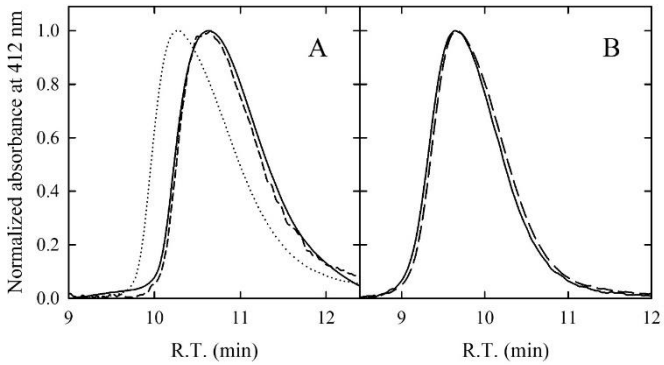

FIGURE 3.2.3: Chromatograms of hSR at different concentrations. For a better comparison, data are normalized to unity. **A)** hSR loaded at 5 μM (dash line), 15 μM (solid line) and 100 μM concentration (dotted line) in the presence of 5 mM EDTA 5; The corresponding AMw were 65.9 kDA, 67.3 kDa and 89.9 kDa respectively. **B)** hSR loaded at 15 μM (solid line) and 100 μM concentration (dashed line), in the presence of 2 mM $MgCl_2$ and 2 mM ATP. The estimated AMws were 152 kDa and 149 kDa, respectively.

In conclusion, in this work, it was demonstrated that ATP and divalent cations clearly modulate the oligomerisation state of hSR, with ionic interactions playing a critical role in the stabilization of higher-order oligomer, as demonstrated by the effect of NaCl (Figure 3.2.4).

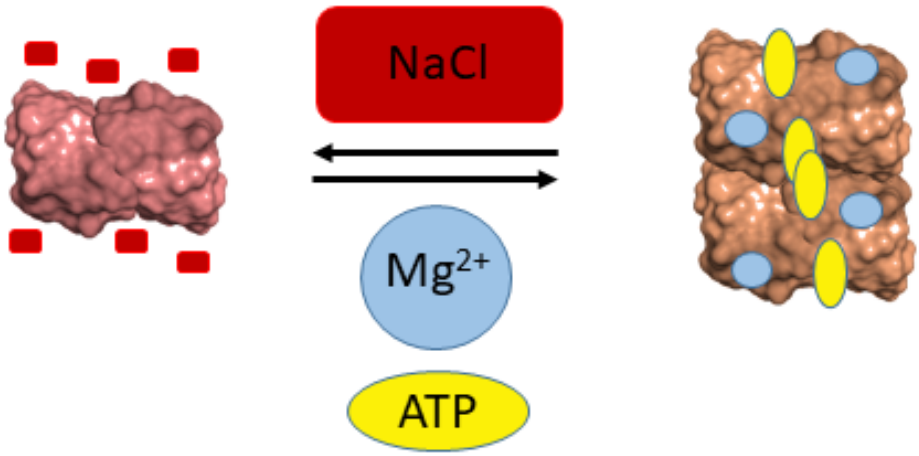

Figure 3.2.4: Model of the quaternary equilibrium of hSR

Chapter 4 - CHARACTERIZATION OF S-NITROSYLATION IN HUMAN SERINE RACEMASE

S-Nitrosylation is an emergent post translational modification (PTM) responsible for several biological events. The effect of nitrosylation on proteins can affect their function, cellular localisation and stability, but it is still poorly understood from a structural point of view. In this chapter, S-nitrosylation of hSR will be discussed in details. Activity assays and fluorescence spectroscopy were used to characterize the functional effect of this PTM on hSR. A mass spectrometry approach was used for the identification of cysteine residues undergoing S-nitrosylation.

Part of this work was published:

Francesco Marchesani, Stefano Bruno, Gianluca Paredi, Samanta Raboni, Barbara Campanini, Andrea Mozzarelli, Human serine racemase is nitrosylated at multiple sites. Biochimica et Biophysica Acta, Proteins and Proteomics (2018). doi: 10.1016/j.bbapap.2018.01.009. Sections of the text and some figures were adapted from the published work, as authorized by the publisher.

Candidate's contribution: I was involved in the functional characterization of the effect of S-nitrosylation on hSR, based on both enzymatic assays and fluorescence spectroscopy.

4.1. MATERIALS AND METHODS

Materials

Chemicals were of the best commercial quality available and were purchased from Sigma-Aldrich (St. Louis, MO, USA), unless otherwise stated. Tris(2-carboxyethyl)phosphine (TCEP) was purchased from Apollo Scientific (Bredbury, UK); Biotin-HPDP and avidin conjugated with horseradish peroxidase were purchased from Thermo Fisher Scientific (Waltham, MA, USA).

Protein expression and purification

Recombinant hSR was expressed as a hexa-His tagged fusion protein encoded in a pET28a-derived plasmid (Dixon et al. 2006) and was expressed in *E. coli* BL21 CodonPlus (DE3)-RIL cells (Merck-Millipore, Darmstadt, Germany), as previously described (Marchetti et al. 2013). D318N and C113S mutants were expressed and purified using the same protocol.

Site-directed mutagenesis

Point mutations C113S and D318N were introduced directly in the pET28a-derived expression vector by the QuikChange site-directed mutagenesis protocol (Stratagene, San Diego, CA, USA) using the primers 5'-gtattgcaagtttttt**act**gtctggagctgtctggg-3' and 5'-cccagacagctccagac**agt**aaaaaacttgcaatac-3' for C113S and 5'gctcagtggtgga<u>aacgtt</u>**aac**ttaacctcctccataacttggg3' and 5'cccaagttatggaggaggttaa**gtt**<u>aacgttt</u>ccaccactgagc-3' for D318N. The codon

bearing the mutations is shown in bold. In the case of D318 mutation, a restriction site was also introduced (underlined) to allow for a faster identification of the recombinants carrying the mutation. All resulting constructs were confirmed by automated sequencing and transformed into *E. coli* BL21 CodonPlus (DE3)-RIL cells.

S-nitrosylation

S-nitrosylation of hSR was produced by incubation with nitrosylglutathione (GSNO) at concentrations ranging from 2 to 500 μM for up to 6 hours, at 25°C, in a buffered solution containing 50 mM triethanolamine (TEA), 150 mM NaCl, 6 mM adenosine triphosphate (ATP), 6 mM $MgCl_2$, 50 μM pyridoxal 5'-phosphate (PLP), pH 8.0. hSR was added at concentrations of 0.5 μM for the enzyme assays, 4 μM for fluorescence measurements or 11 μM for mass spectrometry experiments. For time-dependent experiments, aliquots of the incubation mixtures were assayed for residual activity by adding 50 or 500 mM L-serine, 300 μM NADH and 60 U/ml lactate dehydrogenase (LDH).

Activity assays

Activity assays for L-serine deamination (Foltyn et al. 2005; Marchetti et al. 2015) were carried out in a solution containing 50 mM TEA, 2 mM ATP, 500 mM L-Ser, 50 μM PLP, 2 mM $MgCl_2$, 150 mM NaCl, 60 U/ml lactate dehydrogenase and 300 μM NADH, at pH 8.0. The concentrations of L-serine or ATP were modified in some experiments, as specified. For the determination of the enzyme parameters, the reaction was triggered by addition

of hSR at a final concentration of 0.3-0.5 µM. All reactions were carried out at 37 °C. GSNO was maintained in the assay mixtures at the same concentration as in the incubation mixtures to avoid dilution. Lactate dehydrogenase (LDH), used as the coupled enzyme, was preliminary shown not to be affected by GSNO. For long incubations, a control sample of enzyme in the absence of GSNO was periodically tested for stability and used for correction, when needed.

Fluorescence measurements.

hSR fluorescence spectra in the absence and presence of ligands were collected using a FluoroMax-3 fluorometer (HORIBA-Jobin Yvon), thermostatted at 20.0 ± 0.5 °C on a solution containing 4µM hSR in a buffer containing 50 mM TEA, 150 mM NaCl, 10 mM $MgCl_2$, pH 8.0. The fluorescence of Trp residues was selectively excited at 298 nm. The fluorescence of the cofactor was excited at 445 nm, to avoid any inner filter effect from GSNO, which has an absorption peak centered at about 334 nm. Slits were set for optimal signal-to-noise ratio.

Identification of nitrosylated cysteines by mass spectrometry

Cysteine residues forming stable S-nitroso adducts upon incubation with GSNO were identified using a differential alkylation-based strategy (Wojdyla and Rogowska-Wrzesinska 2015) coupled with mass spectrometry. Purified hSR was first reacted with GSNO at 500 µM concentration for 6 hours, and then with 170 mM methyl methanethiosulfonate (MMTS) for 30 minutes at 50 °C under vigorous stirring to block non-nitrosylated cysteine residues. The protein was precipitated by addition of five volumes of cold acetone followed by centrifugation. The pellet was extensively washed with

cold acetone to remove residual MMTS and then resuspended in a solution containing 50 mM TEA, 2 mM ethylenediaminetetraacetic acid (EDTA), 1% sodium dodecyl sulfate (SDS), pH 8.0. To reduce NO-cysteines and to label nascent thiols, sodium ascorbate and iodoacetamide were added to a final concentration of 1.6 mM and 85 mM, respectively. The control sample underwent the same procedure with the exception of GSNO incubation. For peptide digestion after conjugation with MMTS and iodoacetamide, 5 µg of protein samples were run in a 12 % SDS-PAGE gel in the absence of reducing agents. The gel was extensively washed with water and stained with colloidal Coomassie stain (Bio-rad, CA, USA). The bands corresponding to hSR were excised, incubated with a solution containing 50% ethanol and 10 % acetic acid until fully destained, washed twice with a buffered solution containing 25 mM ammonium bicarbonate and pure acetonitrile (ACN) 1:1 for 20 min and finally incubated with pure ACN for 5 minutes to reach complete dehydration. After removal of ACN, a solution containing trypsin in a 25 mM ammonium bicarbonate solution, pH 7.4, was added for gel rehydration. In-gel digestion was performed at 37°C for 16 hours. The reaction of trypsin was stopped by addition of ACN: 0.1 % trifluoroacetic acid (TFA) 1:1. Peptides were extracted by incubating the gel fragment with ACN: 0.1 % TFA 1:1 twice for 20 minutes at 37 °C, before complete drying using a vacuum concentrator and resuspension with ACN:TFA 0.1 % 1:1 before mass spectrometry experiments.

Mass spectrometry on digested peptides was carried out using either a 4800 Plus MALDI TOF/TOF (AbSciex) or an LTQ Orbitrap (Thermo Fisher Scientific) mass spectrometer. In MALDI experiments, the peptide mixture were analysed using the dried droplet method. Briefly, 1 µL of 10 mg/mL α-cyano-4-hydroxycinnamic acid (HCCA) in ACN:TFA 0.1% 1:1 was mixed with 1 µL of sample and spotted onto MALDI plate. Spectra were acquired in m/z 500-4000 range mediating 500 laser shots for each spectra. In the LTQ

Orbitrap experiments, the peptide mixture was separated in a Phenomenex Aeris™ PEPTIDE 3.6 µm XB-C18 (150 mm x 2.1 mm) reverse-phase column, developed in a 0.2% formic acid/water-0.2% formic acid/acetonitrile gradient (200 µl/min). Peptide identification from LTQ-Orbitrap experiments was carried out using the software PEAKS Studio (version 8.5, Bioinformatics Solutions, Waterloo, Canada), set to a precursor mass tolerance of 10 ppm and a fragment mass error tolerance of 0.1 Da. For recognition of nitrosylation sites, at least three independent experiments were carried out.

Detection of nitrosylated hSR by Western blot

S-nitrosylation of wt hSR and its mutants was confirmed with the biotin-switch technique (Forrester et al. 2009) coupled with Western blots. Briefly, GSNO-treated hSR was reacted with MMTS as described above to block non-nitrosylated cysteines. Sodium ascorbate was added at 1.6 mM concentration to selectively reduce nitrosothiols to free cysteines. At the same time, biotin-HPDP (EZ-link, Thermo Fisher Scientific) was added at 0.6 mM concentration to alkylate the nascent thiols. After 3 hours of incubation in the dark at 25°C, the samples were run on a 12% SDS-PAGE gel, which was then transferred onto a nitrocellulose blotting membrane (Amersham) using a Trans-Blot Turbo transfer system (Bio-rad, CA, USA). The membrane was probed with 5 µg/ml horseradish peroxidase-conjugated avidin (avidin-HRP, Thermo Fisher Scientific). The detection was carried out using the chemiluminescent substrate CheLuminate-HRP PicoDetect (PanReac AppliChem, Darmstadt, Germany). Gels and Western blots images were collected using a Chemidoc MP system (Bio-rad, CA, USA) and analysed with the Image Lab™ software (Bio-rad, CA, USA).

Sequence alignment

Amino acid sequence alignments of hSR and its orthologues were carried out using the software Ugene (Okonechnikov et al. 2012) with the algorithm Clustal Omega (Sievers et al. 2011) with Blosum matrix set at default parameters.

Prediction of S-nitrosylated cysteines in hSR

Four prediction programs were tested to evaluate possible S-nitrosylation sites: GPS-SNO 1.0, iSNOPseAAC, iSNO-AAPair, and SNOSite (Lee et al. 2011; Xu et al. 2013a; Xu et al. 2013b).

Determination of disulphide bonds

To evaluate the number of disulphide bonds, hSR was reacted with 5,5'-dithiobis (2-nitrobenzoic acid) (DTNB) either under native conditions or in the presence of 6 M guanidinium hydrochloride. The extinction coefficient at 280 nm of hSR was determined by the Edelhoch method (Pace et al. 1995). Upon reaction with DTNB, spectra were collected in the range 250-600 nm range to estimate both the protein concentration and the number of reacted cysteine residues.

Data analysis

Graphical and statistical analyses were performed with the software SigmaPlot (Systat Software, San Jose, CA, USA). Where provided, the error bars represent the mean ± s.e.m. of at least two independent experiments on independently prepared samples.

The V_{max} and K_M of hSR and its mutants were determined by fitting the dependence of activity on L-serine concentration with eq. 1:

$$v = \frac{V_{max}[S]}{K_M + [S]} \qquad \text{(eq. 1)}$$

where v is the reaction velocity, V_{max} is the maximal velocity at saturating concentrations of substrate, [S] is the concentration of the substrate and K_M is the Michaelis-Menten constant.

The analysis of the GSNO-mediated inactivation kinetics and fluorescence changes of wild type hSR and mutants were carried out under the assumption of a pseudo-first order kinetic at high GSNO concentrations (Rossi et al. 1997) using a sum of two exponential decays, plus a baseline to account for the residual activity:

$$A = A_0 + a_1 e^{-[GSNO]k_1 t} + a_2 e^{-[GSNO]k_2 t} \qquad \text{(eq. 2)}$$

where A is the enzyme activity, A_0 is the residual activity, a_1 and a_2 the amplitudes of the two inhibition phases; k_1 and k_2 are the second order rate constants.

The analysis of the GSNO inactivation kinetics of C113S hSR were carried out under the assumption of a pseudo-first order kinetic at high GSNO concentrations (Rossi et al. 1997) using a single exponential decay, plus a baseline to account for the residual activity:

$$A = A_0 + a e^{-[GSNO]kt} \qquad \text{(eq. 3)}$$

where A is the enzyme activity, A_0 is the residual activity, a the amplitude of the inhibition time course and k the reaction rate constant.

The determination of the nucleotide binding parameters was determined with a sigmoidal equation to take into account the binding cooperativity (Marchetti et al. 2013).

$$A = A_0 + a\frac{[XTP]^n}{EC_{50}{}^n + [XTP]^n} \qquad \text{(eq. 4)}$$

where A is the enzyme activity, A_0 is the basal activity in the absence of nucleotides, [XTP] is the concentration of either ATP, CTP or GTP, EC_{50} is their half maximal effective concentration and n is the Hill coefficient.

For the analysis of the dependence of fluorescence emission on ATP concentration, a sigmoidal equation was used to take into account the binding cooperativity (Marchetti et al. 2013).

$$y = y_0 + a\frac{[ATP]^n}{K_D{}^n + [ATP]^n} \qquad \text{(eq. 5)}$$

where *y* is the fluorescence emission intensity, [ATP] is the ligand concentration and *n* the Hill coefficient. y_0 is a horizontal offset and *a* the amplitude.

For the analysis of the dependence of fluorescence emission on glycine or ATP (in the presence of glycine) concentration, a binding isotherm was used:

$$y = y_0 + a\frac{[L]}{K_D + [L]} \qquad \text{(eq. 6)}$$

where *y* is the fluorescence emission intensity *[L]* is the ligand concentration and y_0 is a horizontal offset and *a* the amplitude.

4.2 RESULTS AND DISCUSSION

Reactivity of hSR with GSNO

hSR was incubated with GSNO at concentrations ranging from 2 to 80 μM, in the presence of 2 mM ATP, and enzyme activity was evaluated at different incubation times with the deamination assay, in the presence of 50 mM L-serine. Time-courses of hSR inhibition by GSNO are reported in Figure 4.2.1. At 2 and 4 μM GSNO, which correspond to 4- and 8-fold the concentration of hSR, the inhibition was partial, hinting at an equilibrium of the S-transnitrosylation reaction between GSNO and hSR. At 20 μM GSNO, residual activity after equilibration was close to that observed in the absence of ATP (Marchetti et al. 2013). Higher concentrations of GSNO did not decrease further the activity, indicating that the transnitrosylation equilibrium was completely shifted to the right and that the fraction of unreacted SR was negligible.

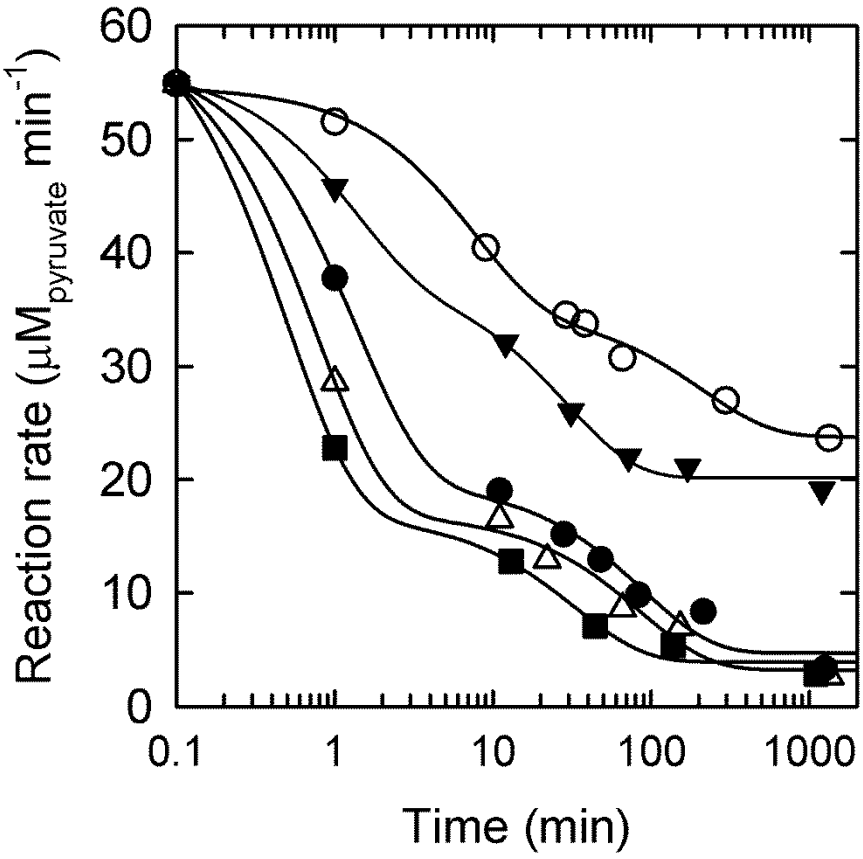

Figure 4.2.1: Inhibition kinetics of hSR in the presence of GSNO at 2 (open circles), 4 (closed triangles), 20 (closed circles), 40 (open triangles) and 80 μM (closed squares). The incubation mixture consisted in a solution containing 50 mM TEA, 2 mM ATP, 50 μM PLP, 2 mM $MgCl_2$, 150 mM NaCl, 0.5 μM hSR and GSNO at various concentration. The assay mixture consisted of the same solution added of 50 mM L-serine, 60 U/ml lactate dehydrogenase and 300 μM NADH. The solid lines represent the analysis of the experimental data using eq 2.

The inhibition kinetics were markedly biphasic, with a fast phase completed within a few minutes and a slow phase completed in timeframes ranging from several minutes to hours, depending on GSNO concentration (Figure 4.2.1). The global fitting of the data point for [GSNO]>20 μM with eq. 2 yielded second order constants of 517 ± 83 $s^{-1}M^{-1}$ and 7.8±2.8 $s^{-1}M^{-1}$. This biphasic time courses suggested the presence of at least two S-nitrosylation sites that react with GSNO at different rates, both causing enzyme inhibition. Addition of 20 mM TCEP resulted in at least 80% recovery of enzyme activity (data not shown), indicating that the inhibition is associated to S-nitrosylation rather than to a non-specific inactivation.

Prediction of secondary nitrosylation sites

To identify the S-nitrosylation sites that account for the observed biphasic inhibition, we carried out an *in silico* prediction based on the sequence of hSR. hSR has 8 cysteine residues in its primary structure, one of which, Cys113, is conserved in all mammals and has already been identified as a site of nitrosylation in the murine orthologue (Mustafa et al. 2007). All other cysteine residues are conserved in mammals except for Cys269, which is unique to humans (Figure 4.2.2). Cys269 is flanked by Asp265 (4.5 Å) and Lys 268 (9 Å), which might constitute the acid-base dyad for S-nitrosothiol stabilization. The results of the *in silico* prediction are summarized in Table 1.

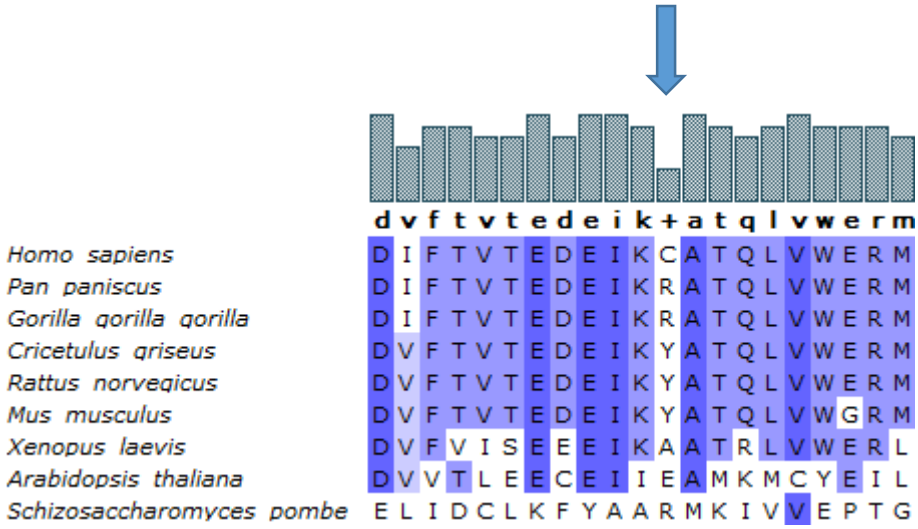

Figure 4.2.2. Multiple alignment of SR sequences covering the region of Cys269 (arrow), indicating its unicity in the human orthologue.

Both iSNO-AAPair and SNO site predicted Cys269 as a possible S-nitrosylation site. Cys217 was predicted only by iSNO-PseAAC. Cys2, Cys6, Cys46, Cys128 and Cys309 were also predicted as possible S-nitrosylation sites. Except for Cys113, which was identified by all the prediction softwares, prediction algorithms yielded highly divergent results, mirroring the incomplete knowledge of the structural features associated with stable S-nitrosylation.

Cysteine residue	GPS-SNO 1.0	iSNO-AAPair	SNO Site	iSNO-PseAAC
Cys 2	X			
Cys6	X			
Cys46			X	X
Cys113	X	X	X	X
Cys128				X
Cys210				X
Cys269		X	X	
Cys309	X			

Table 1: Prediction of S-nitrosylated cysteine residues for hSR according to several prediction softwares

Mass spectrometry detection of disulfide bonds

To ascertain predicted nitrosylation sites of hSR (Table 1), we first investigated the formation of a disulfide bond between Cys2 and Cys6, identified as possible S-nitrosylation candidates by GPS-SNO 1.0. The two residues are adjacent and were not observed in any available crystallographic structure of hSR. Indeed, the protein used for the three-dimensional structure of hSR (PDB: 3L6B) is a C2D, C6D mutant, reported to be more soluble than the wt protein (Smith et al. 2010). Figure 4.2.3 reports a MALDI spectrum of the tryptic digest of hSR incubated with iodoacetamide under non-reducing conditions. A peak at m/z of 2002.85 was assigned to a peptide containing both Cys2 and Cys6 in the carbamidomethylated form, which could be produced only if the cysteine residues were not involved in a disulphide bond. No peak consistent with the peptide forming an intramolecular disulfide bond was detected. Therefore, Cys2 and Cys6 are potentially available for nitrosylation.

Consistently with the mass spectrometry experiments, the reaction of hSR with DTNB under non-reducing conditions yielded a number of free cysteine residues of 7.5 ± 0.1 per monomer after denaturation with 6 M guanidinium hydrochloride, to be compared with 8 cysteine residues present in the primary structure. The same experiment under non-denaturing conditions led to a value of 6.0 ± 0.1, indicating that two cysteine residues are not solvent-accessible in the native conformation (data not shown). The

number of cysteine residues reacting per monomer was calculated by using the preliminarily estimated molecular weight of 34,138.

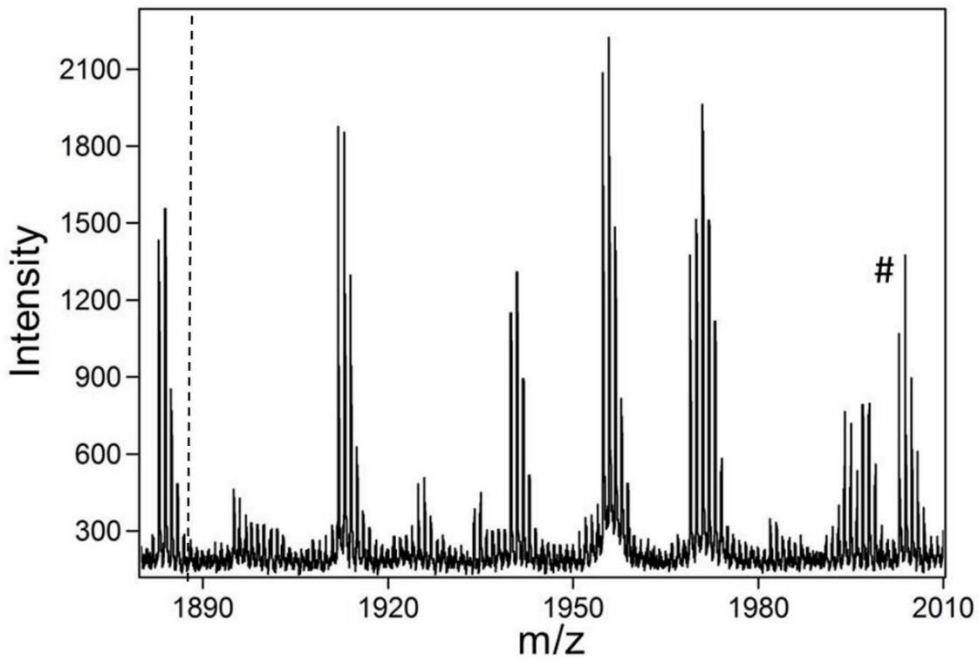

Figure 4.2.3. MALDI spectrum in the region containing peptide GSHMCAQYCISFADVEK, which includes both Cys2 and Cys6. (#) Peak at 2002.85 m/z, corresponding to the peptide in the carboamidomethylated form. The vertical dashed line corresponds to the m\z signal expected for the same peptide with the two cysteine residues involved in a disulphide bond.

Identification of the S-nitrosylated residues

For the identification of nitrosylated cysteine residues, we carried out differential alkylation experiments followed by tryptic digestion and analysis with an LTQ-Orbitrap LC-mass spectrometer. In the differential alkylation procedure that we applied, cysteine residues that were not nitrosylated by GSNO undergo beta-methylthiolation (MW +45.99 Da) upon MMTS incubation, whereas cysteine residues that were originally S-nitrosylated were freed upon incubation with ascorbate in the subsequent step and could undergo

carbamidomethylation (MW +57.02). The two modifications can be easily distinguished by mass spectrometry of proteolytic digests.

The peaks recognized by the software PEAKS Studio 8.5 are reported in Table 2. A selection of the peptides containing cysteine residues are reported in Table 2, where carbamidomethylations are indicated as C and beta-methylthiolations as B. The protein coverage was 92% (95% if excluding the His tag, Table 2) and included peptides containing all 8 cysteine residues. Cys113 was carboamidomethylated in two peptides, confirming that it is a nitrosylation site also in the human ortholog. Peptides containing carboamidomethylated Cys128 and Cys269 were also observed (Table 2), indicating that both were nitrosylated by GSNO. Cys128 is in the small domain (Figure 4.2.4a). It is not close neither to the active site (distance>15 Å), nor to the ATP binding site (distance>19 Å), nor to the metal binding site (distance>17 Å), nor to the dimeric interface (distance>35 Å). Cys269, unique to the human ortholog, is located in a helix involved in the interdimeric interface (Figure 4.2.4a). Cys2, Cys6, Cys46, Cys217 and Cys309 were consistently observed in the beta-methylthiolated form, indicative that they are not nitrosylation sites. In control experiments where hSR underwent all steps apart from nitrosylation, only beta-methylthiolated cysteines were observed (data not shown), confirming the validity of our experimental procedure. Nitrosylation at multiple sites not only account for the biphasic inhibition kinetics observed upon incubation with GSNO, but it could have physiological relevance in consideration that it might alter, in vivo, protein-protein interactions within the rich interactome of hSR (Dumin et al. 2006a; Fujii et al. 2006; Ma et al. 2013; Zhuang et al. 2010).

Peptide	-10lgP	Mass	m/z	z	RT	A.U.C.	PTM	Cys
K.NIC(+45.99)IVLSGGNVDLTSSITWVK.Q	80.61	2264.1545	1133.0853	2	38.80	1.6E6	B	309
K.LEGIPAYIVVPQTAPDC(+45.99)K.K	72.84	1958.9845	980.5008	2	33.35	9.36E6	B	113
K.LAIQAYGASIVYC(+45.99)EPSDESR.E	70.88	2217.0081	740.0107	3	32.15	2.67E6	B	128
K.C(+57.02)ATQLVWER.M	68.73	1161.5601	581.7878	2	23.98	1.32E6	C	269
K.LAIQAYGASIVYC(+57.02)EPSDESR.E	67.94	2228.0420	1115.0282	2	29.11	1.21E6	C	128
K.C(+45.99)ATQLVWER.M	61.95	1150.5264	576.2709	2	26.23	6.16E6	B	269
K.KLAIQAYGASIVYC(+45.99)EPSDESR.E	56.48	2345.1030	782.7089	3	30.20	6.89E5	B	128
K.VYAAEPSNADDC(+45.99)YQSK.L	54.70	1805.7236	903.8698	2	21.25	3.76E6	B	217
K.LEGIPAYIVVPQTAPDC(+57.02)K.K	52.24	1970.0182	657.6806	3	31.32	1.23E6	C	113
Y.GASIVYC(+57.02)EPSDESR.E	49.33	1568.6776	785.3471	2	20.35	3.39E5	C	128
Y.GASIVYC(+45.99)EPSDESR.E	49.23	1557.6439	779.8298	2	24.94	2.24E6	B	128
Y.C(+45.99)ISFADVEK.A	47.14	1056.4619	529.2388	2	26.30	3.09E6	B	6
K.C(+45.99)ELFQK.T	45.66	812.3561	407.1855	2	24.12	1.07E7	B	46
K.LEGIPAYIVVPQTAPDC(+45.99)KK.L	40.96	2087.0793	696.7006	3	30.72	4.34E5	B	113
Y.AAEPSNADDC(+45.99)YQSK.L	31.29	1543.5919	772.8035	2	18.43	9.28E4	B	217
R.GSHMC(+45.99)AQYC(+45.99)ISFADVEK.A	31.04	1979.7708	660.9316	3	31.96	3.35E5	B	2-6
K.KLAIQAYGASIVYC(+57.02)EPSDESR.E	28.68	2356.1370	786.3863	3	27.36	1.77E5	C	128
K.LEGIPAYIVVPQTAPDC(+57.02)KK.L	27.51	2098.1133	700.3787	3	29.36	2.99E5	C	113

Table 2: List of peptides containing cysteine residues upon digestion of GSNO-treated wt hSRas recognized by PEAKS 8.5

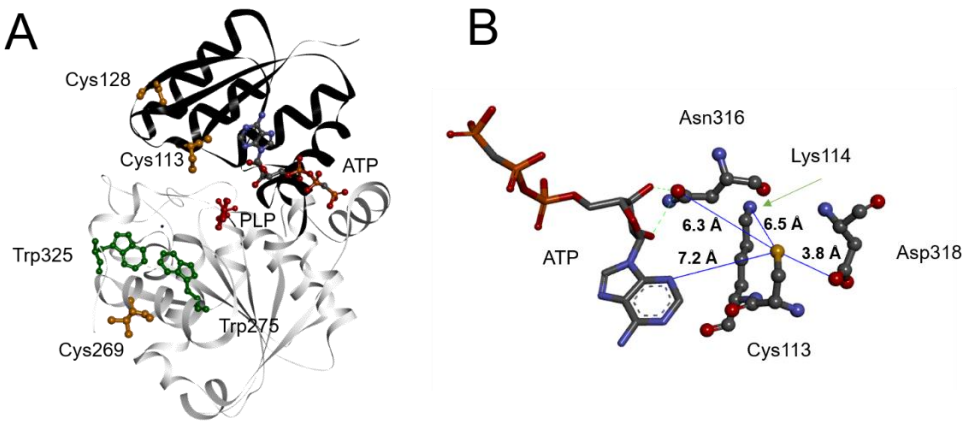

Figure 4.2.4. (A) Model of monomeric of hSR with the S-nitrosylated cysteine residues represented in orange and the tryptophan residues adjacent to Cys269 represented in green. PLP is represented in red. The model is based on PDB entry 3L6B. The ATP binding site was modelled by overlapping the structure of hSR with that from *Schizosaccharomyces pombe* (PDB 1WTC), in complex with the ATP analog AMP-PCP. **(B)** Close-up view of Cys113 in the three-dimensional model of hSR

ATP binding properties of hSR upon S-nitrosylation

After identification of multiple S-nitrosylation sites, we characterized the binding properties of the nitrosylated protein to gain insight into the molecular mechanism that produces inhibition. Considering that Cys113, the only detected nitrosylation site in murine SR, is adjacent to the binding site for ATP, it was proposed that SR nitrosylation causes a marked decrease in ATP affinity and, therefore, a decrease in enzyme activity (Mustafa et al. 2007). To assess whether nitrosylation affects the affinity of ATP, we exploited the fluorescence properties of the enzyme cofactor PLP, which exhibits an emission band centered at 500 nm upon excitation at 445 nm (Bruno et al. 2016; Marchetti et al. 2015). The band did not significantly change upon incubation with GSNO in the absence of ATP (data not shown), indicating that the internal aldimine fluorescence is not sensitive to the nitrosylation state of the protein. However, when 3 mM ATP was added, a 1.3-fold increase in the band intensity was observed for the GSNO-treated protein, in comparison to the 3-fold increase observed for native hSR (Bruno et al. 2016; Marchetti et al. 2015) (Figure 4.2.5a). The addition of 20 mM TCEP to the nitrosylated, ATP-saturated enzyme caused an increase in the fluorescence emission to the levels observed for the native, ATP-saturated protein (Figure 4.2.5a). The dissociation constants of ATP, determined by fitting the dependence of emission at 490 nm on ATP concentration with eq. 5 (Figure 4.2.5b), were 295 ± 13 μM (n=1.66 ± 0.11) and 156 ± 17 μM (n=1.50 ± 0.25) for the native and nitrosylated enzyme, respectively. The observed binding of ATP to S-nitrosylated hSR, with similar K_D and cooperativity to that of native hSR, indicates that, contrary to what was previously suggested for murine SR (Mustafa et al. 2007), S-nitrosylation does not interfere with ATP binding. This finding is confirmed by the lack of any protective effect of ATP against nitrosylation (data not shown). However, since the activity of the enzyme in

the absence of ATP is not affected by nitrosylation (data not shown), we speculated that nitrosylation has nevertheless an effect on the protein dynamics that controls the allosteric modulation of ATP.

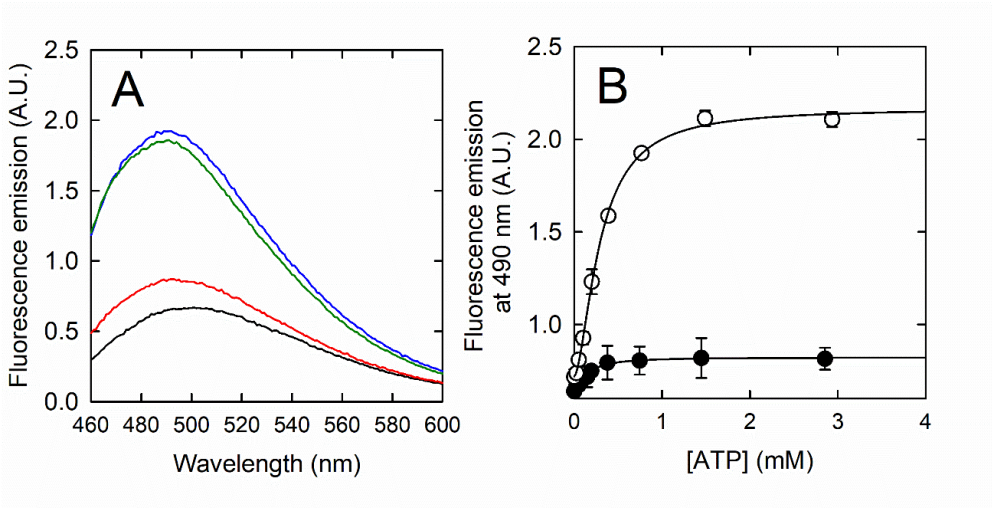

Figure 4.2.5. (A) Fluorescence emission spectra upon excitation at 445 nm of hSR (black line), hSR in the presence of 3 mM ATP (green line), hSR pre-incubated with 150 μM GSNO in the presence of 3 mM ATP (red line) and hSR pre-incubated with 150 μM GSNO in the presence of 3 mM ATP and after addition of 20 mM TCEP for 10 minutes (blue line). The measurements were carried out in a solution containing 50 mM TEA, 150 mM NaCl, 10 mM $MgCl_2$, 4 μM hSR, pH 8.0. **(B)** Dependence of fluorescence emission at 490 nm upon excitation at 445 nm on the concentration of ATP for native hSR (open circles) and for hSR pre-incubated with 150 μM GSNO (closed circles). The measurement was carried out in a solution containing 50 mM TEA, 150 mM NaCl, 10 mM $MgCl_2$, 4 μM hSR, pH 8.0. The solid lines are the fitting of the data points with eq. 5.

Effect of S-nitrosylation on ATP, CTP and GTP binding to hSR

To further investigate whether GSNO-induced inhibition is associated to a conformational transition rather than to a direct displacement of ATP, it was tested if S-nitrosylation produced the same effects in enzyme activity in the presence of ATP or its analogues guanosine trisphosphate (GTP) and cytidine trisphosphate (CTP) (Figure 4.2.6). Indeed, the purine base of ATP is the closest portion of the molecule to Cys113 (7.2 Å) (Figure 4.2.4b) and its substitution with a different base might differentially affect the nucleotide binding to hSR. CTP and GTP both activated hSR, 7 and 3.4-fold, respectively, in a cooperative fashion (Table 3), confirming that the base of trisphosphonucleotides does not confer absolute selectivity in neither the binding nor in the allosteric activation of hSR (De Miranda et al. 2002). Nitrosylation of hSR with 150 μM GSNO produced a similar inhibition in the presence of either CTP, GTP or ATP (Table 3). This finding indicated that a direct interaction between S-nitrosylated Cys113 and the purine base of ATP is not the likely mechanism of inhibition and hints to conformation-based effects.

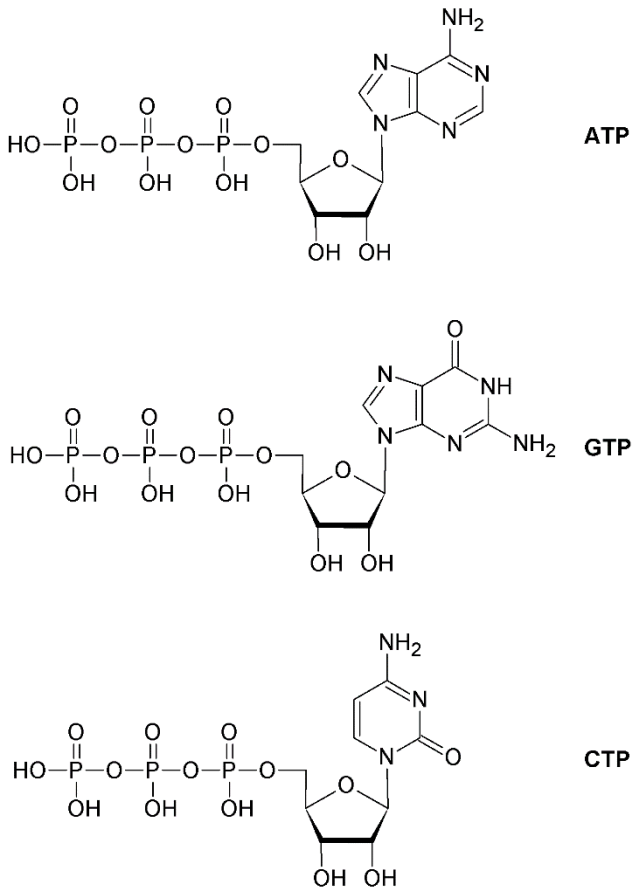

Figure 4.2.6. Triphosphate nucleotides

	Activation at saturating concentrations (-fold)	EC_{50} (mM)	n	Inhibition by 150 µM GSNO (%)
ATP	10	0.21± 0.01	1.8 ± 0.2	86 %
CTP	3.4	3.8 ± 0.2	1.9 ± 0.1	100 %
GTP	7.0	0.65 ± 0.04	1.8 ± 0.1	95 %

Table 3: Binding parameters of ATP, CTP and GTP to hSR

Effect of nitrosylation on the cross-talk between the ATP binding site and the active site

To assess whether hSR activity regulation by NO is predominantly based on a conformational selection, we studied the effect of nitrosylation by using glycine as model active site ligand. Glycine binding to nitrosylated and native hSR in the absence of ATP was followed by fluorescence spectroscopy, since the external aldimine is highly fluorescent (Marchetti et al. 2013). The affinity of glycine was not influenced by treatment with GSNO. Indeed, similar K_D for glycine binding of about 2.64 ± 0.45 mM and 2.83 ± 0.19 mM were obtained for the nitrosylated and native hSR, respectively (Figure 4.2.7a), confirming that the active site is not directly affected by nitrosylation in the absence of ATP.

While trying to titrate nitrosylated hSR with glycine in the presence of saturating ATP, we initially measured an apparently higher dissociation constant (data not shown). We realized that the apparent lower affinity of ATP for glycine-bound SR was indeed due to slow kinetics of signal stabilization. Indeed, at 12 µM ATP, which is the concentration needed to saturate about half of untreated hSR binding sites, the signal requires about 40 minutes to reach equilibrium (Figure 4.2.7b). Once a stable signal was reached, the signal increase nicely overlapped with the one expected for ATP binding on the untreated protein, i.e. 1.1-fold (inset, Figure 4.2.7b). These results indicate that

both ATP and glycine bind to their respective sites with the same affinity regardless of the nitrosylation state.

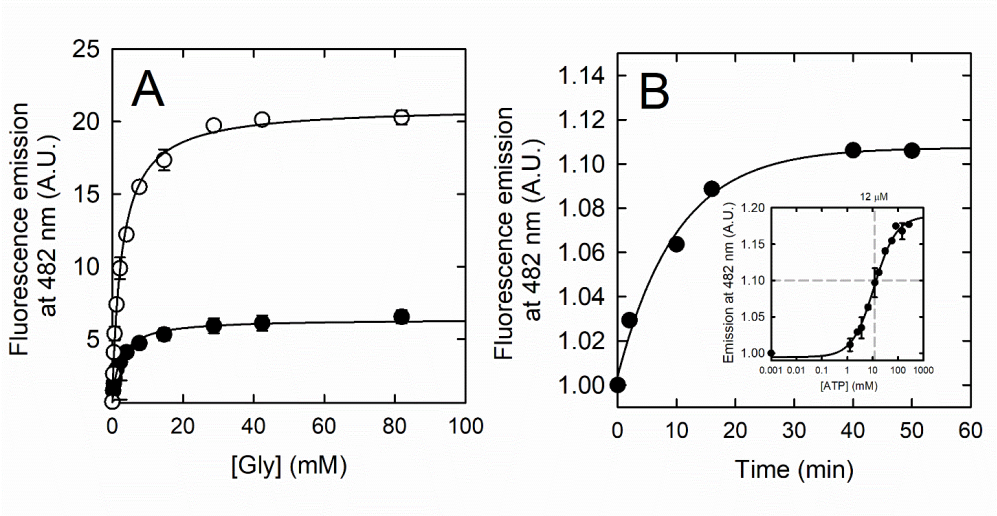

Figure 4.2.7 (A) Dependence of fluorescence emission at 482 nm upon excitation at 445 nm on the concentration of glycine for native hSR (open circles) and hSR pre-incubated with 150 μM GSNO (closed circles). The measurement was carried out in a solution containing 50 mM TEA, 150 mM NaCl, 10 mM $MgCl_2$, 4 μM hSR, pH 8.0. The solid lines are the fitting of the data points with eq. 6. **(B)** Time course of fluorescence emission at 482 nm upon excitation at 445 nm for hSR pre-incubated with 150 μM GSNO and 80 mM glycine following the addition of 12 μM ATP. The measurement was carried out in a solution containing 50 mM TEA, 150 mM NaCl, 10 mM $MgCl_2$, 4 μM hSR, pH 8.0. **Inset:** dependence of fluorescence emission of glycine-bound hSR at 482 nm upon excitation at 445 nm at increasing concentrations of ATP. The experimental points were fitted Eq. 6. The dashed line indicates the signal increase at 12 μM ATP in the titration (i.e. 1.1).

Characterization of the C113S mutant

To confirm inhibition of hSR through S-nitrosylation of residues other than Cys113, we expressed and characterized the C113S hSR mutant. C113S hSR exhibited a K_M for L-serine 3.5-fold higher than wt hSR and a specific activity 3.3-fold lower (Table 4). ATP binding to C113S hSR in the presence of L–serine occurred with a 5-fold higher EC_{50} in comparison with wt hSR, with conserved binding cooperativity (Table 4). The altered kinetic parameters indicated that, independently of nitrosylation, Cys113 might be a hotspot for allosteric enzyme regulation.

ATP binding to C113S hSR in the absence of any active site ligand was followed by fluorescence spectroscopy using the signal increase at 490 nm upon excitation of PLP. The resulting K_D was 453 ± 35 μM (n=1.6 ± 0.2), lower than that assessed from activity assays (1.07 ± 0.06 mM, with n=1.47 ± 0.17), which reflects ATP binding to C113S hSR in the substrate-ligated form. For wt hSR, no such difference was observed (Marchetti et al. 2013). These findings confirmed that Cys113 is important for the cross-talk between the active site and the allosteric ATP binding site and, indirectly, that the nitrosylation of Cys113 residue interfere with the activity of the enzyme.

The GSNO-induced inhibition kinetics of C113S hSR in the presence of 6 mM ATP (Figure 4.2.8a) was fitted as a single exponential decay (eq. 3) yielding a rate of the same order of magnitude as the slow phase of wt hSR inhibition by GSNO ($k_{C113S\ hSR}$ =1.7 s^{-1} M^{-1} ± 0.6 vs $k_{wt\ hSR}$ = 7.8 ± 2.8 s^{-1} M^{-1}, estimated at 150 μM GSNO). Therefore, it can be speculated that the slow phase of GSNO-dependent inhibition of wt hSR is associated to the S-nitrosylation of either Cys269 or Cys128, or both. It is interesting to notice that C113S hSR activity before treatment with GSNO is comparable to that of wt

hSR after the completion of the first phase of inhibition (Figure 4.2.8a), the amplitude of which accounts for around 70% of the total inhibition (Figure 4.2.1). Therefore, it appears that the C113S mutation elicits the same effects on activity as Cys113 nitrosylation.

For the identification of nitrosylated cysteine residues in C113S hSR, we carried out differential alkylation experiments followed by tryptic digestion and analysis with the LTQ-Orbitrap LC-mass spectrometer. Consistently with the mutation, only Cys128 and Cys269 were detected as S-nitrosylation sites (data not shown). For comparison with the C113S murine orthologue, which was not S-nitrosylated by 250 μM GSNO at any sites, as demonstrated by the biotin-switch technique (Mustafa et al. 2007), we carried out the same experiment on C113S hSR. A Western blot of the product, probed with HRP-avidin, led to a band consistent with a nitrosylated protein (Figure 4.2.9). Therefore, both mass spectrometry and the biotin switch techniques confirm that the human ortholog has a nitrosylation pattern different from that of the murine one.

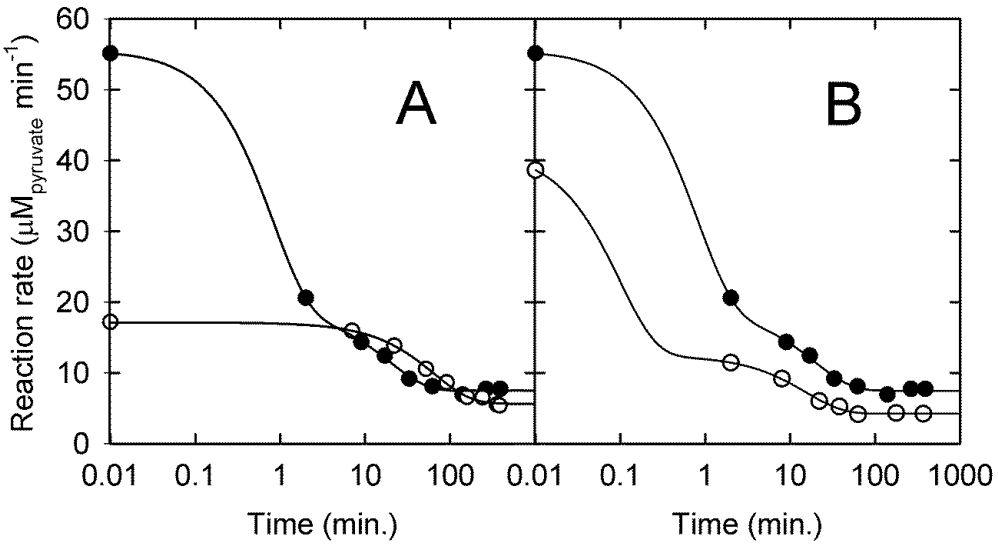

Figure 4.2.8: **(A)** Inhibition kinetics of C113S hSR (open circles) and wt hSR (closed circles) incubated with 150 μM GSNO. The solid lines represent the analysis of the experimental data using a sum of exponential decays plus a baseline for wt hSR and a single exponential decay plus a baseline for C113S hSR. The incubation mixture consisted in a solution containing 50 mM TEA, 6 mM ATP, 50 μM PLP, 6 mM $MgCl_2$, 150 mM NaCl, 0.5 μM hSR. The assay mixture consisted of the same solution added of 500 mM L-serine, 60 U/ml lactate dehydrogenase and 300 μM NADH. **(B)** Inhibition kinetics of D318N hSR (open circles) and wt hSR (closed circles) incubated with 150 μM GSNO. The solid lines represent the analysis of the experimental data using a sum of exponential decays plus a baseline (eq. 2).

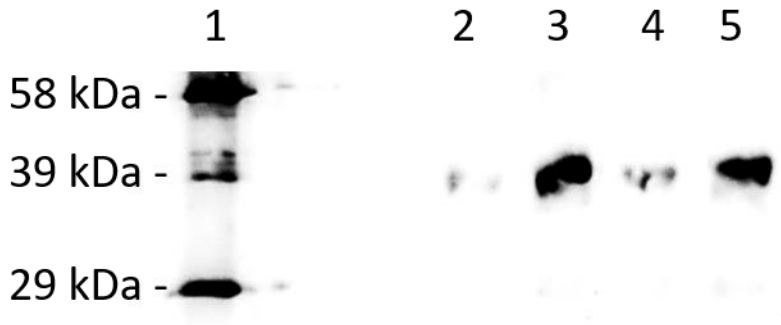

Figure 4.2.9: Biotin-switch analysis of wt hSR and D318N and C113S mutants in Western blot. 1: biotinylated molecular weight marker (Sigma Aldrich) 2: untreated D318N hSR; 3: D318N hSR treated with GSNO at 150 μM concentration; 4: untreated C113S hSR; 5: C113S hSR treated with GSNO at 150 μM concentration. The analysis was carried out with Chemidoc imaging system (Bio-rad, CA, USA).

	K_M for L-serine (mM)	Specific activity ($\mu mol_{pyruvate}$ $min^{-1}mg^{-1}$)	k_{cat} (min^{-1})	k_{cat}/K_M (min^{-1} mM^{-1})	EC_{50}^{ATP} (mM)	n^{ATP}	ATP activation
wt hSR	16 ± 1	4.34 ± 0.09	166 ± 10	10.21 ± 0.46	0.21± 0.01	1.8 ±0.2	10
C113S hSR	54 ± 5	1.34 ± 0.03	51 ± 2	0.95 ± 0.01	1.07 ± 0.06	1.6 ± 0.2	9.48
D318N hSR	50 ± 3	3.00 ± 0.05	115 ± 2	2.30 ± 0.07	0.68 ± 0.03	1.8 ± 0.1	9.52

Table 4: Kinetic parameters of wt hSR and its mutants C113S and D318N

Fluorescence emission spectra of C113S hSR

Fluorescence emission spectra for wt hSR and C113S hSR upon excitation at 445 nm are shown in Figure 4.2.10. Fluorescence increased upon addition of ATP for C113S hSR, as already reported for wt hSR (Marchetti et al. 2013). Interestingly, the emission maximum of PLP of wt hSR blue-shifts from 500 nm to 490 nm at saturating concentrations of ATP while the emission of C113S hSR remains at about 498 nm. The blue shift of the emission spectrum had been associated to a closing of the active site induced by allosteric effectors (Marchetti et al. 2013). The more red-shifted spectrum of the mutant appears to indicate that the cross-talk between the ATP binding site and the active site is partially disrupted, resulting in a partial closure of the site.

This finding is consistent with the lower enzyme activity and confirms that Cys113 is a hotspot for enzyme regulation.

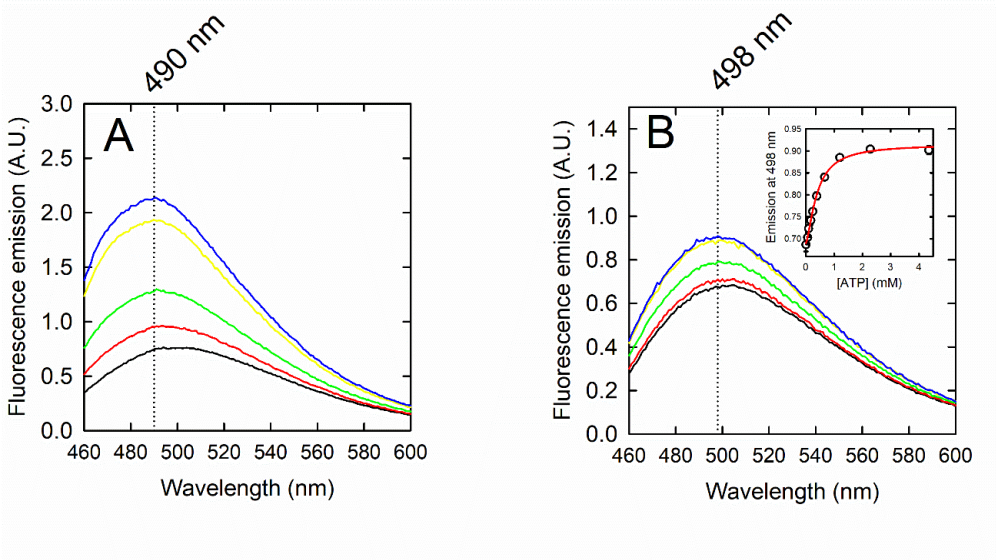

Figure 4.2.10. Fluorescence emission spectra of wt hSR (A) and C113S hSR (B) upon excitation at 445 nm at increasing concentrations of ATP ranging from 0.1 to 4 mM. The hSR emission spectra in the absence of ATP is indicated in black. At higher concentrations of ATP, the emission maximum is at 490 nm for hSR and 498 nm for C113S hSR. In the inset, the dependence of emission at 498 nm on ATP concentration is reported for C113S hSR.

Nitrosylation rates monitored by tryptophan fluorescence in wt hSR and C113S hSR

Finally, to investigate the effects of S-nitrosylation on the conformational equilibria of hSR, we exploited the fluorescence emission of Trp residues as potential probes of conformational changes brought about by nitrosylation. Indeed, hSR has three tryptophan residues in its sequence. Two, Trp275 and Trp325 (Figure 4.2.4a), are located in the large domain. It has been proposed that the fluorescence emission of Trp249 is partially quenched by PLP and is responsible for the emission of the cofactor following excitation at 298 nm (Marchetti et al. 2015). Therefore, the direct emission of tryptophan

residues is mainly attributed to Trp275 and Trp325. These residues are partially solvent-exposed and, consistently, they emit at around 338 nm when selectively exited at 298 nm (Marchetti et al. 2015). Upon addition of 150 μM GSNO to both wt hSR and C113S hSR, emission at 338 nm decreased with time, reaching a stable signal after about 10 minutes (Figure 4.2.11). Since the decrease in the emission intensity is almost identical for wt hSR and C113S hSR and is not accompanied by any shift in the emission maximum, we speculate that the effect is most probably due to a quenching by the nitroso group of Trp(s) close to a nitrosylation site (Akhter et al. 2002), other than Cys113, which is missing in the mutant. Cys269 appears a more likely candidate, as it is in close proximity to Trp325 and Trp275 (Figure 4.2.4a). Both phases monitored in fluorescence exhibit rates in the same order of magnitude as the fast phase of wt hSR inhibition, as monitored by activity assays (Figure 4.2.11), indicating that the nitrosylation of Cys269 takes place at a rate similar to that of Cys113, albeit without affecting the enzyme activity, as demonstrated by the lack of a fast inhibition phase in the C113S mutant. Further studies are required to assess the origin of the biphasic behavior of nitrosylation-induced quenching kinetics.

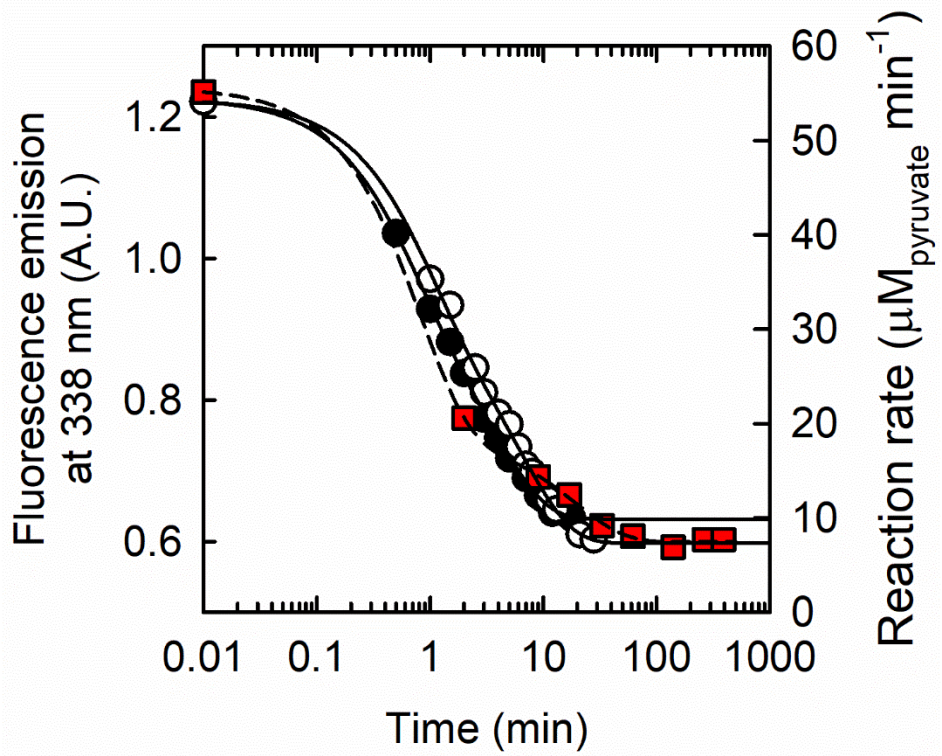

Figure 4.2.11. Fluorescence emission kinetics at 338 nm upon excitation at 298 nm of wt hSR (closed circles) and C113S hSR (open circles) in the presence of 150 μM GSNO, TEA 50 mM, NaCl 150 mM, MgCl2 10 mM, 4 μM hSR, pH 8. The experimental points are fitted with a double exponential decay equation (eq. 2). For comparison, the inhibition kinetic from Figure 4.2.1 is also reported (red squares, right axes).

Role of aspartate 318 in S-nitrosothiol stabilization

Cys113 is surrounded by an asparagine residue in position 316, a lysine residue in position 114 and an aspartate residue in position 318 (Figure 4.2.4b). It was speculated (Mustafa et al. 2007) that Asp318, only 3.8 Å apart from Cys113, is the acidic amino acid often located in the proximity of cysteine residues that undergo stable S-nitrosylation (Greco et al. 2006). To test whether this residue is crucial in the stabilization of the nitrosothiol, we expressed and characterized mutant D318N hSR.

D318N hSR exhibited a K_M for L-serine 3.5-fold higher than wt hSR, with a specific activity 1.5 –fold lower (Table 4). ATP binding occurred with an EC_{50} 3-times higher than that of wt hSR, with the same degree of cooperativity (Table 4). These altered kinetic parameters confirmed that the region in proximity of ATP might be relevant for both ATP binding and for the allosteric regulation of enzyme activity. Inhibition of D318N hSR by GSNO occurred with a time course almost identical to that of wt hSR (Figure 4.2.8b). Particularly, the fast inhibition phase that we attributed to Cys 113 nitrosylation was unchanged, indicating that an acidic residue in position 318 is not crucial for GSNO-induced nitrosylation of Cys113. Indeed, it is known that the acid-base dyad recognized around some S-nitrosylated cysteines is not present in others (Marino and Gladyshev 2010).

In conclusion, unlike the murine orthologue, human serine racemase is nitrosylated by the nitroso group donor GSNO at three cysteine residues, Cys113, Cys269 and Cys128. The inhibition kinetic is biphasic, indicating that at least two of these residues are responsible for enzyme inhibition, as confirmed by site-directed mutagenesis of Cys113. Cys113 is associated to the fast inhibition phase, whereas Cys128 is associated to the slow phase. The S-nitrosylation of Cys269 does not affect activity but is detected by fluorescence emission of tryptophan residues, which is quenched due to proximity to the modified cysteine. S-nitrosylated hSR binds ATP with unchanged affinity and cooperativity, indicating that hSR inhibition by S-nitrosylation arises from conformational modifications that affect the allosteric communication between the ATP binding site and the active site.

Chapter 5 - Conformation-dependence of human serine racemase S-nitrosylation

S-Nitrosylation is still poorly understood from a structural point of view; in particular, a detailed characterisation of the conformational changes occurring upon S-nitrosylation has been carried out only for hemoglobin and for a few other proteins. Indeed, hemoglobin is the only well-characterised example in which nitrosylation controls the conformation equilibrium and viceversa. In this chapter, the conformational equilibrium of hSR was explored in association with the S-nitrosylation of a residue close to the ATP binding site (Cys113).

I carried out all the work described herein, including the optimization of a fluorimetric method for the detection of S-nitrosylation.

5.1 MATERIALS AND METHODS

Materials

Chemicals were of the best commercial quality available and were purchased from Sigma-Aldrich (St. Louis, MO, USA), unless otherwise stated. Tris(2-carboxyethyl)phosphine (TCEP) was purchased from Apollo Scientific (Bredbury, UK).

Site-directed mutagenesis and protein expression

Mutants D318A, N316A and K114Q were obtained by site directed mutagenesis of the plasmid encoding for wt hSR (Dixon et al. 2006) by the QuikChange protocol (Stratagene, San Diego, CA, USA) using the primers indicated in Table 1. In the case of the N316A mutations, a restriction site was also introduced (underlined) to allow for a faster identification of the recombinants carrying the mutation. The artificial gene encoding for mutant C2S, C4S, C128S, C269S, C309S (Δ5Cys), codon-optimized for *Escherichia coli*, was synthetized by GeneArt (Regensburg, Germany) and subcloned in a pET28 expression vector. All mutants were then expressed and purified as described for wt hSR in *E. coli* BL21 CodonPlus (DE3)-RIL cells (Merck-Millipore, Darmstadt, Germany) (Marchetti et al. 2013), modified with the co-expression of GroEL and GroES (Canosa et al. 2018). Mutagenesis, expression and purification of mutants C113S, D318N and Q89M were reported elsewhere (Canosa et al. 2018; Marchesani et al. 2018).

mutations	Primer forward	Primer reverse
D318A	tcagtggtggaaatgtag**cct**taacc tcctccataac	gttatggaggaggtta**agg**ctacatttccacca ctga
N316A	gctcagtggtgga**gct**gtagatctaa cctcctccataacttggg	cccaagttatggaggaggttagatctac**agc**t ccaccactgagc
K114Q	ccagacagctccagactgtcag**aa a**cttgcaatacaagcct	aggcttgtattgcaag**ttt**ctgacagtctggag ctgtctgg

Table 1

S-nitrosylation

S-nitrosylation of wt hSR and its mutants was produced by incubation with GSNO at concentrations ranging from 150 to 500 μM for up to 90 minutes, at 25°C, in a buffered solution containing 50 mM triethanolamine (TEA), 150 mM NaCl, pH 8.0 either in the presence or absence of: i) 6 mM adenosine triphosphate (ATP) ii) 10 mM $MgCl_2$ iii) 80 mM glycine iv) 5 mM ethylenediaminetetraacetic acid (EDTA).

GSNO-induced nitrosylation was carried out with wt hSR or its mutants at concentrations of 0.5 μM for the enzyme assays, 4 μM for fluorescence measurements and 11 μM for the in-gel S-nitrosylation detection method (see below) and for mass spectrometry experiments.

Activity assays

Activity assays for L-serine demination (Foltyn et al. 2005; Marchetti et al. 2015) were carried out in a solution containing 50 mM TEA, 2 mM ATP, 500 mM L-Ser, 50 µM PLP, 2 mM $MgCl_2$, 150 mM NaCl, 60 U/ml lactate dehydrogenase and 300 µM NADH, at pH 8.0. The concentrations of L-serine or ATP were modified in some experiments, as specified. In some experiments, glycine was also added at 3 mM concentration, as specified. For the determination of enzyme parameters of hSR mutants, the reaction was triggered by addition of the enzyme at a final concentration of 0.3-0.5 µM. For the evaluation of GSNO-inhibition, aliquots of the incubation mixtures were assayed for residual activity by adding 500 mM L-serine, 300 µM NADH and 60 U/ml lactate dehydrogenase (LDH). It was preliminarily shown that LDH was not directly inhibited by GSNO (data not shown). GSNO was maintained in the assay mixtures at the same concentration as in the incubation mixtures to avoid dilution. All reactions were carried out at 25 °C.

Fluorescence measurements

Fluorescence kinetic measurements of wt hSR and its mutants were performed in the absence and presence of GSNO, ATP and\or glycine using a FluoroMax-3 fluorometer (HORIBA-Jobin Yvon), thermostatted at 20.0 ± 0.5 °C, in a solution containing 4 µM hSR, 50 mM TEA, 150 mM NaCl, 10 mM $MgCl_2$, pH 8.0. The fluorescence of the pyridoxal 5‘-phosphate was excited at 445 nm, to avoid any inner filter effect from GSNO, which has an absorption peak centred at about 334 nm. Slits were set for optimal signal-to-noise ratio. Emission was collected at 490 nm when working in the absence of glycine and 482 nm when working in its presence (Marchetti et al. 2013). Data points were

collected at 30 s intervals with the shutter closed in-between to avoid photobleaching.

Molecular modelling

The model of hSR bound to ATP was built using the crystallographic structure of the complex between *Saccharomyces pombe* SR (SpSR) and adenylylmethylenediphosphonate (AMP-PCP) (Goto et al. 2009) using the Swiss-model server (Waterhouse et al. 2018).

Detection of S-nitrosocysteines by differential tagging

Detection of S-nitrosylation was carried out using a differential tagging approach (Devarie-Baez et al. 2013) with 5-iodoacetamidefluoresceine and iodoacetamide (5IAF\IAA method). Cysteine residues forming stable S-nitroso adducts upon incubation with GSNO were identified using the 5IAF\IAA method coupled with mass spectrometry. Purified hSR was reacted with 500 μM GSNO for 90 minutes in a 50 mM TEA, 150 mM NaCl, solution at pH 8.0 modified to give five conditions i) +5 mM EDTA; ii) +10 mM MgCl2; iii) +6 mM ATP and 10 mM MgCl2; iv) +80 mM glycine and 10 mM MgCl2; v) +6 mM ATP, 10 mM MgCl2 and 80 mM glycine. The 5IAF\IAA was then applied. The samples were incubated with 10 mM iodoacetamide (IAA) for 30 minutes at 50°C in the dark, followed by precipitation with nine volumes of cold ethanol at 80 °C. After centrifugation the pellet was extensively washed with cold ethanol to remove residual IAA and then resuspended in a solution containing 50 mM TEA, 2 mM ethylenediaminetetraacetic acid (EDTA), 1% sodium dodecyl sulfate (SDS), pH 8.0. To reduce NO-cysteines and to label nascent thiols, sodium ascorbate and 5IAF were added to a final concentration of 10 mM and 0.3 mM, respectively; samples are incubated at 25 °C for two

hours in the dark. After the conjugation with 5IAF the samples were precipitated in an ice bath with one volume of 10% TCA followed by centrifugation; the pellets are then extensively washed with acetone, to remove unreacted 5IAF. Finally, the samples are resuspeded in sample buffer solution in the absence of β-mercaptoethanol. The control sample underwent the same procedure with the exception of GSNO incubation. Samples were run in a 12 % SDS-PAGE gel in the absence of reducing agents. After the run, the gel was extensively washed with water and fluoresceine was detected with a Chemidoc instrument, followed by staining with colloidal Coomassie stain (Bio-rad, CA, USA). Comassie staining allow for the normalization of the fluorescence signals.

The bands corresponding to hSR were excised, incubated with a solution containing 50% ethanol and 10 % acetic acid until fully destained, washed twice with a buffered solution containing 25 mM ammonium bicarbonate and pure acetonitrile (ACN) 1:1 for 20 min and finally incubated with pure ACN for 5 minutes to reach complete dehydration. After removal of ACN, a solution containing trypsin in a 25 mM ammonium bicarbonate solution, pH 7.4, was added for gel rehydration. In-gel digestion was performed at 37°C for 16 hours. The reaction of trypsin was stopped by addition of ACN: 0.1 % trifluoroacetic acid (TFA) 1:1. Peptides were extracted by incubating the gel fragment with ACN: 0.1 % TFA 1:1 twice for 20 minutes at 37 °C, before complete drying using a vacuum concentrator and resuspension with ACN:TFA 0.1 % 1:1 before mass spectrometry experiments. Mass spectrometry on digested peptides was carried out using an LTQ Orbitrap (Thermo Fisher Scientific) mass spectrometer. The peptide mixture was separated in a Phenomenex Aeris™ PEPTIDE 3.6 µm XB-C18 (150 mm x 2.1 mm) reverse-phase column, developed in a 0.2% formic acid/water-0.2% formic acid/acetonitrile gradient (200 µl/min). Peptide identification from

LTQ-Orbitrap experiments was carried out using the software PEAKS Studio (version 8.5, Bioinformatics Solutions, Waterloo, Canada), set to a precursor mass tolerance of 10 ppm and a fragment mass error tolerance of 0.2 Da.

Data analysis

Graphical and statistical analyses were performed with the software SigmaPlot (Systat Software, San Jose, CA, USA). Where provided, the error bars represent the mean ± s.e.m. of at least two independent experiments on independently prepared samples.

The V_{max} and K_M of wt hSR and its mutants were determined by fitting the dependence of activity on L-serine concentration with eq. 1:

$$v = \frac{V_{max}[S]}{K_M + [S]} \qquad \text{(eq. 1)}$$

where v is the reaction velocity, V_{max} is the maximal velocity at saturating concentrations of substrate, [S] is the concentration of the substrate and K_M is the Michaelis-Menten constant.

The analysis of the GSNO-mediated inactivation kinetics and fluorescence changes of wt hSR and mutants were carried out under the assumption of a pseudo-first order kinetic at high GSNO concentrations (Rossi et al. 1997) using a sum of two exponential decays, plus a baseline to account for the residual activity:

$$A = A_0 + a_1 e^{-[GSNO]k_1 t} + a_2 e^{-[GSNO]k_2 t} \qquad \text{(eq. 2)}$$

where A is the enzyme activity or the initial fluorescence signal, A_0 is the residual activity or the residual fluorescence signal, a_1 and a_2 the amplitudes of the two inhibition phases; k_1 and k_2 are the second order rate constants.

The analysis of the GSNO inactivation kinetics for the mutants that did not exhibit a biphasic behaviour were carried out under the assumption of a pseudo-first order kinetic at high GSNO concentrations (Rossi et al. 1997) using a single exponential decay, plus a baseline to account for the residual activity:

$$A = A_0 + ae^{-[GSNO]kt} \qquad \text{(eq. 3)}$$

where A is the enzyme activity or the initial fluorescence signal, A_0 is the residual activity or the residual fluorescence signal, *a* the amplitude of the inhibition time course and k the reaction rate constant.

The determination of the ATP binding parameters was determined with a sigmoidal equation to take into account the binding cooperativity (Marchetti et al. 2013).

$$A = A_0 + a\frac{[ATP]^n}{EC_{50}{}^n + [ATP]^n} \qquad \text{(eq. 4)}$$

where A is the enzyme activity, A_0 is the basal activity in the absence of nucleotides, [ATP] is the concentration of ATP, EC_{50} is their half maximal effective concentration and n is the Hill coefficient.

5.2 RESULTS AND DISCUSSION

In the presence of 6 mM ATP, the deaminase activity of wild type (wt) hSR is inhibited by addition of 150 μM GSNO in a time-dependent biphasic fashion, with an observed rate constant of 0.59 ± 0.02 min^{-1} for the fast phase (Figure 5.2.1a). When glycine, a non-productive substrate analogue, was also added at 3 mM final concentration, the time course of the inhibition induced by GSNO was severely slowed down (Figure 5.2.1a). The events triggered by GSNO could also be monitored by fluorescence spectroscopy upon excitation at 445 nm, following the emission at 490 nm (in the absence of glycine) or 482 nm (in the presence of glycine) (Figure 5.2.1b). When GSNO was added to the ATP-bound enzyme, fluorescence intensity decreased over time around 3.3-fold, with an observed rate constant for the fast phase of 0.380 ± 0.005 min^{-1}, fully consistent with the event monitored through enzyme assays. Unlike enzyme assays, fluorescence experiments could be carried out at saturating concentrations of glycine. At 80 mM concentration, only a slow phase could be detected (Figure 5.2.1b). All fluorescence and enzyme activity changes were reversed by addition of the reducing agent TCEP (data not shown).

Mutant hSR C2S, C4S, C128S, C269S, C309S (Δ5Cys, Table 2) was designed to isolate the effects of Cys113, as it lacks both Cys128 and Cys269, which can undergo S-nitrosylation (Marchesani et al. 2018), as well as the other solvent-exposed residues Cys2, Cys4 and Cys309, all mutated to Ser. The remaining Cys residues – Cys46 and Cys217 and Cys113 – were shown to be critical for protein function and folding (Mustafa et al. 2007). The Δ5Cys mutant exhibited a behaviour similar to wt hSR (Figure 5.2.1c) - albeit with a smaller fluorescence decrease – further confirming that the conformation-

dependent effect of S-nitrosylation is mainly associated with Cys113. The pseudo first-order rate constant of 0.14 ± 0.02 min^{-1} is only slightly lower than that observed for wt hSR.

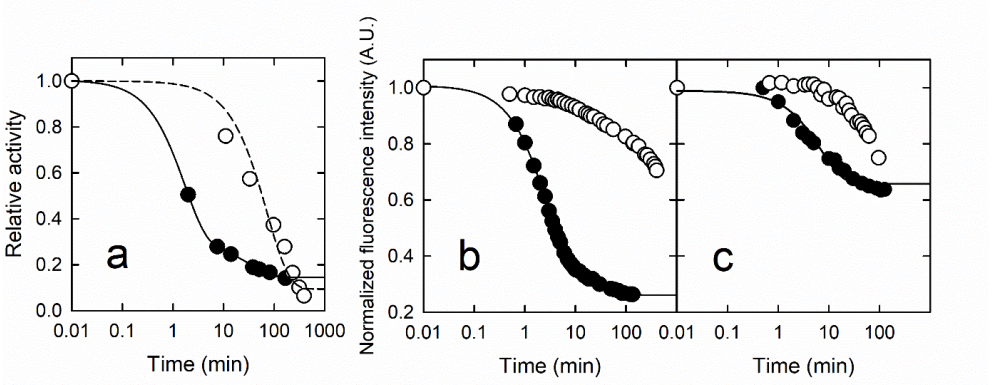

Figure 5.2.1: (a) Kinetics of wt hSR activity loss upon incubation with 150 μM of GSNO in a buffered solution containing 50 mM TEA, 150 mM NaCl, 6 mM ATP 10 mM $MgCl_2$ at pH 8.0 in the absence (closed circles) and presence (open circles) of 3 mM glycine. **(b)** Fluorescence kinetics of wt hSR upon incubation with 150 μM of GSNO in a buffered solution containing 50 mM TEA, 150 mM NaCl, 6 mM ATP and 10 mM $MgCl_2$ at pH 8.0, in the absence (closed circles) and presence (open circles) of 80 mM glycine. **(c)** Fluorescence kinetics of the Δ5Cys mutant in a buffered solution containing 50 mM TEA, 150 mM NaCl, 6 mM ATP and 10 mM $MgCl_2$ at pH 8.0, in the absence (closed circles) and presence (open circles) of 80 mM glycine. The lines are the fitting of the experimental data to a sum of two exponential decays, with the exception of the kinetic of wt hSR activity in the presence of both ATP and glycine and fluorescence kinetics of the Δ5Cys mutant in the presence of ATP, which were fitted with a mono exponential decay.

Differential tagging of cysteine residues with the 5-iodoacetamide-fluoresceine\iodoacetamide S-nitrosylation detection method (5IAF\IAA method) allowed comparing the extent of GSNO-induced S-nitrosylation under different conditions, known to correspond to different protein conformations, as inferred from the crystal structures of SpSR, rat SR and hSR

(Goto et al. 2009; Smith et al. 2010; Takahara et al. 2017; Yamauchi et al. 2009). Incubation with GSNO was carried out for 90 minutes, approximately the time required for the fast phase of wt hSR to complete in the absence of glycine (Figure 5.2.1a).

In the presence of Mg^{2+}, which binds at a specific site in the large domain and activates the enzyme 10-fold (Bruno et al. 2017; Cook et al. 2002; Goto et al. 2009; Ito et al. 2012; Smith et al. 2010), only a faint fluorescence band was observed (Figure 5.2.2a). Under these conditions, SR is known to exhibit an open conformation from the crystallographic structure of all orthologues (Goto et al. 2009; Smith et al. 2010; Takahara et al. 2017; Yamauchi et al. 2009). In the presence of EDTA, which chelates Mg^{2+}, a similarly faint band was detected. No crystallographic structure under this condition is available, but fluorescence experiments suggested an open-like conformation (Bruno et al. 2017). In the presence of ATP, which produces a change in relative orientation between the two monomers, according to the crystallographic structure of SpSR (Goto et al. 2009), the fluorescence band is 6-fold more intense (Figure 5.2.2a), suggesting that the conformation it stabilizes is significantly more prone to nitrosylation. Glycine alone marginally increased fluorescence in comparison with the forms not incubated with ATP (Figure 5.2.2), as did malonate (data not shown). Both are known to stabilize a closed conformation, characterized by a rotation of 20° of the small domain towards the large one (Smith et al. 2010). When both glycine and ATP are present, a fluorescence band similar to that observed in the presence of ATP alone could be seen (Figure 5.2.2a). It is interesting to notice that in this conformation nitrosylation takes place (Figure 5.2.2) but the nitrosylation kinetics is severely slowed down, with around 20% reduction in fluorescence signal after 90 minutes (Figure 5.2.1).

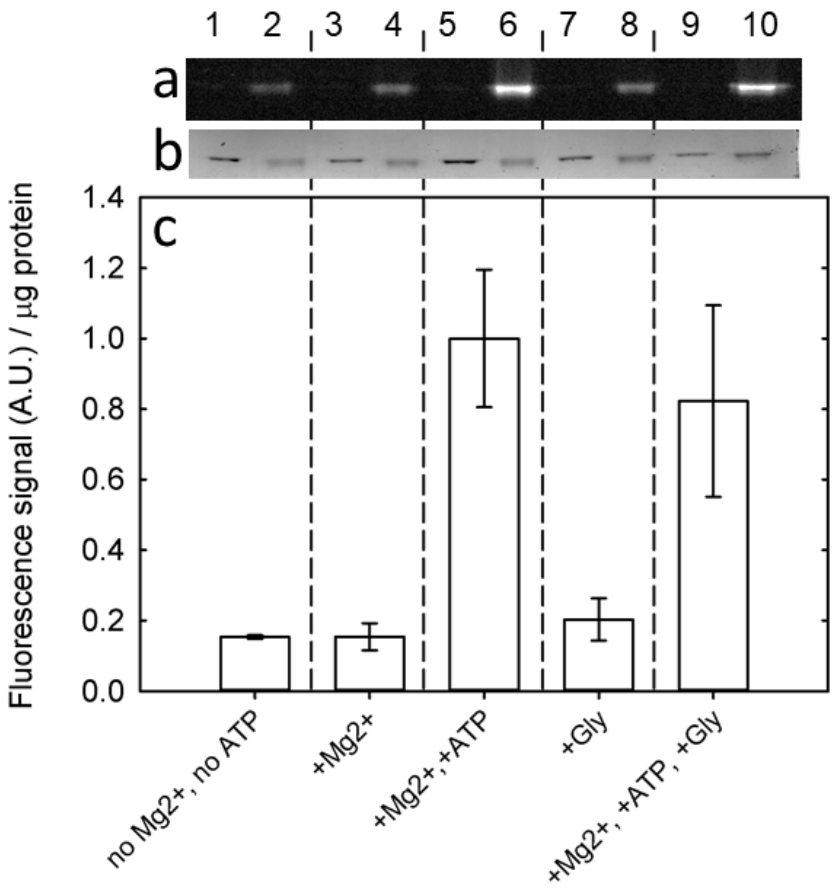

Figure 5.2.2: 5-IAF\IAA method applied to wt hSR in a 50 mM TEA, 150 mM NaCl, solution at pH 8.0 added of: i) 5 mM EDTA (lanes 1 and 2); ii) 10 mM $MgCl_2$ (lanes 3 and 4) iii) 6 mM ATP and 10 mM $MgCl_2$ (lanes 5 and 6); iv) 80 mM glycine (lanes 7 and 8); v) 6 mM ATP,10 mM $MgCl_2$ and 80 mM glycine (lanes 9 and 10). For each condition, hSR was either preincubated with 150 µM GSNO for 90 minutes (lanes 2, 4, 6, 8, 10) or not (lanes 1, 3, 5, 7, 9). 0.2 µg of hSR were loaded in each lane of an SDS-PAGE gel. Both the fluorescence signal (a) and the Coomassie blue staining signal (b) were collected. The bars in plot (c) are the ratios between the fluorescence signal and the Coomassie blue staining signal, subtracted of the respected control. Values were then normalized to 1. The error bars are the s.e.m. of at least two independent experiments.

The different nitrosylation pattern in the different conditions was confirmed by mass-spectrometry (Table 2). Peptide LEGIPAYIVVPQTAPDCK, containing Cys113, was identified in all samples either modified by carboamidomethylation (as double charged species, +57.02) or modified by covalent binding with 5IAF (triple charged species, +387.07). In the presence of ATP alone and of both ATP and glycine, a higher MS\MS coverage was observed in comparison with the other conditions, with 6 y ions.

	Peptide: LEGIPAYIVVPQTAPDC(+387.07)K			Peptide: LEGIPAYIVVPQTAPDC(+57.02)KK		
	m/z	R.T. (min)	MOD.	m/z	R.T. (min)	MOD.
EDTA	767.6970 (z = 3)	36.25	5IAF	986.0158 (z = 2)	31.27	IAA
Mg^{2+}	767.6962 (z = 3)	36.29	5IAF	986.0148 (z = 2)	31.33	IAA
ATP	767.6965 (z = 3)	36.16	5IAF	986.0151 (z = 2)	31.14	IAA
Gly	767.6970 (z = 3)	36.34	5IAF	986.0165 (z = 2)	31.32	IAA
ATP + Gly	767.6978 (z = 3)	36.27	5IAF	986.0159 (z = 2)	31.25	IAA

Table 2

A targeted relative quantification based on the chromatographic peaks was performed for peptide LEGIPAYIVVPQTAPDCK, which exhibited a retention time of 31.2 minutes in the carboamidomethyled form and 36.2 in the 5IA-conjugated form. The ratios between the intensities are reported in Figure 5.2.3. The results are fully consistent with the evaluation of total nitrosylation

(Figure 5.2.2), albeit a reduced relative level was observed for Cys113 in the mass spectrometry experiment in the presence of both ATP and glycine.

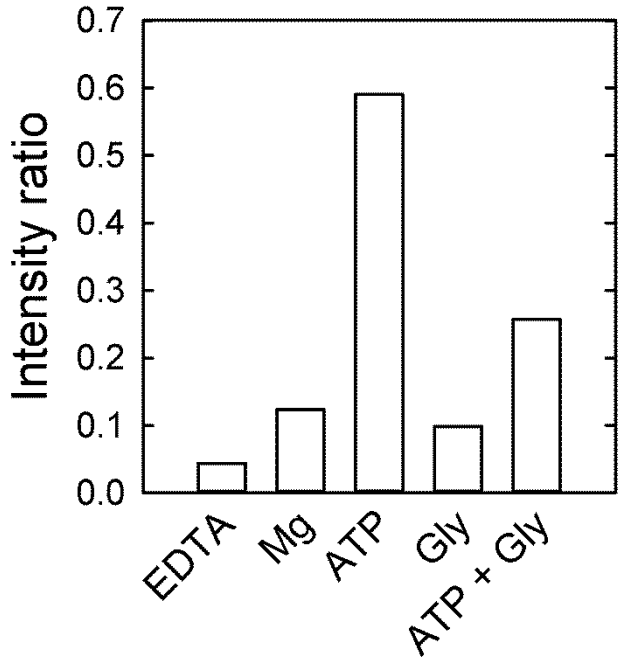

Figure 5.2.3: intensity ratios of the peaks of the peptide modified with 5-IAF (LEGIPAYIVVPQTAPDC(+387.07)K) normalized for the sum between the intensity of the peptide modified with 5-IAF and the one modified with IAA (LEGIPAYIVVPQTAPDC(+57.02)KK)

Cys113 lies on the N-terminus of helix H5 in the small domain and the closest neighbouring residues are on the large domain, in the loop between β-strand S10 and helix H14. In the absence of ATP and active-site ligands, Cys113 is exposed to the solvent (Figure 5.2.4a). Upon ligation of ATP, hSR – as modelled on the basis of the SpSR complex with AMP-PCP (Goto et al. 2009) – undergoes local changes within an open conformation, with Asp318

getting closer to Cys113 (5.2 Å), possibly within reach of the S-nitroso derivative (Figure 5.2.4b). Considering a length of the nitroso group of around 2 Å, also Lys114, Gln89 and Asn316 become within reach of direct interactions. The adenine ring of ATP is around 6 Å apart from Cys113 (Figure 5.2.4b). However, we had ruled out the possibility of a direct and specific interaction between ATP and Cys113 (Marchesani et al. 2018). Malonate, similarly to serine and supposedly glycine (Smith et al. 2010), stabilizes a closed conformation, bringing about a significant rearrangement of the surroundings of Cys113 (Figure 5.2.4c). In particular, the distances from the lateral chain of Asp318 (3.8 Å), as well as from the backbone carbonyl group of Val317 (3.9 Å), become consistent with hydrogen bonds. It is possible that, in the presence of malonate or glycine, and without ATP, Cys113 is partially buried and therefore S-nitrosylation is not favoured. The binding of ATP could shift the position of Cys113, both in the absence and presence of an active-site ligand, towards a conformation in which Cys113 has an intermediate position between the closed and open form, which is more prone to nitrosylation.

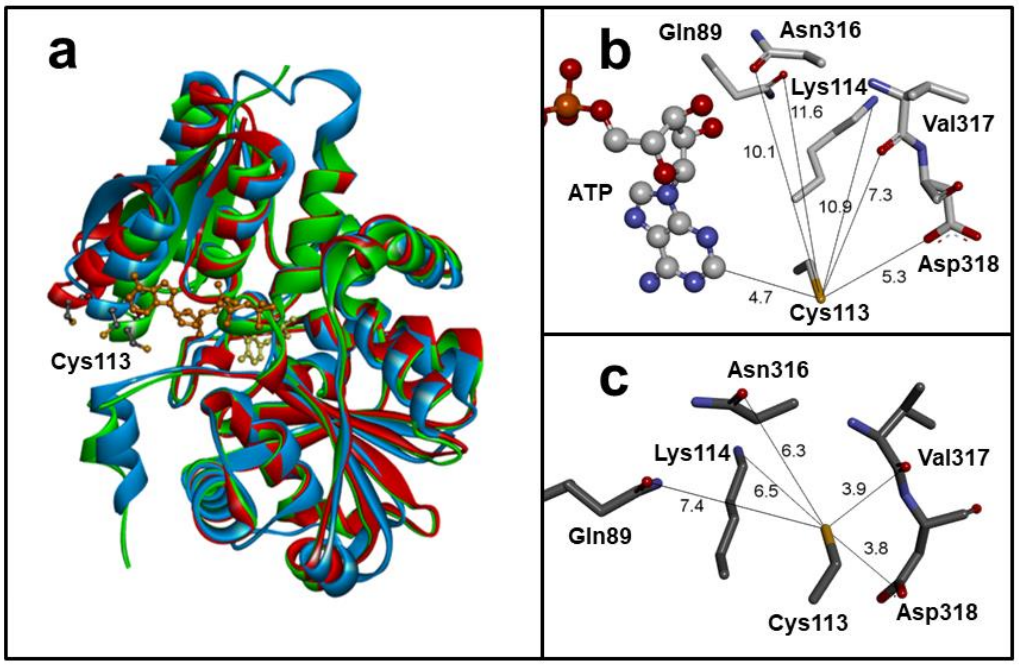

Figura 5.2.4: (a) Superimposition of the structures of hSR crystallized in the absence of ATP and active-site ligands (pdb 5X2L, in red), in the presence of ATP, as modelled on the structure of SpSR in complex with AMP-PCP (in blue) and in the presence of malonate (pdb 3L6B in green). Cys113 is represented in ball and sticks. PLP is represented in yellow, ATP is represented in orange. **(b)** Detail of the environment of Cys113 in the model of hSR bound to ATP based on the structure of SpSR in complex with AMP-PCP. ATP is represented in ball and sticks. **(c)** Detail of the environment of Cys113 in the structure of hSR in complex with malonate (**c**, pdb 3L6B). All distances are in Å.

In search of the structural determinants that promote and stabilize Cys113 S-nitrosylation, we have already shown that the spatially adjacent acidic residue Asp318 is not crucial for nitrosylation (Marchesani et al. 2018). Moreover, Cys113 is within the sequence Pro-Asp-Cys113-Lys-Lys, which does not correspond to the recognition motif required for iNOS-S100A8/A9-mediated S-nitrosylation (Jia et al. 2014). Therefore, we comprehensively evaluated by site-directed mutagenesis the effect of all the residues

surrounding Cys113, since this pocket undergoes significant conformational changes depending on the ligation state of SR, modulating its nitrosylation, as suggested for other. Based on the structural observations, we expressed, purified and characterized mutants K114Q, N316A and D318A (Table 3). The characterization of mutants Q89M and D318N has already been reported (Canosa et al. 2018; Marchesani et al. 2018).

Mutant	**$K_{M,\ L\text{-serine}}$ (mM)**	**k_{cat} (min^{-1})**	**k_{cat}/K_M ($min^{-1}mM^{-1}$)**	**$K_{50}/K_{d\ ATP}$ (mM)**	**n_{ATP}**	**Ref.**
Wt hSR	16 ± 1	166 ± 10	10	0.21 ± 0.01	1.8 ± 0.2	(Marchesani et al. 2018)
C113S	54 ± 5	51 ± 2	0.9	1.07 ± 0.06	1.6 ± 0.2	(Marchesani et al. 2018)
D318N	50 ± 3	115 ± 2	2.3	0.68 ± 0.03	1.8 ± 0.1	(Marchesani et al. 2018)
D318A	33 ± 6	70 ± 0,9	2.1	0.55 ± 0.05	1.7 ± 0.3	This work
N316A	40.6 ± 1.19	7.64 ± 0.05	0.2	n. a.	n. a.	This work
K114Q	18.7 ± 1.3	6.31 ± 0.08	0.4	0.11 ± 0.03	0.8 ± 0.2	This work
Q89M	19±2	56±1	3	0.15 ± 0.01	non coop	(Canosa et al. 2018)
C2S, C4S, C128S, C269S, C309S (Δ5Cys)	48 ± 9	56.6 ± 2.9	1.2	0.24 ± 0.04	1.67 ± 0.5	This work

Table 3: Kinetic parameters and ATP binding parameters for mutants used in this study

For all mutants, S-nitrosylation kinetics were followed by fluorescence spectroscopy in the presence of ATP or with both ATP and glycine (Figure 5.2.5). K114Q and Q89M mutants exhibited a behaviour similar to wt hSR, with fast nitrosylation kinetics in the presence of ATP alone (Figure 5.2.5a) and a much slower one when glycine was also added (Figure 5.2.5b). However, nitrosylation of K114Q hSR exhibited a rate constant 5.5-fold lower than wt hSR (0.0690 ± 0.002 min^{-1} vs 0.380 ± 0.005 min^{-1}), indicating that this residue plays a role in the stabilization of the nitroso derivative. As for wt hSR, the time course for Q89M hSR was biphasic, but with a larger amplitude of the slow phase, confirming that the perturbation of the surroundings of Cys113 modulates the nitrosylation kinetics.

Mutant N316A exhibited an opposite behaviour in comparison with K114Q and Q89M, with no decrease in fluorescence intensity when incubated with GSNO in the presence of ATP alone (data not shown). It should be noticed that Asn316 is involved in a hydrogen bond with the ribose group of ATP (Goto et al. 2009) and its mutation largely prevent its binding.

The nitrosylation of mutant D318N – unlike wt hSR and all other mutants – was only modestly slowed down in the presence of both glycine and ATP (Figure 5.2.5b), with a pseudo first order constant for the fast phase of 0.052 ± 0.003 min^{-1}. This behaviour could be explained in light of the direct hydrogen bond between Asp318 and Cys113 in the closed conformation (Figure 5.2.4), which could be crucial to prevent the allosteric inhibition by S-nitrosylation. Indeed, once Asp318 is mutated to asparagine, with substitution of the charged carboxylic group, the glycine-stabilized conformation becomes more susceptible to inhibition by S-nitrosylation, unlike wt hSR and all other mutants. In the presence of ATP alone, Cys113 nitrosylation was faster than

for wt hSR, with a pseudo first-order constant of 1.934 ± 0.100 min^{-1}, with a different amplitude for the fast and slow phase (Figure 5.2.5a).

Mutant C113S did not exhibit any fast phase in the presence of ATP (Figure 5.2.5a), confirming the association between the fluorescence signal and Cys113 nitrosylation. In the presence of both ATP and glycine, the slow phase observed for C113S hSR was superimposable to that of wt hSR, confirming that this slow phase is not associated to Cys113 (Figure 5.2.5), but, possibly, to nitrosylation of Cys128 and Cys269, which were previously identified as alternative nitrosylation sites (Marchesani et al. 2018). It is possible that in the closed conformation (with glycine or malonate) the pKa of Cys113 is higher, due to the presence of the negatively charged group of Asp318 at 3.8 Å distance. When no ligand is present at the active site, on the other hand, Asp318 shifts with respect to the sulphur atom of Cys113 and therefore the formation of the stronger nucleophile thiolate might be favoured, thus promoting S-nitrosylation.

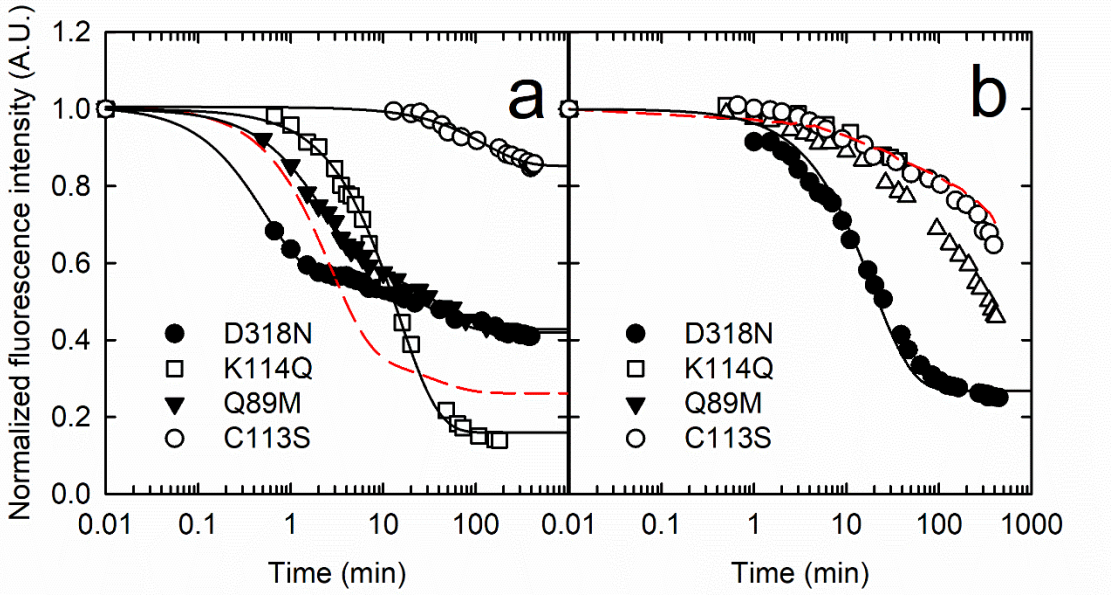

Figure 5.2.5: Fluorescence kinetics of wt hSR and hSR mutants upon incubation with 150 μM of GSNO in **(a)** a buffered solution containing 50 mM TEA, 150 mM NaCl, 6 mM ATP 10 mM $MgCl_2$ at pH 8.0 and **(b)** in the same solution added of 80 mM glycine. The red dashed lines are the fitting of the experimental points obtained for wt hSR in both conditions (Figure 5.2.1). The solid lines are the fitting of the experimental points with a sum of two exponential decays, with the exception of the fluorescence kinetics of K114Q hSR and C113S hSR in the presence of ATP and D318N hSR in the presence of both ATP and glycine, which were fitted with a mono exponential decay.

S-nitrosylation was then directly evaluated using the 5-IAF\IAA method for all the mutants of residues surrounding Cys113 (Figure 5.2.6). All of them, in the presence of 6 mM ATP and 10 mM $MgCl_2$, exhibited a nitrosylation degree comparable to wt hSR, indicating that no single residue is strictly crucial for the nitrosylation to take place.

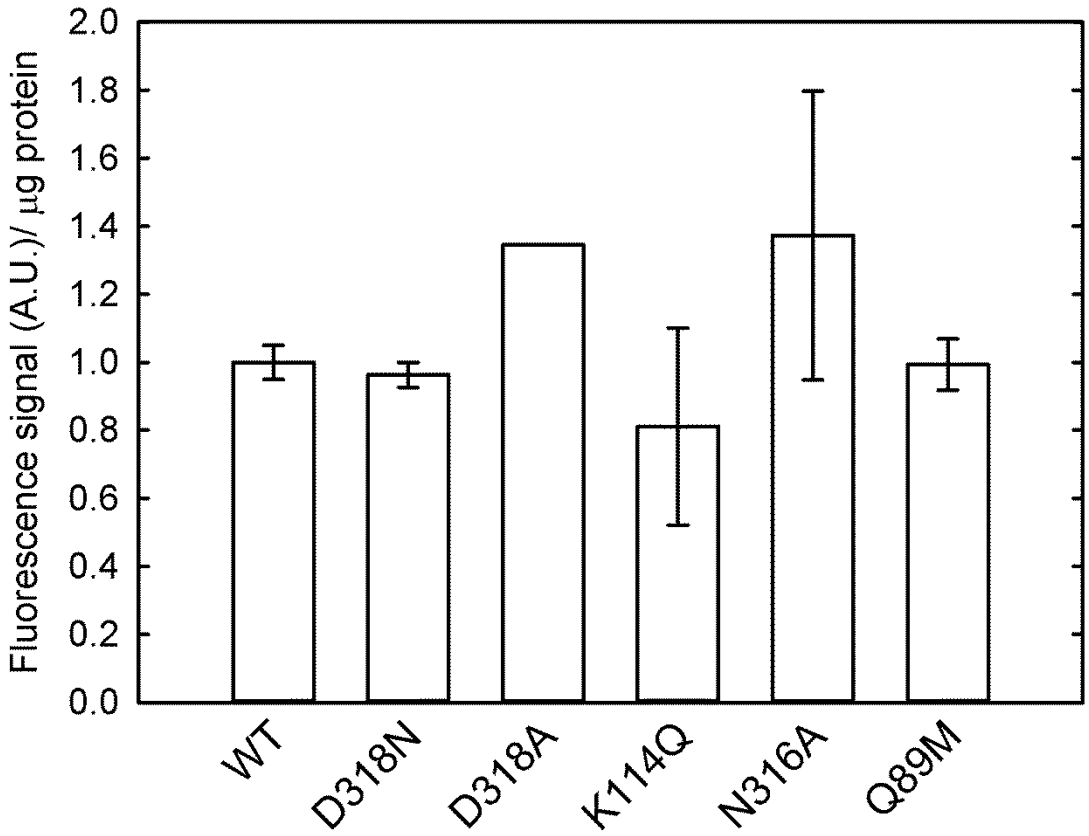

Figura 5.2.6: 5-IAF\IAA method applied to hSR mutants in a 50 mM TEA, 150 mM NaCl, 6 mM ATP and 10 mM $MgCl_2$ solution at pH 8.0. Each mutant was pre-incubated with 150 μM GSNO for 90 minutes. 0.8 μg of hSR mutants were loaded in each lane of an SDS-PAGE gel. Both the fluorescence signal and the Coomassie blue staining signal were collected. The bars in plot are the ratios between the fluorescence signal and the Coomassie blue staining signal, subtracted of the respective control. Values were then normalized to the value measured for wt hSR. The error bars are the s.e.m. of at least two independent experiments.

From the results of fluorescence kinetics (Figure 5.2.1) and differential labelling method (Figure 5.2.2), it appears that the closed pocked stabilized by either malonate or glycine does not prevent nitrosylation but it prevents the conformational rearrangement responsible for allosteric inhibition. In the absence of ATP, nitrosylation takes place only to limited extent (Figure 5.2.2).

6. CONCLUSIONS

Human serine racemase (hSR) is strongly regulated by post-translational modifications, small ligands and protein interactors. It is also a promising target for neurodegenerative diseases, being the only enzyme involved in both the synthesis and degradation of D-serine, the obligatory co-agonist of the NMDA receptor for glutamate. Unfortunately, the efforts made to target the active site of this enzyme did not yield molecules endowed with drug-like properties. In this work, the possibility to target hSR at different sites has been investigated by characterizing the complex conformational space of the protein and its regulation by allosteric ligands.

Firstly, we characterized the inhibition of hSR by NADH and we concluded that 1,4 dihydro nicotinamide derivatives are partial, allosteric inhibitors, binding in a cleft close to the ATP binding site. The redox state of the nicotinamidic ring is crucial, as only the partially reduced form is effective. From a physiological point of view, the ratio between NAD and NADH is strongly shifted towards the oxidized species. Conversely, NADPH is the predominant species in the redox equilibrium with $NADP^+$, but its cytosolic concentrations are very low (Ying et al. 2008). These considerations suggest that, considering the relatively high IC50s, the partial inhibition and the low physiological concentrations, it appears unlikely that NADH or NADPH may have a role in hSR modulation *in vivo*. However, NMN was recently shown to accumulate after nerve damage, reaching concentrations in the micromolar range and promoting axon degeneration (Magni et al. 2004). These findings might suggested that NMN acts as a hSR modulator in response to nerve injury.

Secondly, we have characterized the oligomerisation state of this enzyme in the presence of allosteric ligands such as divalent metals (Mg^{++} and Ca^{++}) and ATP. Considering the physiological concentrations of ATP, Mg^{2+} and Na^{+} in neurons, it is possible to speculate that a tetrameric state is indeed stabilized within the cell, depending on its ligation state and on ionic interactions. Inhibitors of the protein-protein interactions involved in the tetramerization might be a possible strategy to modulate the activity of hSR.

Finally, we have shown that S-nitrosylation produces inhibition in a time-dependent manner, involving three cysteine residues. NO-induced inhibition depends on hSR conformation; in particular, it is faster in the presence of ATP or glycine and markedly slower in the presence of both. Therefore, we concluded that hSR can be a target of NO – shown to be produced at the NMDA synaptic system – depending on its ligation state. As hSR is around 50% glycine-saturated at its physiological concentration of around 1 mM and nearly fully ATP-saturated, we suggest that slight changes in the concentrations of ATP and glycine – another NMDA co-agonist – might affect D-serine production through the conformation-dependent nitrosylation of hSR. These observations open the possibility to target this enzyme at alternative sites that have never been considered before. Indeed, S-nitrosylation sites in proteins have been evaluated only recently for targeting enzyme. For example, S-nitrosylated glyceraldehyde 3-phosphate dehydrogenase (GAPDH) binds the protein Siah1 and the complex co-translocate in the nucleus, leading to apoptosis. The drugs deprenyl and omigapil prevent GAPDH S-nitrosylation and disrupt the formation of the complex, blocking the apoptotic process (Hara et al. 2006).

REFERENCES

Akhter S, Vignini A, Wen Z, English A, Wang PG, Mutus B (2002) Evidence for S-nitrosothiol-dependent changes in fibrinogen that do not involve transnitrosation or thiolation. Proc Natl Acad Sci U S A 99:9172-9177 doi:10.1073/pnas.142136499.

Anand P, Stamler JS (2012) Enzymatic mechanisms regulating protein S-nitrosylation: implications in health and disease. J Mol Med (Berl). 2012 Mar; 90(3): 233–244.

Balu, D.T., Li, Y., Puhl, M.D., Benneyworth, M.A., Basu, A.C., Takagi, S., Bolshakov, V.Y., and Coyle, J.T. (2013). Multiple risk pathways for schizophrenia converge in serine racemase knockout mice, a mouse model of NMDA receptor hypofunction. Proc. Natl. Acad. Sci. U.S.A. 110**,** E2400-E2409.

Baumgart F, Mancheño J, Rodríguez-Crespo I (2007) Insights into the activation of brain serine racemase by the multi-PDZ domain glutamate receptor interacting protein, divalent cations and ATP. vol 274. doi:10.1111/j.1742-4658.2007.05986.x.

Beato, C., Pecchini, C., Cocconcelli, C., Campanini, B., Marchetti, M., Pieroni, M., Mozzarelli, A., and Costantino, G. (2015). Cyclopropane derivatives as potential human serine racemase inhibitors: unveiling novel insights into a difficult target. Journal of Enzyme Inhibition and Medicinal Chemistry**,** 1-8.

Bettati, S., Benci, S., Campanini, B., Raboni, S., Chirico, G., Beretta, S., Schnackerz, K.D., Hazlett, T.L., Gratton, E., and Mozzarelli, A. (2000). Role of pyridoxal 5'-phosphate in the structural stabilization of O-acetylserine sulfhydrylase. Journal of Biological Chemistry 275, 40244-40251.

Blankenhorn G, Moore EG (1980) Sulfoxylate ion (HSO2-), the hydride donor in dithionite-dependent reduction of NAD+ analogs. J Am Chem Soc 102:1092-1098 doi:10.1021/ja00523a028.

Bruno S, Marchesani F, Dellafiora L, Margiotta M, Faggiano S, Campanini B, Mozzarelli A (2016) Human serine racemase is allosterically modulated by NADH and reduced nicotinamide derivatives. Biochem Journal 473:3505-3516 doi:10.1042/BCJ20160566.

Bruno, S., Margiotta, M., Marchesani, F., Paredi, G., Orlandi, V., Faggiano, S., Ronda, L., Campanini, B., and Mozzarelli, A. (2017). Magnesium and calcium ions differentially affect human serine racemase activity

and modulate its quaternary equilibrium toward a tetrameric form. Biochim Biophys Acta 1865, 381-387.

Campanini, B., Raboni, S., Vaccari, S., Zhang, L., Cook, P.F., Hazlett, T.L., Mozzarelli, A., and Bettati, S. (2003). Surface-exposed tryptophan residues are essential for O-acetylserine sulfhydrylase structure, function, and stability. Journal of Biological Chemistry 278, 37511-37519.

Canosa, A.V., Faggiano, S., Marchetti, M., Armao, S., Bettati, S., Bruno, S., Percudani, R., Campanini, B., and Mozzarelli, A. (2018). Glutamine 89 is a key residue in the allosteric modulation of human serine racemase activity by ATP. Sci Rep 8, 9016.

Canu N, Ciotti MT, Pollegioni L (2014) Serine racemase: a key player in apoptosis and necrosis. Frontiers in synaptic neuroscience 6:9 doi:10.3389/fnsyn.2014.00009.

Conti P, Tamborini L, Pinto A, Blondel A, Minoprio P, Mozzarelli A, De Micheli C (2011) Drug discovery targeting amino acid racemases. Chem Rev 111:6919-6946 doi:10.1021/cr2000702.

Cook SP, Galve-Roperh I, del Pozo AM, Rodriguez-Crespo I (2002) Direct calcium binding results in activation of brain serine racemase J Biol Chem 277:27782-27792 doi:10.1074/jbc.M111814200.

Copeland RA (2000) Enzymes: A Practical Introduction to Structure, Mechanism, and Data Analysis. Wiley-VCH, Inc.

De Miranda J, Panizzutti R, Foltyn VN, Wolosker H (2002a) Cofactors of serine racemase that physiologically stimulate the synthesis of the N-methyl-D-aspartate (NMDA) receptor coagonist D-serine. Proc Natl Acad Sci USA 99:14542-14547 doi:10.1073/pnas.222421299.

Dellafiora, L., Marchetti, M., Spyrakis, F., Orlandi, V., Campanini, B., Cruciani, G., Cozzini, P., and Mozzarelli, A. (2015). Expanding the chemical space of human serine racemase inhibitors. Bioorganic & Medicinal Chemistry Letters.

Devarie-Baez NO, Zhang D, Li S, Whorton AR, Xian M (2013) Direct methods for detection of protein S-nitrosylation. Methods 62:171-176 doi:10.1016/j.ymeth.2013.04.018.

Di Stefano M, Nascimento-Ferreira I, Orsomando G, Mori V, Gilley J, Brown R, Janeckova L,Vargas M E, Worrell L A,Loreto A,Tickle J, Patrick J, Webster J R M, Marangoni M,Carpi F M,Pucciarelli S,Rossi F,Meng W, Sagasti A, Ribchester R R, Magni G,Coleman MP, Conforti L (2014) A rise in NAD precursor nicotinamide mononucleotide (NMN)

after injury promotes axon degeneration. Cell Death and Differentiation (2015) 22, 731–742; doi:10.1038/cdd.2014.164;

Dixon SM, Li P, Liu R, Wolosker H, Lam KS, Kurth MJ, Toney MD (2006a) Slow-binding human serine racemase inhibitors from high-throughput screening of combinatorial libraries J Med Chem 49:2388-2397 doi:10.1021/jm050701c.

Dumin E, Bendikov I, Foltyn VN, Misumi Y, Ikehara Y, Kartvelishvily E, Wolosker H (2006) Modulation of D-serine levels via ubiquitin-dependent proteasomal degradation of serine racemase J Biol Chem 281:20291-20302 doi:10.1074/jbc.M601971200.

Foltyn, V.N., Bendikov, I., De Miranda, J., Panizzutti, R., Dumin, E., Shleper, M., Li, P., Toney, M.D., Kartvelishvily, E., and Wolosker, H. (2005). Serine racemase modulates intracellular D-serine levels through an alpha,beta-elimination activity. Journal of Biological Chemistry 280, 1754-1763.

Forrester MT, Foster MW, Benhar M, Stamler JS (2009) Detection of protein S-nitrosylation with the biotin-switch technique Free Radic Biol Med 46:119-126 doi:10.1016/j.freeradbiomed.2008.09.034.

Fujii, K., Maeda, K., Hikida, T., Mustafa, A.K., Balkissoon, R., Xia, J., Yamada, T., Ozeki, Y., Kawahara, R., Okawa, M., Huganir, R.L., Ujike, H., Snyder, S.H., and Sawa, A. (2005). Serine racemase binds to PICK1: potential relevance to schizophrenia. Molecular Psychiatry 11, 150.

Genc S, Kurnaz IA, Ozilgen M (2011) Astrocyte - neuron lactate shuttle may boost more ATP supply to the neuron under hypoxic conditions - in silico study supported by in vitro expression data BMC System Biology 5:162 doi:10.1186/1752-0509-5-162.

Goto, M., Yamauchi, T., Kamiya, N., Miyahara, I., Yoshimura, T., Mihara, H., Kurihara, T., Hirotsu, K., and Esaki, N. (2009). Crystal Structure of a Homolog of Mammalian Serine Racemase from Schizosaccharomyces pombe. Journal of Biological Chemistry 284, 25944-25952.

Greco TM, Hodara R, Parastatidis I, Heijnen HF, Dennehy MK, Liebler DC, Ischiropoulos H (2006) Identification of S-nitrosylation motifs by site-specific mapping of the S-nitrosocysteine proteome in human vascular smooth muscle cells Proc Natl Acad Sci U S A 103:7420-7425 doi:10.1073/pnas.0600729103.

Gribble FM, Loussouarn G, Tucker SJ, Zhao C, Nichols CG, Ashcroft FM (2000) A Novel Method for Measurement of Submembrane ATP

Concentration J Biol Chem 275:30046-30049 doi:10.1074/jbc.M001010200.

Hanley, J.G. (2008). PICK1: A multi-talented modulator of AMPA receptor trafficking. Pharmacol Ther 118, 152-160.

Hara MR, Thomas B, Cascio MB, Bae BI, Hester LD, Dawson VL, Dawson TM, Sawa A, Snyder SH (2006) Neuroprotection by pharmacologic blockade of the GAPDH death cascade. Proc Natl Acad Sci U S A. 2006 Mar 7;103(10):3887-9. Epub 2006 Feb 27.

Henneberger C, Papouin T, Oliet SHR, Rusakov DA (2010) Long term potentiation depends on release of D-serine from astrocytes. Nature. 2010 Jan 14;463(7278):232-6. doi: 10.1038/nature08673.

Hikida, T., Mustafa, A.K., Maeda, K., Fujii, K., Barrow, R.K., Saleh, M., Huganir, R.L., Snyder, S.H., Hashimoto, K., and Sawa, A. (2008). Modulation of D-serine levels in brains of mice lacking PICK1. Biological Psychiatry 63, 997-1000.

Hoffman HE, Jiraskova J, Cigler P, Sanda M, Schraml J, Konvalinka J (2009) Hydroxamic acids as a novel family of serine racemase inhibitors: mechanistic analysis reveals different modes of interaction with the pyridoxal-5'-phosphate cofactor J Med Chem 52:6032-6041 doi:10.1021/jm900775q.

Ito T, Hayashida M, Kobayashi S, Muto N, Hayashi A, Yoshimura T, Mori H (2016) Serine racemase is involved in d-aspartate biosynthesis J Biochem 160:345-353 doi:10.1093/jb/mvw043.

Ito, T., Murase, H., Maekawa, M., Goto, M., Hayashi, S., Saito, H., Maki, M., Hemmi, H., and Yoshimura, T. (2012). Metal ion dependency of serine racemase from Dictyostelium discoideum. Amino Acids 43, 1567-1576.

Jager J, Moser M, Sauder U, Jansonius JN (1994) Crystal structures of Escherichia coli aspartate aminotransferase in two conformations. Comparison of an unliganded open and two liganded closed forms J Mol Biol 239:285-305 doi:10.1006/jmbi.1994.1368.

Jansonius JN, Vincent MG (1987). In: Jurnak FA, and McPherson A (ed) Biological Macromolecules and Assemblies, vol 3. J. Wiley & Sons, Inc., New York, pp 187–285.

Jia J, Arif A, Terenzi F, Willard B, Plow EF, Hazen SL, Fox PL (2014) Target-selective protein S-nitrosylation by sequence motif recognition Cell 159:623-634 doi:10.1016/j.cell.2014.09.032.

Jiraskova-Vanickova J, Ettrich R, Vorlova B, Hoffman HE, Lepsik M, Jansa P, Konvalinka J (2011) Inhibition of human serine racemase, an emerging target for medicinal chemistry Curr Drug Targets 12:1037-1055.

Kiriyama Y, Nochi H (2016) D-Amino Acids in the Nervous and Endocrine Systems vol 2016. doi:10.1155/2016/6494621.

Koskiniemi S, Garza-Sánchez F, Sandegren L, Webb JS, Braaten BA, Poole SJ, Andersson DI, Hayes CS, Low DA (2014) Selection of orphan Rhs toxin expression in evolved Salmonella enterica serovar Typhimurium PLoS Genet 10:e1004255 doi:10.1371/journal.pgen.1004255.

Labrie, V., Fukumura, R., Rastogi, A., Fick, L.J., Wang, W., Boutros, P.C., Kennedy, J.L., Semeralul, M.O., Lee, F.H., Baker, G.B., Belsham, D.D., Barger, S.W., Gondo, Y., Wong, A.H., and Roder, J.C. (2009). Serine racemase is associated with schizophrenia susceptibility in humans and in a mouse model. Human Molecular Genetics 18, 3227-3243.

Lee TY, Chen YJ, Lu TC, Huang HD, Chen YJ (2011) SNOSite: exploiting maximal dependence decomposition to identify cysteine S-nitrosylation with substrate site specificity PLoS ONE 6:e21849 doi:10.1371/journal.pone.0021849.

Ma, T.M., Abazyan, S., Abazyan, B., Nomura, J., Yang, C., Seshadri, S., Sawa, A., Snyder, S.H., and Pletnikov, M.V. (2013). Pathogenic disruption of DISC1-serine racemase binding elicits schizophrenia-like behavior via D-serine depletion. Molecular Psychiatry 18, 557-567.

Ma, T.M., Paul, B.D., Fu, C., Hu, S., Zhu, H., Blackshaw, S., Wolosker, H., and Snyder, S.H. (2014). Serine racemase regulated by binding to stargazin and PSD-95: potential N-methyl-D-aspartate-alpha-amino-3-hydroxy-5-methyl-4-isoxazolepropionic acid (NMDA-AMPA) glutamate neurotransmission cross-talk. J Biol Chem 289, 29631-29641.

Magni G, Amici A, Emanuelli M, Orsomando G, Raffaelli N, Ruggieri S (2004) Enzymology of NAD+ homeostasis in man. Cell Mol Life Sci 61:19-34 doi:10.1007/s00018-003-3161-1.

Marchesani F, Bruno S, Paredi G, Raboni S, Campanini B, Mozzarelli A (2018) Human serine racemase is nitrosylated at multiple sites Biochim Biophys Acta 1866:813-821 doi:10.1016/j.bbapap.2018.01.009.

Marchetti M, Bruno S, Campanini B, Bettati S, Peracchi A, Mozzarelli A (2015) Regulation of human serine racemase activity and dynamics by

halides, ATP and malonate Amino Acids 47:163-173 doi:10.1007/s00726-014-1856-2.

Marchetti M, Bruno S, Campanini B, Peracchi A, Mai N, Mozzarelli A (2013) ATP binding to human serine racemase is cooperative and modulated by glycine FEBS J 280:5853-5863 doi:10.1111/febs.12510.

Marino SM, Gladyshev VN (2010) Structural Analysis of Cysteine S-Nitrosylation: A Modified Acid-Based Motif and the Emerging Role of Trans-Nitrosylation J Mol Biol 395:844-859 doi:10.1016/j.jmb.2009.10.042.

Maruyama K (1990) Activation of Pseudomonas ochraceae 4-Hydroxy-4-Methyl-2-Oxoglutarate Aldolase by Inorganic Phosphate The Journal of Biochemistry 108:334-340.

Miladi B, El Marjou A, Boeuf G, Bouallagui H, Dufour F, Di Martino P, Elm'selmi A (2012) Oriented immobilization of the tobacco etch virus protease for the cleavage of fusion proteins J Biotechnol 158:97-103 doi:10.1016/j.jbiotec.2012.01.010.

Mori, H., Wada, R., Li, J., Ishimoto, T., Mizuguchi, M., Obita, T., Gouda, H., Hirono, S., and Toyooka, N. (2014). In silico and pharmacological screenings identify novel serine racemase inhibitors. Bioorganic and Medicinal Chemistry Letters 24, 3732-3735.

Mozzarelli, A., Bettati, S., Campanini, B., Salsi, E., Raboni, S., Singh, R., Spyrakis, F., Kumar, V.P., and Cook, P.F. (2011). The multifaceted pyridoxal 5'-phosphate-dependent O-acetylserine sulfhydrylase. Biochimica et Biophysica Acta 1814, 1497-1510.

Mustafa, A.K., Kim, P.M., and Snyder, S.H. (2004). D-Serine as a putative glial neurotransmitter. Neuron glia biology 1, 275-281.

Mustafa, A.K., Kumar, M., Selvakumar, B., Ho, G.P., Ehmsen, J.T., Barrow, R.K., Amzel, L.M., and Snyder, S.H. (2007). Nitric oxide S-nitrosylates serine racemase, mediating feedback inhibition of D-serine formation. Proc Natl Acad Sci U S A 104, 2950-2955.

Neidle, A., and Dunlop, D.S. (2002). Allosteric Regulation of Mouse Brain Serine Racemase. Neurochemical Research 27, 1719-1724.

Okamoto A, Higuchi T, Hirotsu K, Kuramitsu S, Kagamiyama H (1994) X-ray crystallographic study of pyridoxal 5'-phosphate-type aspartate aminotransferases from Escherichia coli in open and closed form J Biochem 116:95-107.

Okonechnikov K, Golosova O, Fursov M, team U (2012) Unipro UGENE: a unified bioinformatics toolkit Bioinformatics 28:1166-1167 doi:10.1093/bioinformatics/bts091.

Pace CN, Vajdos F, Fee L, Grimsley G, Gray T (1995) How to measure and predict the molar absorption coefficient of a protein Protein Sci 4:2411-2423 doi:10.1002/pro.5560041120.

Paoletti P, Bellone C, Zhou Q (2013) NMDA receptor subunit diversity: impact on receptor properties, synaptic plasticity and disease Nat Rev Neurosci 14:383-400 doi:10.1038/nrn3504.

Raboni S, Bettati S, Mozzarelli A (2009) Tryptophan synthase: a mine for enzymologists Cell Mol Life Sci 66:2391-2403 doi:10.1007/s00018-009-0028-0.

Raboni S, Pioselli B, Bettati S, Mozzarelli A (2003) The molecular pathway for the allosteric regulation of tryptophan synthase Biochim Biophys Acta 1647:157-160.

Rossi R, Lusini L, Giannerini F, Giustarini D, Lungarella G, Di Simplicio P (1997) A method to study kinetics of transnitrosation with nitrosoglutathione: reactions with hemoglobin and other thiols Anal Biochem 254:215-220.

Ruhe ZC, Hayes CS (2010) The N-terminus of GalE induces tmRNA activity in Escherichia coli PLoS ONE 5:e15207 doi:10.1371/journal.pone.0015207.

Sievers F, Wilm A, Dineen D, Gibson TJ, Karplus K, Li W, Lopez R, McWilliam H, Remmert M, Söding J, Thompson JD, Higgins DG (2011) Fast, scalable generation of high-quality protein multiple sequence alignments using Clustal Omega Mol Syst Biol 7:539 doi:10.1038/msb.2011.75.

Smith, M.A., Mack, V., Ebneth, A., Moraes, I., Felicetti, B., Wood, M., Schonfeld, D., Mather, O., Cesura, A., and Barker, J. (2010). The structure of mammalian Serine Racemase: evidence for conformational changes upon inhibitor binding. Journal of Biological Chemistry 285, 12873-12881.

Strisovsky K, Jiraskova J, Mikulova A, Rulisek L, Konvalinka J (2005) Dual substrate and reaction specificity in mouse serine racemase: Identification of high-affinity dicarboxylate substrate and inhibitors and analysis of the beta-eliminase activity Biochemistry 44:13091-13100 doi:10.1021/bi051201o.

Suzuki, M., Sasabe, J., Miyoshi, Y., Kuwasako, K., Muto, Y., Hamase, K., Matsuoka, M., Imanishi, N., and Aiso, S. (2015). Glycolytic flux controls D-serine synthesis through glyceraldehyde-3-phosphate dehydrogenase in astrocytes. Proc Natl Acad Sci U S A 112, E2217-2224.

Takahara, S., Nakagawa, K., Uchiyama, T., Yoshida, T., Matsumoto, K., Kawasumi, Y., Mizuguchi, M., Obita, T., Watanabe, Y., Hayakawa, D., Gouda, H., Mori, H., and Toyooka, N. (2017). Design, synthesis, and evaluation of novel inhibitors for wild-type human serine racemase. Bioorg Med Chem Lett.

Uda K, Abe K, Dehara Y, Mizobata K, Sogawa N, Akagi Y, Saigan M, Radkov AD,Moe LA (2016). Distribution and evolution of the serine/aspartate racemase family in invertebrates. Amino Acids 48, 387–402. doi: 10.1007/s00726-015-2092-0

Vorlova, B., Nachtigallova, D., Jiraskova-Vanickova, J., Ajani, H., Jansa, P., Rezac, J., Fanfrlik, J., Otyepka, M., Hobza, P., Konvalinka, J., and Lepsik, M. (2015). Malonate-based inhibitors of mammalian serine racemase: kinetic characterization and structure-based computational study. European Journal of Medicinal Chemistry 89, 189-197.

Wang W, Barger SW (2012) Cross-linking of serine racemase dimer by reactive oxygen species and reactive nitrogen species. J Neurosci Res. 2012 Jun;90(6):1218-29. doi: 10.1002/jnr.22832. Epub 2012 Feb 22.

Waterhouse A, Bertoni M, Bienert S, Studer G, Tauriello G, Gumienny R, Heer FT, de Beer TAP, Rempfer C, Bordoli L, Lepore R, Schwede T. (2018) SWISS-MODEL: homology modelling of protein structures and complexes Nucleic Acids Res 46:W296-W303 doi:10.1093/nar/gky427.

Wild JR, Belser WL, O'Donovan GA (1976) Unique aspects of the regulation of the aspartate transcarbamylase of Serratia marcescens J Bacteriol 128:766-775.

Wojdyla K, Rogowska-Wrzesinska A (2015) Differential alkylation-based redox proteomics--Lessons learnt Redox biology 6:240-252 doi:10.1016/j.redox.2015.08.005.

Wolosker H, Balu DT, Coyle JT (2016) The Rise and Fall of the d-Serine-Mediated Gliotransmission Hypothesis Trends Neurosci doi:10.1016/j.tins.2016.09.007.

Wolosker H, Dumin E, Balan L, Foltyn VN (2008) D-amino acids in the brain: D-serine in neurotransmission and neurodegeneration. FEBS J. 2008 Jul;275(14):3514-26. doi: 10.1111/j.1742-4658.2008.06515.x.

Wolosker H, Sheth KN, Takahashi M, Mothet JP, Brady RO, Ferris CD, Snyder SH (1999) Purification of serine racemase: Biosynthesis of the neuromodulator D-serine Proc Natl Acad Sci USA 96:721-725 doi:10.1073/pnas.96.2.721.

Xu Y, Ding J, Wu LY, Chou KC (2013a) iSNO-PseAAC: predict cysteine S-nitrosylation sites in proteins by incorporating position specific amino acid propensity into pseudo amino acid composition PLoS ONE 8:e55844 doi:10.1371/journal.pone.0055844.

Xu Y, Shao XJ, Wu LY, Deng NY, Chou KC (2013b) iSNO-AAPair: incorporating amino acid pairwise coupling into PseAAC for predicting cysteine S-nitrosylation sites in proteins PeerJ 1:e171 doi:10.7717/peerj.171.

Yamauchi, T., Goto, M., Wu, H.Y., Uo, T., Yoshimura, T., Mihara, H., Kurihara, T., Miyahara, I., Hirotsu, K., and Esaki, N. (2009). Serine Racemase with Catalytically Active Lysinoalanyl Residue. J. Biochem. 145, 421-424.

Ying W (2008) NAD+/NADH and NADP+/NADPH in cellular functions and cell death: regulation and biological consequences Antioxid Redox Signal 10:179-206 doi:10.1089/ars.2007.1672.

Zhuang Z, Yang B, Theus MH, Sick JT, Bethea JR, Sick TJ, Liebl DJ (2010) EphrinBs regulate D-serine synthesis and release in astrocytes J Neurosci 30:16015-16024 doi:10.1523/JNEUROSCI.0481-10.2010.

PUBLISHED WORKS

- Daniela Coppola, Daniela Giordano, Stefania Abbruzzetti, **Francesco Marchesani**, Marco Balestrieri, Guido di Prisco, Cristiano Viappiani, Stefano Bruno, Cinzia Verde, "Functional characterization of the haemoglobins of the migratory notothenioid fish Dissostichus eleginoides", Hydrobiologia (2015) 761:315–333 DOI 10.1007/s10750-015-2439-2
- Gianluca Paredi, Samanta Raboni, **Francesco Marchesani**, Stella A. Ordoudi, Maria Z. Tsimidou and Andrea Mozzarelli, "Insight of Saffron Proteome by Gel-Electrophoresis", Molecules (2016), 21, 167; doi:10.3390/molecules21020167
- Stefano Bruno, **Francesco Marchesani**, Luca Dellafiora, Marilena Margiotta, Serena Faggiano, Barbara Campanini, Andrea Mozzarelli, "Human serine racemase is allosterically modulated by NADH and reduced nicotinamide derivatives", Biochemical Journal (2016) DOI: 10.1042/BCJ20160566
- Stefano Bruno, Marilena Margiotta, **Francesco Marchesani**, Gianluca Paredi, Valentina Orlandi, Serena Faggiano, Luca Ronda, Barbara Campanini, Andrea Mozzarelli, "Magnesium and Calcium ions differentially affect human serine racemase activity and modulate its quaternary state toward a tetrameric form". Biochimica et Biophysica Acta, Proteins and Proteomics (2016) DOI: 10.1016/j.bbapap.2017.01.001.
- Roberta Russo, Daniela Giordano, Gianluca Paredi, **Francesco Marchesani**, Lisa Milazzo, Giovanna Altomonte, Pietro Del Canale, Stefania Abbruzzetti, Paolo Ascenzi, Guido di Prisco, Cristiano Viappiani, Angela Fago, Stefano Bruno, Giulietta Smulevich, Cinzia Verde, "The Greenland shark Somniosus microcephalus—Hemoglobins and ligand-binding properties". PLOS ONE (2017) 12(10):e0186181
- **Francesco Marchesani**, Stefano Bruno, Gianluca Paredi, Samanta Raboni, Barbara Campanini, Andrea Mozzarelli, "Human serine racemase is nitrosylated at multiple sites". Biochimica et Biophysica Acta, Proteins and Proteomics (2018) DOI: 10.1016/j.bbapap.2018.01.009
- Samanta Raboni, Marialaura Marchetti, Serena Faggiano, Barbara Campanini, Stefano Bruno, **Francesco Marchesani**, Marilena

Margiotta, Andrea Mozzarelli. “The Energy Landscape of Human Serine Racemase”. Front. Mol. Biosci., (2019) https://doi.org/10.3389/fmolb.2018.00112

PhD SCHOOLS AND MEETINGS ATTENDED

- "Watching at the D-side: D-amino acids and their significance in neurobiology", Lake Como school of advanced studies, Como, June 5-9th 2016
- "In silico/in vitro approaches for food science" EFSA, Parma September 09th 2016
- “Proteins as drug target, proteins as drug, and protein degradation as therapeutic strategy” - Organized by the Group Protein of the Italian Biochemical Society and the Division of Medicinal Chemistry of the Italian Chemistry Society - May 8th, 2017, Congress Hall, Plesso Didattico Q02, Viale delle Scienze, Campus, Università di Parma, Parma.
- “NGP-net Winter School on Experimental Methods forProtein Disorder & Aggregation” - Marseille, France 13–17th February 2017
- “Advanced fluorescence methods to explore dynamics and mechanisms of molecular machines” - Training School (COST); February 7-9th 2018, University of Parma, Italy
- “Macromolecular crystallography”; May 8-14th 2018, University of Parma, Italy
- “ULLA Summer school”; Leuven, Belgium 8-13th July 2017
- “PROTEINE 2018”, Verona, May 28-30th 2018 (congress of the Italian Biochemical Society). ORAL PRESENTATION (“Insights on s-nitrosylation in human serine racemase”)
- “ULLA Workshop”, Helsinki, July 1-4th 2018